Journal of Machine Construction and Maintenance

Łukasiewicz
ITEE

SCIENTIFIC BOARD

Ladies and Gentlemen,

Exactly 30 years have passed since the first number of the scientific magazine *Maintenance Problems* was issued, which was renamed as the *Journal of Machine Construction and Maintenance* in 2017 under the auspices of the Committee on Machine Building of the Polish Academy of Sciences.

Throughout this thirty-year period, the subject areas of the articles presented in the journal mainly concerned the scientific and technical issues of machine construction and maintenance, as well as important complementary issues in the fields of surface engineering, advanced manufacturing technologies, environmental technologies, research and testing equipment, technology transfer, and methods of computer-aided support for technical systems. It should be strongly stressed that the area of research and technical interests almost perfectly fits the paradigm of the sustainable development of the global economy widely recognised as extremely important from the beginning of the 21st century. The magazine's program line assumed that basic and applied research in technical sciences should support the development of advanced technologies, and that the achieved research results should find useful industrial applications and be economically efficient. Therefore, in our journal, in addition to advanced cognitive work and scientific research, interesting examples of the implementation of innovative technical solutions were presented, as well as barriers to their transfer to economic applications, and the scientific, system, and operational ways of the elimination or mitigation of these barriers.

The thirty-year history of the journal, which was listed in several international databases, comprises 125 volumes and more than 2,600 scientific articles by both Polish and foreign authors. It also includes over 300 monographs, mainly of professors' books and habilitation theses, which were published in the associated with the journal publishing series *Problems of Machine Construction and Maintenance Library*, also under the patronage of the Committee on Machine Building of the Polish Academy of Sciences.

Unfortunately, despite the very positive opinions of the readers of our magazine, its subscribers and database administrators in which the journal is listed, as well as reviewers of the Ministry of Science and Higher Education competition under the program "Support for scientific journals," who assessed "It is a good, needed and valued scientific journal in Poland," it not only did not receive funding (without which it could still be published), but above all was granted a low level of scoring, conditioning the interest of the scientific community. Therefore, despite waiting for the final evaluation of the journal in the Web of Science database, to which it was submitted almost three years ago, which, according to a recent declaration by a representative of this database, should be made by the end of the first quarter of 2020, and also due to structural and personal changes at the Institute for Sustainable Technologies in Radom, which is the publisher of the magazine, we decided to suspend its publication. I would like to warmly thank the authors, reviewers, scientific and editorial committees, and specially the readers, for many years of cooperation.

Yours faithfully,
Adam Mazurkiewicz
Editor-in-chief

CONTENTS

Joanna KACPRZYŃSKA-GOŁACKA[a,*], **Piotr WIECIŃSKI**[b], **Halina GARBACZ**[b],
Adam MAZURKIEWICZ[a], **Sylwia SOWA**[a], **Jerzy SMOLIK**[a]

[a] Łukasiewicz Research Network – Institute for Sustainable Technologies, Radom, Poland
[b] Faculty of Materials Engineering, Warsaw University of Technology, Warsaw, Poland
* Corresponding author: joanna.kacprzynska@itee.radom.pl

THE INFLUENCE OF MICROSTRUCTURE OF Cr/CrN NANOMULTILAYER COATINGS ON THEIR TRIBOLOGICAL AND MECHANICAL PROPERTIES

Key words: multilayer coatings, PVD, tribological tests.

Abstract: One of the most effective ways of shaping the operating parameters of functional elements is the modification of the surface layer by modern surface engineering technologies. The most perspective directions in the development of surface engineering solutions are multilayer coatings. The appropriate selection of parameters of multi-layered structure such as thickness, chemical composition, microstructure, and the number of component layer in these type coatings enable effective shaping of their properties. However, a characteristic of the mechanical and tribological properties as a function of parameters of a multilayer structure are still unclear in literature.

The paper presents the influence of multilayer structure on mechanical and tribological properties of the coatings prepared by arc vacuum technics. The analysis of mechanical properties included hardness, Young's modulus, and adhesion tests. The analysis of microstructure was performed using Scanning Transmission Electron Microscopy (STEM). The tribological properties were examined using the pin-on-disc produced by the DUCOM Company. The authors indicated that the multilayer coatings Cr/CrN were characterized by good mechanical and tribological properties. In this paper, the authors confirmed that parameters of the process of the multilayer creation are important in shaping the unique tribological properties of the multilayer coatings.

Wpływ mikrostruktury na właściwości mechaniczne oraz trybologiczne powłok nanowielowarstwowych Cr/CrN

Słowa kluczowe: powłoki wielowarstwowe, PVD, badania trybologiczne.

Streszczenie: Jednym z najbardziej efektywnych sposobów kształtowania właściwości eksploatacyjnych elementów użytkowych jest modyfikowanie warstwy wierzchniej poprzez zastosowanie nowoczesnych technologii inżynierii powierzchni. Głównym kierunkiem rozwoju rozwiązań inżynierii powierzchni stały się w ostatnich latach między innymi powłoki wielowarstwowe. Stwarzają one bardzo duże możliwość w zakresie kształtowania ich właściwości poprzez odpowiedni dobór struktury wielowarstwowej, w tym: grubość, ilość, mikrostruktura oraz skład chemiczny warstw składowych. Nadal jednak charakterystyka ich właściwości mechanicznych oraz trybologicznych w funkcji parametrów ich wielowarstwowej konfiguracji pozostaje niejasna w dostępnej literaturze.

W artykule przedstawiono wpływ parametrów budowy wielowarstwowej powłok Cr/CrN wytwarzanych metodą łukowo-próżniową na ich właściwości mechaniczne oraz trybologiczne. Analiza właściwości mechanicznych obejmowała badania twardości, modułu Younga oraz badania adhezji metodą zarysowania. Analizę mikrostruktury przeprowadzono z wykorzystaniem skaningowej mikroskopii transmisyjnej (STEM). Badania właściwości trybologicznych zostały przeprowadzone w temperaturze pokojowej z wykorzystaniem testera trybologicznego firmy DUCOM typu pin-on-disc. Autorzy wskazują, iż powłoki nanowielowarstwowe Cr/CrN charakteryzują się dobrymi właściwościami mechanicznymi oraz dobrymi właściwościami trybologicznymi. W artykule autorzy potwierdzili wpływ parametrów budowy wielowarstwowej powłok PVD w procesie kształtowania ich właściwości trybologicznych.

Introduction

One of the most effective ways of shaping the operating parameters of functional elements is to modify the surface layer using modern technologies of surface engineering. In recent years, the main directions in the development of surface engineering solutions are multilayer coatings, which enable effective shaping of surface layer properties [1–3]. One example of a multilayer coating is Cr/CrN coating, whose properties are very well described (reported) in the literature [4–6]. Coatings are characterized by excellent mechanical and tribological properties due to the presence of hard layers based on nitrides and a plastic metallic layer in the structure. In this connection, the plastic layer of metallic Cr can absorb excessive plastic deformation, while the phase of hard chromium nitride ensures good wear resistance. In addition, the presence of boundaries between the component layers in the Cr/CrN coating structure ensures high brittle cracking resistance. The presence of transition layers could change the cracking mechanism of the coating from a single-step, which is characteristic for single-layer coatings, to a multi-stage/ steps mechanism. The initiation of cracks in the coating can come from both the substrate and from the surface. The propagation of cracks in the single-layer coating can destroy it in the whole cross-section. However, in the multi-layer coating, the boundaries between the component layers are places of energy dissipation. The directions of microcracks propagation can change, thus preventing their further spreading in the coating. This phenomenon prolongs the path of a single crack. At the same time, the energy is reduced and significantly improves the resistance of multi-layer coatings to brittle fracture [7–8].

Thanks to these properties, the Cr/CrN multilayer coating can be successfully used to improve durability on plastic deformation and erosion processes, which was confirmed in the many research works [9–10]. The large possibilities of using Cr/CrN multilayer coating are connected with the possibility of practically optional designing of the surface layer properties by shaping of parameters of their multilayer structure (phase composition, chemical composition, microstructure, grain size, and state of stress) and the whole coating (number and thickness of component layers).The literature analysis confirmed the possibility of shaping the mechanical properties of the Cr/CrN coating by changing the multi-layer configuration [11]. It should be noted that the characteristic of tribological properties as a function of the parameters of the multilayer configuration of Cr/CrN coatings is still unclear in the available literature.

The authors of article present the analysis of the properties of Cr/CrN coatings that are produced by the arc vacuum method depending on the number of component layer in the range of 10–100. An analysis of the impact of the multilayer configuration on their tribological properties is also presented. The research methods which were presented in the article include the analysis of mechanical properties and microstructure and the analysis of tribological properties of selected nano-multilayer coating in the function of the number and thickness of component layers.

1. Experimental details

1.1 Deposition of coatings

Samples for investigations were made of titanium alloy Ti6Al4V. Before the deposition process, substrates were cleaned and mechanically polished using the procedure reported in literature [12].

The investigated PVD multilayers coating were created by means of the Arc Evaporation method, with the use of CDS-Standard device designed and produced by the Łukasiewicz Research Network-Institute for Sustainable Technologies, Radom. The technological processes include the formation of three coatings of different thicknesses and the number of component layers. All coatings were made using four pure Cr targets. Parameters of the surface treatment technology are presented in Table 1.

Table 1. Parameters of the deposited PVD coatings

Coating	Layer	Atmosphere	Temperature T [^{o}C]	Pressure p [mbar]	Voltage U_{bias} [V]	Current I_{bias} [A]	Time t [min]
Cr/CrN 10	Cr	100%Ar	350	5.0×10^{-3}	- 50	4x50	15
	CrN	100%N_2		3.5×10^{-2}	- 200	4x50	7
Cr/CrN 50	Cr	100%Ar	360	5.0×10^{-3}	- 50	4x50	3
	CrN	100%N_2		3.5×10^{-2}	- 200	4x50	1.4
Cr/CrN 100	Cr	100%Ar	340	5.0×10^{-3}	- 50	4x50	1.5
	CrN	100%N_2		3.5×10^{-2}	- 200	4x50	0.7

1.2. Characteristics of the mechanical properties of coatings

1.2.1. Hardness and Young's modulus test

Mechanical properties like hardness and Young's modulus for investigated coatings were measured by means of the nanoindentation method using a Nano-Hardness Tester by CSM Instruments with a Berkovich diamond indenter. The hardness and Young's modulus measurements of selected PVD coatings were carried out according to parameters presented in Table 2. The maximum penetration of the indenter is $h_{max} < 0.1$ (10%) of the thickness of the layer. Parameters used in measurements of Young's modulus using the Nano-Hardness Tester are given in Table 2.

Table 2. Results of measurements of hardness and Young's modulus by means of the Nano-Hardness

Coating	Maximum penetration of indenter h_{max} [nm]	Maximum load of indenter F_{max} [mN]	Number of load cycles	Dwell time of maximum load [s]	Type of indenter
Cr/CrN 10	400	61	1	1	Berkovich
Cr/CrN 50	400	62	1	1	Berkovich
Cr/CrN 100	400	63	1	1	Berkovich

The load and displacement of intender were recorded during all measurements. The next step was the plotting of the displacement-dependence curve as a function of the load.

In accordance with the mathematical principles developed by Oliver and Pharr, both of values of the hardness of the tested coatings and the Young's modulus were determined [13]. Based on the results of the hardness and Young's modulus, the "plasticity index" H^3/E^2 was determined, which is widely quoted as a valuable measure in determining the limit of elastic behaviour in a surface contact, and it was clearly important for the avoidance to wear [14].

1.2.2. Adhesion test

Adhesions were measured using a scratch-test method with the use of a Revetest (CSM Instruments) equipped with a diamond Rockwell indenter with a radius of 200 µm and an apex angle of 120º. The indenter's load force increased linearly in the range of 0-200N, and the loading rate was 10 N/min. The scratches were 5 mm. During the test, the changes of acoustic emission (AE) and friction forces (Ft) as a function of the force loading the indenter (Fn) were registered. Each sample was subjected to three such tests. The scratch specimens were also subjected to a detailed examination by SEM after the test series had been completed. Based on the changes in acoustic emission and friction force, three critical loads were determined corresponding to completely damage of the coating. The Fc1 parameter described the value of the load on the penetrator under which the first fractures were observed, the Fc2 parameter described the load under which the next adhesive damages in the form of spalling occurred, and the Fc3 parameter was related to the load under which decohesion occurred in the entire layer from the substrate.

1.3. Surface and microstructure characterization

The microstructures of coatings were characterized with Scanning Transmission Electron Microscopy (STEM) Hitachi HD2700. The measurements were investigated on samples which were made of titanium alloy Ti6Al4V. For the preparation of samples, a Hitachi FB2100 was used with a focused ion beam (FIB) system equipped with a Ga+ion source with accelerating voltage in the range 10–40 kV and the current in the range 0.01–45 nA. The thickness of STEM thin foil was about 100 nm.

1.4. Tribological properties of coatings

Tribological tests of samples were executed using the pin-on-disc tribometer produced by the DUCOM Company. The investigated samples were prepared from the Ti6Al4V alloy. For all of our samples, the tests were performed at room temperatures for the combination with Al_2O_3 ball–shield covered with the test coating in accordance with the parameters shown in Table 3.

Table 3. Parameters of pin-on-disc tribological tests

Temperature [°C]	Ball load force [N]	Wear track [m]	Number of cycles	Sliding distance [m/s]	The diameter of wear track [mm]	The radius of wear track [mm]
25	2	350	6370	0.2	15	6

After the tests, wear tracks were scanned using an Interferometric Profilometer, and the volume of the removed coating material was measured. Based on the volume of removed coatings material, the wear index W was calculated, according to the following formula:

$$W = V / F \cdot s,$$

where

V – volume of removed coatings material [mm^3],

F – ball load force [N],

s – length of wear track [m].

To determine the dominant mechanism of the destruction during the scratch test, the created wear tracks were also subjected to microscopic observation and measurements of chemical composition by using the EDS technique.

2. Results and discussion

2.1. Microstructure and chemical composition

The results of the microstructure and cross section analysis are presented in Fig.1. The surface analysis of coatings revealed a small variation of the surface roughness. As the number of component layers increased, the significant roughness was changed.
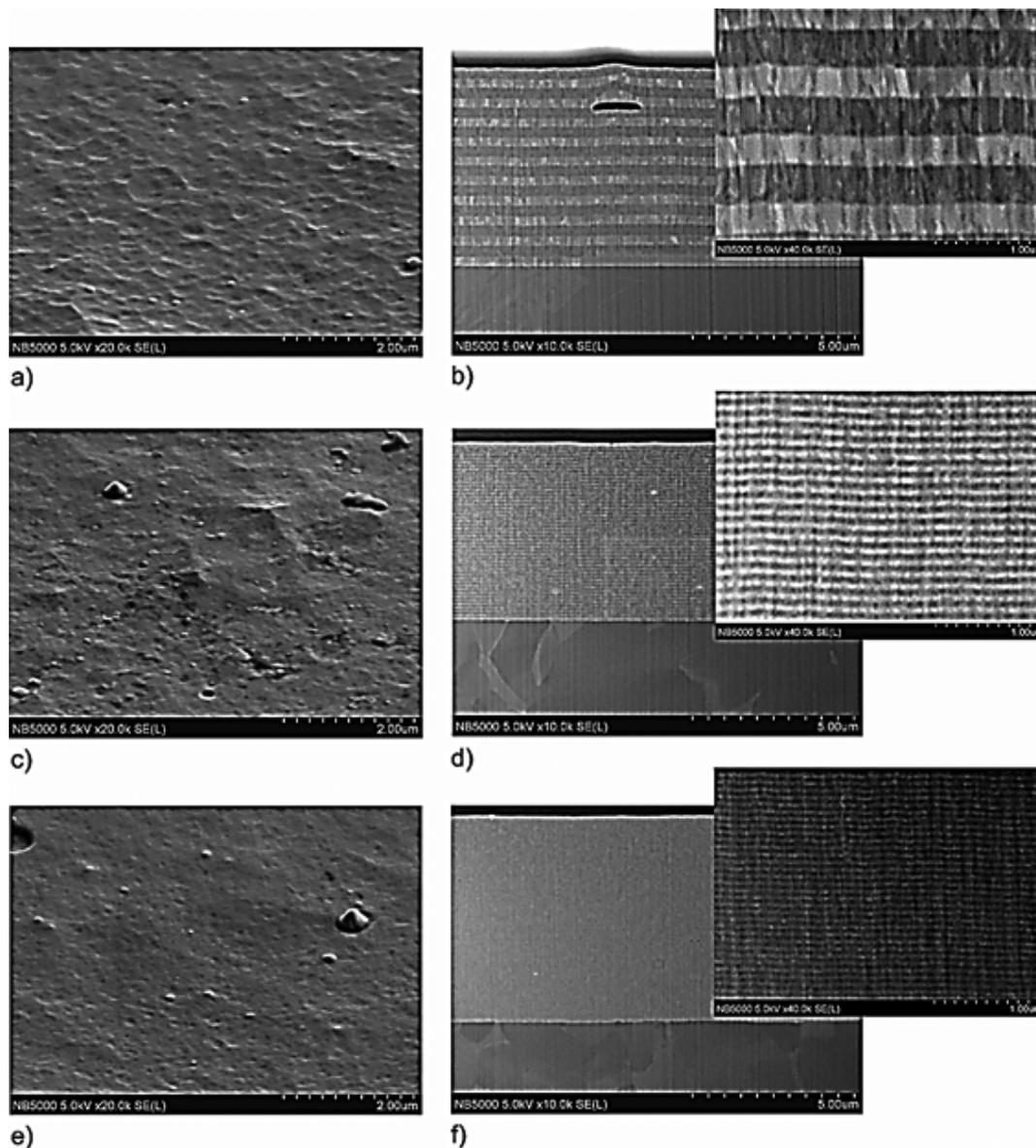
Fig. 1. Microstructure of investigated coatings: a) Cr/CrNx10 coating-surface, b) Cr/CrNx10 coating–cross-section, c) Cr/CrNx50 coating-surface, b) Cr/CrNx50 coating-cross-section, e) Cr/CrNx100 coating-surface, f) Cr/CrNx100 coating-cross-section

The conducted analysis has also confirmed a significant differentiation in the thickness for the component layers in the obtained coatings. The parameters of the multilayer coating are presented in Table 4. In all cases, the total thicknesses of the deposited coatings were similar and were in the range of 5.2–5.8 μm. It was observed that coatings also have a homogeneous thickness for all component layers. The increasing number of the component layers can affect the reduction in the thickness of individual of Cr/CrN layers. The ratio for the thickness of metallic Cr layer and CrN layer is at the level of about 1:1. In the case of the coating which consists of 10 Cr/CrN layers, the thickness of the individual layer was about $g_{Cr/CrNx10}$=0.57 μm. In the case of coatings that consisted of 50 and 100 layers, the thicknesses of individually layer were significantly smaller and were respectively p: $g_{Cr/CrNx50}$=0.08 μm, $g_{Cr/CrNx100}$=0.05 μm.

Table 4. Parameters of multilayers coatings

	Thickness			Bi-layer period [μm]	width of columnar grains [μm]
	Total thickness [μm]	Cr [μm]	CrN [μm]		
Cr/CrN 10	5.8	0.24	0.33	0.57	0.09
Cr/CrN 50	5.8	0.03	0.05	0.08	0.05
Cr/CrN 100	5.2	0.02	0.03	0.05	0.04

The detailed observation of multilayer microstructure has indicated that all investigated coatings were characterized by non-porous microstructure with fine dense fibrillar crystallites. This microstructure is typical for the structure of the transition zone T according to the Thorton model proposed for PVD coatings [15]. The increasing of the component layers contributed to a significant fragmentation of the structure. The highest reduction of grain size reduction was observed when the number of Cr/CrN complexes increased from 10 to 50. For the Cr/CrNx10 coating, the size of the columnar grains was about 0.09 μm. For Cr/CrNx50 coating, the size of the grains was about 0.05 μm. Increasing the number of layers did not influence the clear fragmentation of the structure. The grain size for the Cr/CrNx100 coating was decreasing to a value of about 0.04 μm.

2.2. Mechanical properties

The results of the investigations of mechanical properties for coatings are presented in Table 4. The measurements of the hardness and the Young's modulus results showed that increasing number of component layers to 50 causes a significant increase in the value of hardness and Young's modulus. Further increasing of the number of component layers contributed to the decrease of Young's modulus and the lack of changes in hardness. The Young's modulus decreases and changes the elastic properties defined by the H/E plasticity index, which is an important criterion of resistance against plastic deformation of hard coatings. The high H/E value at high hardness indicates very good wear resistance for thin coatings [16]. The analysis of the elastic properties demonstrated that, with the increase in the number of layers, the susceptibility of deformation is reduced, i.e. for all coatings, $H/E_{Cr/CrNx10}$=0.7 and $H/E_{Cr/CrNx50}$=0.8, and, for the coating which consists of 100 layers, $H/E_{Cr/CrNx100}$=0.9. With an increasing thickness of component layers, the resistance to the plastic deformation, which is defined the H^3/E^2index, increases (Table 5). Coatings with high hardness and a small modulus of elasticity will be able to transfer much higher loads, and they not induce plastification [17].

Table 5. Mechanical properties of deposited layers

Coating PVD	Hardness [GPa]	The Young's modulus [GPa]	H/E	H3/E2
Cr/CrN 10	20±2	291±20	≈0.07	≈0.09
Cr/CrN 50	26±2	311±20	≈0.08	≈0.18
Cr/CrN 100	26±1	297±11	≈0.09	≈0.20

The adhesion tests were carried out making three scratches for each of the tested coatings, and then the average values of critical loads were determined. The obtained results showed that the best adhesion to the substrate was characterized by (Cr, CrN)x10 coating. The complete removal of the coating from the substrate was observed at $Fc3_{Cr/CrNx10}$ = 80 N. In the scratch test, the first cracks for this coating were observed with a critical load $Fc1_{Cr/CrN10}$ = 9 N. These cracks were curved opposite to the direction of the indenter movement and propagated outside the area of scratches, and increasing the load generated their multiplication.

For $Fc2_{Cr/CrN10}$ = 59 N, it was observed that the coating was only removed on the edges of scratches. Chips were not observed over the entire length of the scratches.

For other coatings, the load values when the total coating was removed from the crack area were significantly lower and were, respectively, $Fc3_{Cr/CrNx50}$ = 75 N and $Fc3_{Cr/CrNx100}$ = 69 N. The first cracks for these coatings also appeared at a lower load than in the case of the coating which consists of 10 layers ($Fc1_{Cr/CrNx50}$ = 6 N and $Fc1_{Cr/CrNx100}$ = 5 N). These cracks have only appeared on the edges of the scratches and were arranged parallel to the indenter movement. The appearance of the first adhesive defects in the form of chips were observed when further increasing the load. These chips were observed at $Fc2_{Cr/CrN50}$ =24 N and $Fc2_{Cr/CrN100}$ = 26 N. The surfaces of chips were larger for the coating which consists of 100 component layers than for the coating which consists of 50 component layers.

2.3. Tribological properties

The results of the tribological tests at the room temperature are shown in Table 6. In accordance with the calculated the wear index, the best resistance was characterized by the coatings with 100 component layers ($Wz_{Cr/CrN}$=1.08^{-3} mm^3/N*km). The coating which consists 50 component layers were characterized by a lower wear index ($Wz_{Cr/CrN50}$ = 5.93^{e-3} mm^3/N*km). The worst resistance for tribological tests were recorded for the coating which consisted of 10 component layers (Cr/CrN 10). The wear index for Cr/CrN50 ($Wz_{Cr/CrN50}$ = 5.47^{e2} mm^3/N*km) was lower. The results of research showed that the wear resistance of the Cr/CrN multilayer coatings depends on the thickness of the Cr and CrN layers. The wear indexes of component layers are decreasing with increasing the thickness of coatings.
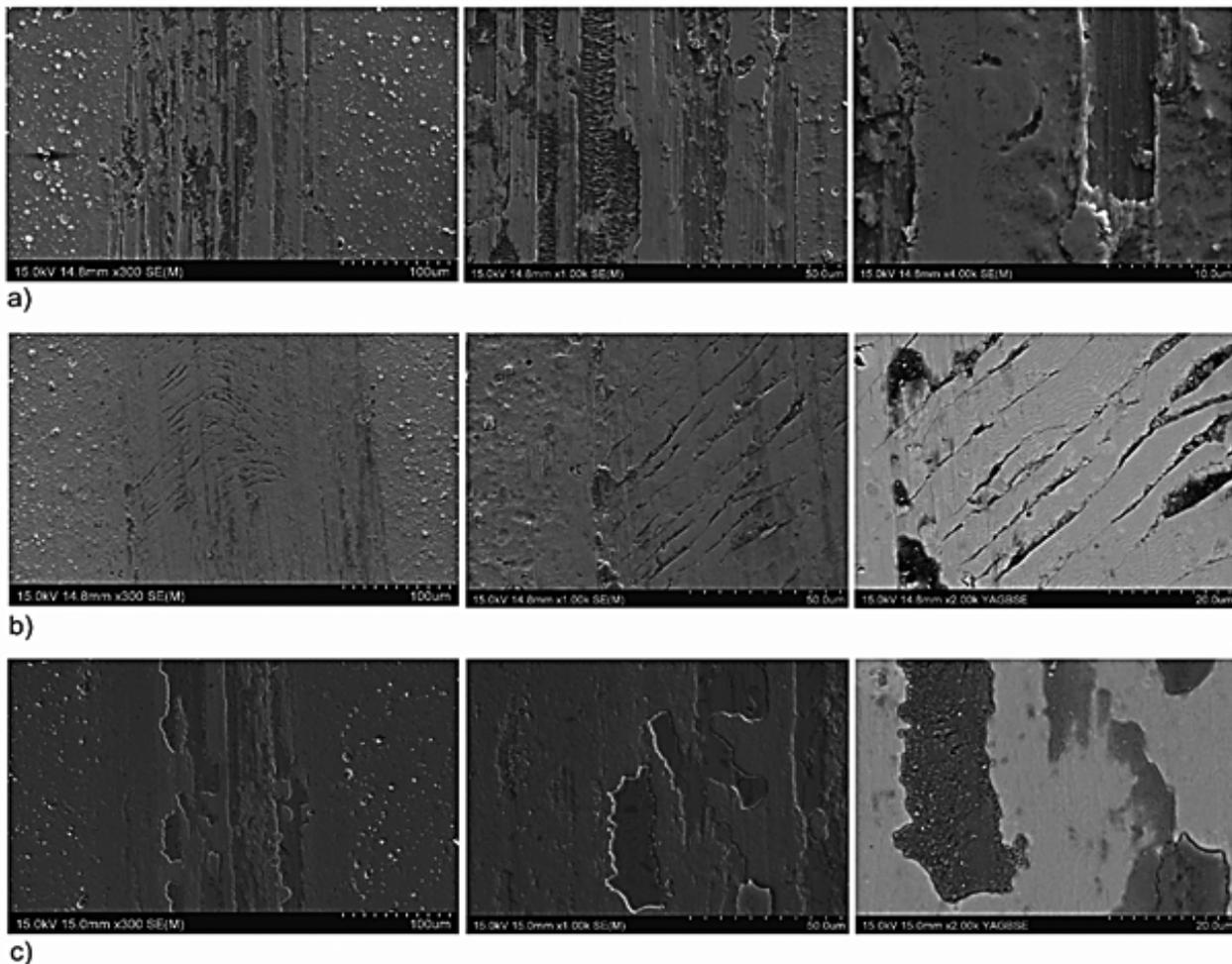
Fig. 2. Images of wear tracks after tribological tests at room temperature: a) Cr/CrNx10 (300x,1000x,4000x), b) Cr/CrNx50 (300x, 1000x, 2000x), c) Cr/CrNx100 (300x, 1000x, 2000x)

Table 6. The wear track index based on the tribological tests

Coating	Volume of wear track [mm^3]			Average volume of wear track [mm^3]	Wear index Wz [mm^3/N*km]
Cr/CrN 10	5.98E-03	9.93E-02	9.58E-03	3.83E-02	5.47E-02
Cr/CrN 50	9.57E-03	1.64E-03	1.24E-03	4.15E-03	5.93E-03
Cr/CrN 100	6.95E-04	8.60E-04	7.07E-04	7.54E-04	1.08E-04

The analysis of wear tracks after tribological tests (Fig. 2) showed that different destruction mechanisms of the coating were observed. The results of the tribological tests depended on the number of multilayers parameters. The area of the wear for 10 layers (Cr/CrN10) was characterized by non-homogenous surface (Fig. 2a). We can observe a lot of grooves and indentations which were characteristic of the abrasive wear mechanism through grooving. In the results of this phenomenon, cooperation at the interfaces of layers was worse, and this leads to faster damage of the coating. The abrasive wear of this coating was increased by surface fatigue. It led to separating relatively large fragments which were crushed, and they were present at friction contact. The analysis of the chemical composition did not show the presence of aluminium, which indicates a lack of wear products of the Al_2O_3 counter-sample.

The analysis of wear track for other samples (Cr/CrN50 and Cr/CrN100) showed a different mechanism of the destruction of these materials in friction processes. The wear destructions, small cracks, and chips were dominant in the scratch which was formed on Cr/CrN50 coating (Fig. 2b). Abrasive and adhesive wear was also observed. We can observe that aluminium was present in wear tracks. It can be information for us about abrasion and the transferring of material from the counter-sample. The larger adhesive destructions in the form of chips were noticed for the Cr/CrN100 coating in the abrasion track (Fig. 2c). The chemical analysis showed that the wear material from counter-body was absent. We can observe the high content of oxygen and chromium on the wear surface. It indicates the oxidation of the coating. It was reported in literature that the Cr_xO_y [18] was formed on the surface of Cr at room temperatures. The presence of Cr_xO_y in a friction pair can reduce the wear [19]. We can observed a typical abrasive wear of the interlayer in the form of a chromium oxide lubricating film (CrxOy), which protected surface coatings against wear [20–21].

of hardness was observed with the increasing number of component layer from 10 to 50. This is due the fact that the increasing of the thickness Cr/CrN layer can reduce the thickness of the plastic chromium phase Cr characterized by the low hardness (H_{Cr}=4GPa). The observed decrease in the thickness of the chromium metal layer also caused an increase in the resistance to plastic deformation ($H/E_{Cr/CrN10}$=0.7, $H/E_{Cr/CrN10}$=0.8, $H/E_{Cr/CrN10}$=0.9) for whole complex. This was also confirmed by the results of adhesion tests. For the coating which can be characterized by a low H/E index, chips were not observed over the entire length of the crack. There was only the loosening of the coating from the substrate at the edges of the crack mainly due to the uplift of the material, which is characteristic for materials with high susceptibility to plastic deformation. The critical normal force tends to increase with increasing coating hardness. In the case of other coatings, the appearance of many chips characteristic for brittle materials was observed. Increasing the number of Cr/CrN layers contributed to increasing the wear tracks.

The authors also confirmed the significant effect of the parameter of multilayer configuration of the coatings on tribological properties. The analysis of the results indicated that, with the increasing number of component layers, the abrasion resistance of the tested coatings increase. The change in the thickness of the component layers also affects the change of destructive mechanisms occurring in the process of tribological wear from typical wear for soft materials through grooving on abrasive and adhesive wear. Important is the fact that, with increasing the number of the component layers to 100, Cr/CrN complexes caused an increase in the number of defects in the form of shallow adhesive chips. It caused that the layer of metallic chromium was exposed and was oxidized. The phenomenon of the formation of the Cr_xO_y oxide layer in accordance with the literature has a positive effect on the reduction of wear intensity in tribological friction processes.

3. Conclusion

The analysis of the obtained results confirmed the significant influence of the parameter of the multilayer configuration of coatings in the formation of tribological and mechanical properties. The increasing

Acknowledgements

References

1. Huang S-H., Chen S-F., Kuo Y-Ch., Wang Ch-J., Lee J-W., Chan Y-Ch., Chen H-W., Duh J-G., Hsieh T-E.: Mechanical and tribological properties evaluation of cathodic arc deposited CrN/ZrN multilayer coatings. *Surface & Coatings Technology*, 2011, 206, pp. 1744–1752.
2. Li P., Chen L., Wang S.Q., Yang B., Du Y., Li J., Wu M.J.: Microstructure, mechanical and thermal properties of TiAlN/CrAlN multilayer coatings. *Int. Journal of Refractory Metals and Hard Materials*, 2013, 40, pp. 51–57.
3. Ibrahim R.N., Rahmat M.A., Oskouei R.H., Singh Raman R.K.: Monolayer TiAlN and multilayer TiAlN/CrN PVD coatings as surface modifiers to mitigate fretting fatigue of AISI P20 steel. *Engineering Fracture Mechanics*, 2015, 137, pp. 64–78.
4. Wieciński P., Smolik J., Garbacz H., Kurzydlowski K.J.: Microstructure and mechanical properties of nanostructure multilayer CrN/Cr coatings on titanium alloy. *Thin Solid Films*, 2011, 519(12), pp. 4069–4073.
5. Chim Y.C., Ding X.Z., Zeng X.T., Zhang S.: Oxidation resistance of TiN, CrN, TiAlN and CrAlN coatings deposited by lateral rotating cathode arc. *Thin Solid Films*, 2009, 517, pp. 4845–4849.
6. Yonekura D., Fujita J., Miki K.: Fatigue and wear properties of Ti–6Al–4V alloy with Cr/CrN multilayer coating. *Surface & Coatings Technology*, 2015, 275, pp. 232–238.
7. Kot M., Major Ł., Lackner J., Rakowski W.: Analysis of influence of sublayer thickness on the deformation mechanism and fracture of Ti/TiN multilayer. *Tribologia*, 2010, 4, pp. 181–189 [in Polish].
8. Chen L., Xu Y.X., Du Y., Liu Y.: Effect of bilayer period on structure, mechanical and thermal properties of TiAlN/AlTiN multilayer coatings. *Thin Solid Films*, 2015, 592, pp. 207–214.
9. Wieciński P., Smolik J., Garbacz H., Kurzydłowski K.J.: Erosion resistance of the nanostructured Cr/CrN multilayer coatings on Ti6Al4V alloy. *Vacuum*, 2014, 107, pp. 277–283
10. Wieciński P., Smolik J., Garbacz H., Kurzydłowski K.J.: Microstructure and mechanical properties of nanostructure multilayer CrN/Cr coatings on titanium alloy. *Thin Solid Films*, 2011, 12, pp. 4069–4073.
11. Wieciński P., Smolik J., Garbacz H., Bonarski J., Mazurkiewicz A., Kurzydłowski K.J.: Microstructure and properties of metal/ceramic and ceramic/ceramic multilayer coatings on titanium alloy Ti6Al4V. *Surface and Coatings Technology*, in press, corrected proof.
12. Kacprzyńska-Gołacka J., Smolik J., Mazurkiewicz A.: The comparison of antiwear and fatigue properties in higher temperature for PN+CrN and PN+AlCrTiN layer composites. *Int. J. Microstructure and Materials Properties*, 2014, 9, pp. 15–24.
13. Pharr M., Oliver W.C., Brotzen F.R.: On the generality of the relationship between contact stiffness, contact area, and Elastic moduli during indentation. *Journal of Materials Research,* 1992, 7, pp. 613–617.
14. Halling J.: Surface films in tribology. *Tribologia*, 1982, 1, p. 15.
15. Thornton J.A.: High rate thick film growth. *Annual Review of Materials Science*, 1977, 7, pp. 239–260.
16. Pei Y.T., Galvan D., De Hosson J.Th.M., Cavaleiro A.: Nanostructured TiC/a-C coatings for low friction and wear resistant applications. *Surface and Coatings Technology*, 2005, 198, pp. 44–50.
17. Leyland A., Matthews A.: On the significance of the H/E ratio in wear control: a nanocomposite coating approach to optimised tribological behavior. *Wear*, 2000, 246, pp. 1–11.
18. Ezirmik V., Senel E., Kazmanli K., Erdemir A., Ürgen M.: Effect of copper addition on the temperature dependent reciprocating wear behaviour of CrN coatings. *Surf. Coat. Technol.*, 2007, 202, pp. 866–870.
19. Bhushan B., Lowry J.A.: Friction and wear studies of various head materials and magnetic tapes in a linear mode accelerated test using a new nanoscratch wear measurement technique. *Wear*, 1995, 190, pp. 1–15.
20. Polcar T., Parreira N.M.G., Novák R.: Friction and wear behaviour of CrN coating at temperatures up to 500 ˚C. *Surf. Coat. Technol.*, 2007, 201, pp. 5228–5235.
21. Zhou F., Chen K., Wang M., Xu X., Meng H., Yu M., Dai Z.: Friction and wear properties of CrN coatings sliding against Si3N4 balls in water and air. *Wear*, 2008, 265, pp. 1029–1037.

**Sylwia SOWA*, Daniel PAĆKO, Adam MAZURKIEWICZ,
Joanna KACPRZYŃSKA-GOŁACKA, Jerzy SMOLIK**
Łukasiewicz Research Network – Institute for Sustainable Technologies, Radom, Poland
* Corresponding author: sylwia.sowa@itee.radom.pl

A STUDY ON EROSIVE WEAR RESISTANCE OF DIFFERENT MULTILAYER COATINGS TYPES Cr/CrN/(CrN-Me_1Me_2N)$_{MULTINANO}$/(Me_1Me_2N-VN)$_{MULTINANO}$

Key words: multilayer coatings, erosive wear resistance.

Abstract: In the article, the authors present the results of erosion tests of five different material solutions of surface engineering, i.e. multilayer coatings type Cr/CrN/(CrN-Me_1Me_2N)$_{multinano}$/(Me_1Me_2N-VN)$_{multinano}$, where metals Me_1 and Me_2 were chosen from Al, Cr, Ti, Zr and Si. Multilayer coatings used for testing were deposited by the Arc Evaporation method. The research methods presented in the article focused on the analysis of surface topography of the multilayer coatings after erosion test. The erosive wear resistance of tested coatings was carried out by the modern research equipment designed and produced by Łukasiewicz Research Network- Institute for Sustainable Technologies in Radom. The erosive craters were analysed by using the interference microscope Talysurf CCI by Taylor Hobson. The chemical composition of the craters were analysed by using a Scanning Electron Microscope – SEM (Hitachi TM3000).

Badanie odporności na zużycie erozyjne różnych powłok wielowarstwowych typu Cr/CrN/(CrN-Me_1Me_2N)$_{multinano}$/(Me_1Me_2N-VN)$_{multinano}$

Słowa kluczowe: powłoki wielowarstwowe, odporność na zużycie erozyjne.

Streszczenie: W artykule autorzy zaprezentowali wyniki badań odporności na zużycie erozyjne dla pięciu różnych rozwiązań materiałowych typu powłoka wielowarstwowa Cr/CrN/(CrN-Me_1Me_2N)$_{multinano}$/(Me_1Me_2N-VN)$_{multinano}$, gdzie metale Me_1 and Me_2 wybrano spośród Al, Cr, Ti, Zr i Si. Powłoki wielowarstwowe wykorzystane do badań wykonano metodą Arc Evaporation. Metody badawcze przedstawione w artykule koncentrowały się na analizie topografii powierzchni powłok wielowarstwowych po testach erozyjnych. Badanie odporności na zużycie erozyjne wykonano przy zastosowaniu nowoczesnego urządzenia do badania erozji zaprojektowanego przez Sieć Badawczą Łukasiewicz – Instytut Technologii Eksploatacji w Radomiu. Kratery erozyjne zbadano przy zastosowaniu mikroskopu interferometrycznego Talysurf CCI firmy Taylor Hobson. Skład chemiczny powstałych kraterów zbadano przy zastosowaniu Skaningowego Mikroskopu Elektronowego – SEM (Hitachi TM3000).

Introduction

Multilayer coating create many possibilities for shaping the functional properties of machine elements and tools in many industries area. Their complex structure allows one to give several functional properties at the same time. These coatings, through the possibility of shaping the properties of individual component layers, are characterized by good resistance to complex mechanisms of destruction including the simultaneous action of several destructive factors. Erosion wear is this type of a complex mechanism of destruction. It is known from the literature that erosive wear is caused by the impact of solid or liquid particles on the surface of the object causing the following wear mechanisms [1-4]: micro-cutting, grooving, cracking and chipping of the material, fatigue wear, chemical and electrochemical reactions causing creating products of these reactions and their mechanical removal. Due to the complex mechanism of destruction, multilayer coatings seem to be the best material solution that can counteract these phenomena.

The authors proposed a certain material solution to improve erosive wear resistance. The proposed PVD coating includes three zones [5], where each zone has different properties (Fig. 1). Zone 1 is the Cr/CrN complex located directly on the tool surface, providing the required adhesion to the substrate. Zone 2 is a nano-multilayered coating CrN-Me_1Me_2N$_{multinano}$, which is a transition zone between the "adhesive complex,"

and Zone 3 is responsible for cooperation with the external material. In the coating CrN-Me_1Me_2N$_{multinano}$, where Me_1 and Me_2 are metals which are components of the nano-multilayer coating in Zone 3. In the case of the designed multilayer coating, Zone 3 consists of alternately applied layers of Me_1Me_2N and VN, with nanometric thicknesses, where Me_1, $Me_2 \approx$ Al, Cr, Ti, Zr, Si.
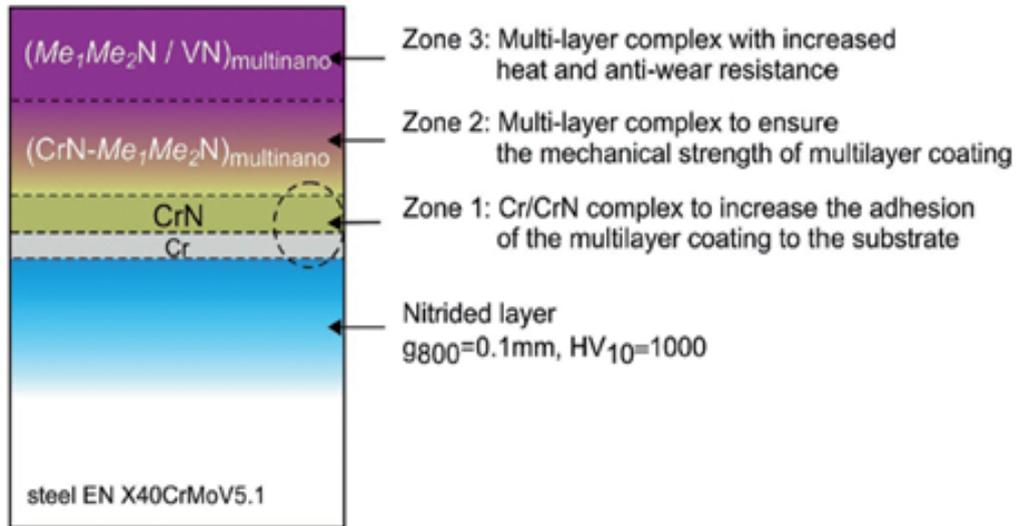
Fig.1. Scheme of multilayer coatings selected for testing [5]

The authors developed an extensive methodology of testing the properties of erosive wear resistance and conducted an analysis of how the chemical composition of the component layers in a multilayer coating can influence wear resistance.

A detailed description about composition of the multilayer coatings and their preparation method was presented in the publication [5].

1. Methodology

The samples were prepared for the research on nitrided steel ENX40CrMoV5.1 (nitride layer: HV10=1000-1100 HV, gHV800 $\approx$0.07mm), according to

the Fig. 1. Multilayer coatings for testing were deposited by the Arc Evaporation method using the a MZ383 technological device produced by Metaplas Ionon in accordance with the parameters shown in Table 1.

Table 1. Parameters of PVD treatment

Component layer of multilayer coatings	Pressure in the chamber p_k [mbar]	U_{BIAS} [V]	I_z [A]	Temperature T [°C]	Time t [min.]
Cr- CrN / (CrN-CrAlN)$_{multinano}$ /	5.0×10^{-3} 3.5×10^{-2} 3.5×10^{-2}	-50 -150 -150	3x55 (Cr) 3x55 (Cr) 2x55 (Cr) 2x55 (CrAl)	T_k=400	10 22 30
(CrAlN-VN)$_{multinano}$	3.5×10^{-2}	-150	2x55 (CrAl) 2x55 (V)		54
Cr- CrN / (CrN-TiAlN)$_{multinano}$ /	5.0×10^{-3} 3.5×10^{-2} 4.0×10^{-2}	-50 -150 -150	3x55 (Cr) 3x55 (Cr) 2x55 (Cr) 2x55 (TiAl)	T_k=400	10 22 35
(TiAlN-VN)$_{multinano}$	4.0×10^{-2}	-100	2x55 (TiAl) 2x55 (V)		57

Cr -CrN / (CrN-TiZrN)multinano / (TiZrN-VN)multinano	5.0×10^{-3} 3.5×10^{-2} 3.5×10^{-2} 3.5×10^{-2}	50 -150 -150 -150	3x55 (Cr) 3x55 (Cr) 2x55 (Cr) 2x55 (TiZr) 2x55 (TiZr) 2x55 (V)	T_k=400	10 22 35 47
Cr -CrN / (CrN-CrSiN)multinano / (CrSiN-VN)multinano	5.0×10^{-3} 3.5×10^{-2} 3.5×10^{-2} 3.5×10	50 -150 -150 -150	3x55 (Cr) 3x55 (Cr) 2x55 (Cr) 2x55 (CrSi) 2x55 (CrSi) 2x55 (V)	T_k=400	10 22 24 40
Cr -CrN / (CrN-VN)multinano	5.0×10^{-3} 3.5×10^{-2} 3.5×10^{-2}	-50 -150 -150	3x55 (Cr) 3x55 (Cr) 2x55 (Cr) 2x55 (V)	Tk=400	10 63 51

In all cases, the total thicknesses of the deposited coatings were similar and were in the range of 3.1 to 3.7 µm (Table 2). The basic mechanical properties of the obtained multilayer coatings are presented in Table 2 [5].

Table 2. The basic mechanical properties of five multilayer coatings selected for erosion tests [5]

Multilayer coatings	Thickness of coating [µm]	Hardness of the coating H [GPa]	Young Modulus E [GPa]	Resistance to elastic deformation H/E	Resistance to plastic deformation H³/E²
Cr-CrN / (CrN-CrAlN)multinano / (CrAlN-VN)multinano (P1.5)	3.5	25.4 ± 1.2	373 ± 28	0.068	0.117
Cr-CrN / (CrN-TiAlN)multinano / (TiAlN-VN)multinano (P2.5)	3.4	25.6 ± 1.4	400 ± 37	0.064	0.105
Cr-CrN / (CrN-TiZrN)multinano / (TiZrN-VN)multinano (P3.5)	3.7	24.9 ± 1.7	353 ± 16	0.071	0.124
Cr-CrN / (CrN-CrSiN)multinano / (CrSiN-VN)multinano (P4.5)	3.1	23.2 ± 1.5	333 ± 20	0.070	0.113
Cr-CrN / (CrN-VN)multinano (P5.5)	3.7	21.8 ± 1.6	327 ± 21	0.067	0.097

The erosive wear resistance tests were carried out in dust erosion conditions using a technological device designed and manufactured by Łukasiewicz Research Network – National Research Institute in Radom presented in Fig. 2. The authors described the precise construction and methodology of the device in the publication [6].

The detailed parameters were selected in accordance with the procedure described in standard ASTM G76-07, which is applicable to the study of erosion. Three steps of preparation were necessary to obtain repeatability and were carried out before proceeding with erosion tests. They are as follows:

1. Heating the abrasive particles Al_2O_3.
2. Heating of channels, that are responsible for mobilising the abrasive materials. (Stabilization of temperature in laboratory room).
3. Test of the repeatability the flow of abrasive flow.

Table 3 presents the parameters of the erosion test for five multilayer coatings.

Table 3. Parameters of erosion tests.

Parameters of erosion tests	Unit	Value
Velocity of the abrasive particles Al_2O_3	[m/s]	70
The angle of incidence of abrasive particles	[°]	40
The flow of abrasive particles	[g/min]	2
Time of the singe test	[min]	10
Temperature of test	[°C]	22
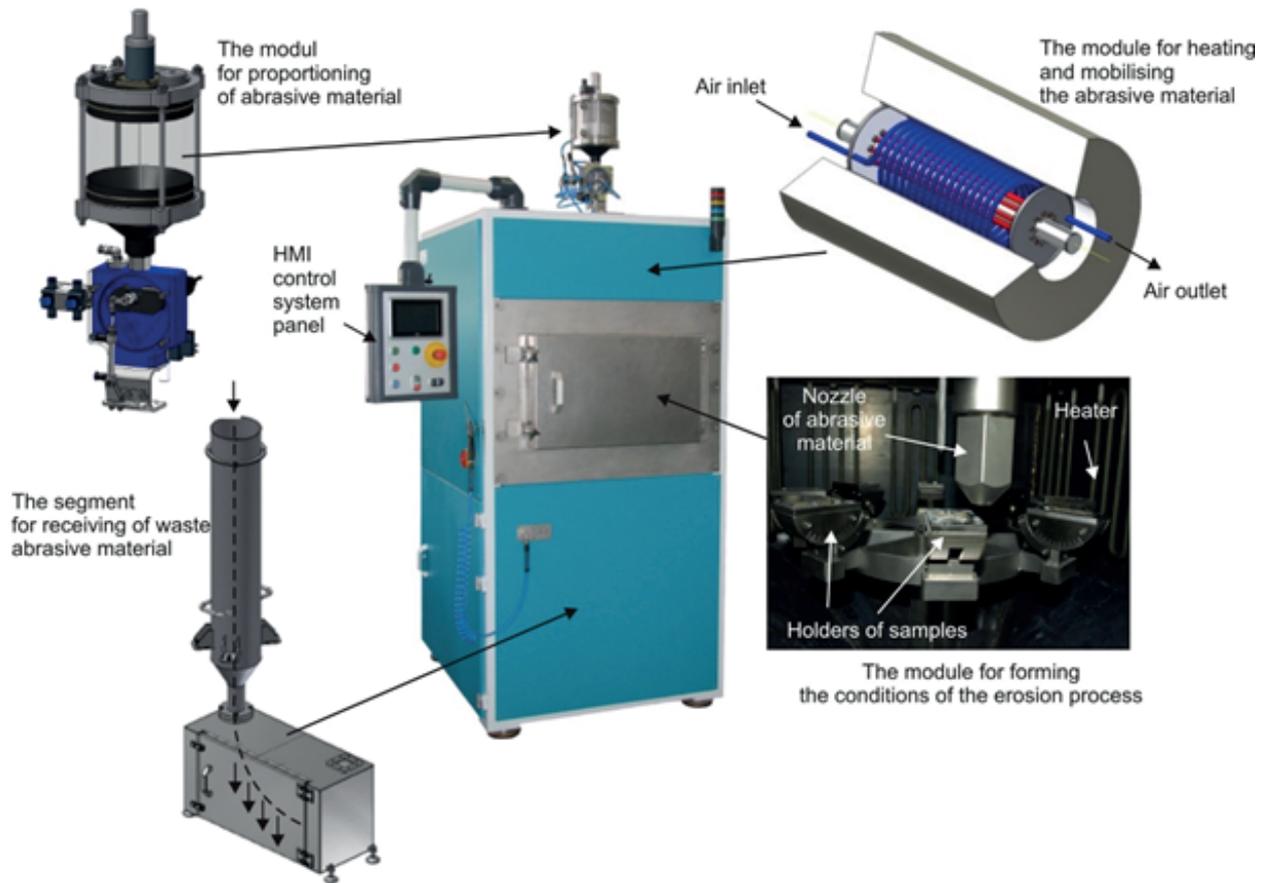
Fig. 2. The universal test equipment to carry out erosion tests

For each of the five multilayer coatings, three erosion tests were carried out. Before the next test cycle, the flow of abrasive particles was checked. The images of samples with marked craters formed after erosion tests and the direction of the abrasive particles are shown in Figure 3.
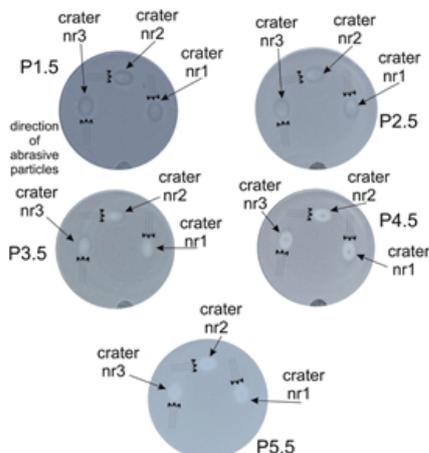
Fig. 3. Samples with craters which were formed after erosion tests

The obtained erosive craters were scanned using an interference microscope Talysurf CCI made by Taylor Hobson, which allows one to shape measurements by optical method with magnification 2.5 The craters analyses were performed by Mountains Map Universal 7.4.8737 program with possibility of 2D (profile) and 3D (topography) images. Based on the received results, the authors calculated the maximum depth and volume of the craters.

The analyses of the erosive mechanisms in tested multilayer coatings were made using the Scanning Electron Microscope – SEM (Hitachi TM3000) with the accelerating voltage of 15 kV. The quantitative analysis of the chemical composition and surface analysis of the chemical composition were performed in 3 selected places: on the surface outside the erosive crater, within ¼ of the resulting erosive crater, and within ½ of the resulting erosive crater as shown in Fig. 4.
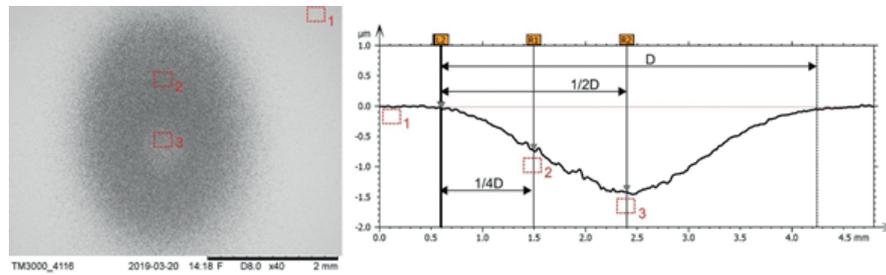
Fig. 4. Scheme of selected crater formed after erosion tests

2. Results and discussion

The results of erosive tests are presented in Figures 5 and 6. Figure 5 presents an analysis of erosive craters to assess their depth and surface. In the case of the two tested coatings, i.e., Cr-CrN/(CrN-CrSiN)$_{multinano}$/(CrSiN-VN)$_{multinano}$ (P 4.5) and Cr-CrN/(CrN-VN)$_{multinano}$ (P5.5), one can observe the formation of craters with much greater depth (approx. 1.5 μm) compared to other coatings. Within these craters is also visible a rough and heterogeneous surface, which indicates damage to the coating due to material chipping during erosion test. The craters formed on the remaining samples were characterized by a much smoother surface and much smaller depth (in the range of 0.5 to 1 μm), which proves their better resistance to abrasive particles.
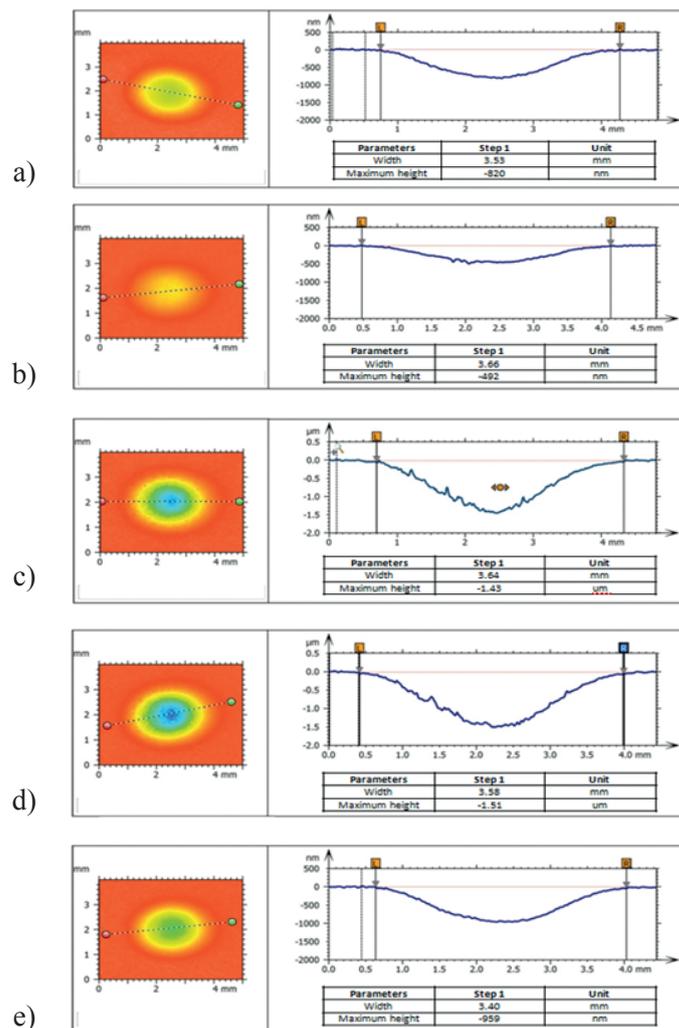
Fig. 5. Profile formed from the intersection of the erosive craters as a result of the erosive wear resistance test for coatings:
a) Cr-CrN/(CrN-CrAlN)$_{multinano}$/(CrAlN-VN)$_{multinano}$ (P1.5), b) Cr-CrN/(CrN-TiAlN)$_{multinano}$/(TiAlN-VN)$_{multinano}$ (P2.5);
c) Cr-CrN/(CrN-TiZrN)$_{multinano}$/(TiZrN-VN)$_{multinano}$ (P3.5); d) Cr-CrN/(CrN-CrSiN)$_{multiano}$/(CrSiN-VN)$_{multinano}$ (P4.5);
e) Cr-CrN/(CrN-VN)$_{multiano}$ (P5.5)

Analysis of the chemical composition of the erosive craters surface showed the presence of Al_2O_3 particles originating from the erosive stream, in all tested coatings. The presence of these particles indicates the fatigue wear of the material and its plastic deformation. In the case of coatings Cr-CrN/(CrN-CrSiN)$_{multinano}$/(CrSiN-VN)$_{multinano}$ (P 4.5) and Cr-CrN/(CrN-VN)$_{multinano}$ (P 5.5), one can observe a much higher density of these particles in the crater area. This indicates a lower fatigue resistance of these materials compared to other coatings.

Similar results were also shown by the analysis of the volume of formed craters. In the case of two coatings i.e., Cr-CrN/(CrN-CrSiN)$_{multinano}$/(CrSiN-VN)$_{multinano}$ (P 4.5) and Cr-CrN/(CrN-VN)$_{multinano}$ (P5.5), a significantly larger volume of removed material (4.06E -03 ± 4.90E-04 mm^3) in comparison with other coatings was noted. The coating Cr-CrN/(CrN-TiZrN)$_{multinano}$/(TiZrN-VN)$_{multinano}$ (P3.5) was characterized by the smallest volume of formed craters (1.27E-03 ± 9.09E-05 mm^3) and the best erosion resistance.
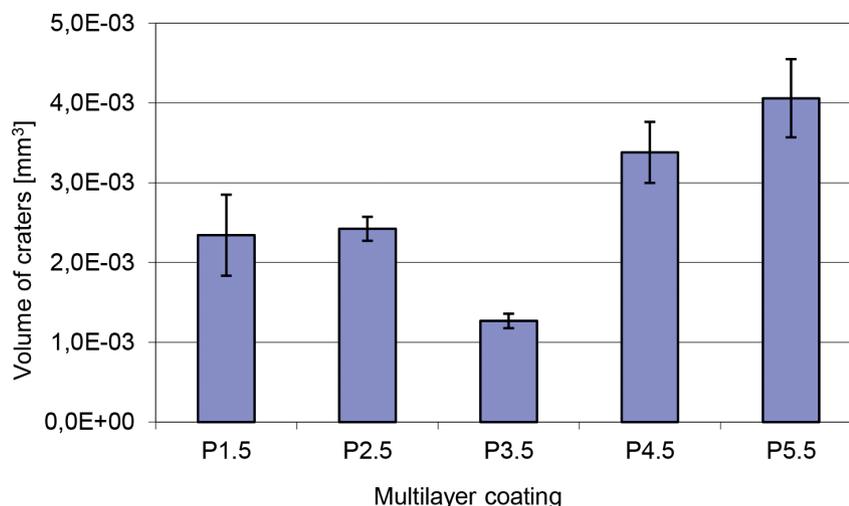
Fig. 6. The results of volume of erosive craters for the tested multilayer coatings

Conclusion

The analysis of the performed tests clearly showed that the coating Cr-CrN/(CrN-TiZrN)$_{multinano}$/(TiZrN-VN)$_{multinano}$ (P 3.5) was characterized by the best resistance to plastic deformation ($H^3/E^2 = 0.124$) and also exhibits the best erosive wear resistance. The research showed that the coatings characterized by the worst erosive wear resistance among the analysed samples were Cr-CrN/(CrN-CrSiN)$_{multinano}$/(CrSiN-VN)$_{multinano}$ (P 4.5) and Cr-CrN/(CrN-VN)$_{multinano}$ (P 5.5). The craters formed as a result of the erosion tests of these coatings were characterized by the greatest depth, rough surface and the presence of a large amount of abrasive particles. It was confirmed that the dominant mechanism of wear material in the erosion process was intensive plastic deformation and fatigue wear. The low fatigue resistance of these coatings is associated with the low hardness (H4.5 = 23.2 ± 1.5 H5.5 = 21.8 ± 1.6) and the Young's modulus (E4.5 = 333 ± 20, E5.5 = 327 ± 21) of these materials.

Acknowledgements

References

1. Kula P.: *Inżynieria warstwy wierzchniej.* Wydawnictwo Politechniki Łódzkiej, 2000 [in Polish].

2. Bitter J.G.: A study of erosion phenomena – Part I. *Wear,* 1963, 6(1), pp. 5–21.

3. Blicharski M.: *Inżynieria Powierzchni.* Warszawa: Wydawnictwo Naukowo-Techniczne, 2009 [in Polish].

4. Stachowiak G.W., Batchelor A.W.: *Engineering Tribology.* 2nd ed. Butterworth-Heinemann, 2001.

5. Smolik J., Mazurkiewicz A., Bujak J., Paćko D., Rogal Ł.: Analysis of fatigue strength of multi-layer coatings type Cr/CrN/(CrN-*Me1Me2*N)$_{multinano}$/(*Me1Me2*N-VN)$_{multinano}$. *Journal of Machine Construction and Maintenance*, 2019, 114, pp. 31–38.

6. Mazurkiewicz A., Smolik J., Mizak W., Mężyk J., Paćko D.: Universal research instrumentation for erosion tests. *Solid State Phenomena,* 2015, 237, pp. 21–26.

Matthew GUTOWSKI[a],*, Blair KUYS[a], Sheng LI[b]
[a] Swinburne University of Technology, Melbourne, Australia
[b] CSIRO Manufacturing Flagship, Melbourne, Australia
* Corresponding author: mgutowski@swin.edu.au

MODULAR DESIGN & CONSTRUCTION IN AUTOMOTIVE AND BUILDING STRUCTURES: ELIMINATING 'SHOW-STOPPERS' IN THE USE OF WOOD-BASED FAÇADE CLADDING

Key words: products modularisation, automotive industry, building & construction, residential and commercial building, façade cladding, wood products, paints, clear coatings, paint durability, wood durability.

Abstract: The key demands on manufacturers in the modern-age markets globalisation are: (i) short development cycle, (ii) cost effectiveness, (iii) excellent product quality, and (iv) in-built product variability and upgradability. Development of new products under such dynamic market conditions necessitates an integrated approach to all stages of company operations, including product design, prototyping, productionising and manufacturing and extending it to the lifetime serviceability. Such competitive requirements cannot be dealt with by conventional, sequential model of product development and require switching to the modular approach, which additionally enables effective accommodation of growing needs of customers for products variety and their immediate or future customisation.

This paper addresses modular product development, including design and assembly in application to building & construction industry. The focus is on paving the path for new generation high-quality/high durability products, such as modular cladding components for low- and high-rise residential and commercial buildings with the emphasis on product sustainability and long-lasting aesthetics. It also considers: (i) identification of principal causes of diminishing market share of wood-based cladding of building facades, and (ii) highlights key aspects of development of a breakthrough technology providing high-quality, high-durability surface finish of painted exterior wood products offering a platform for reversal of decades-long decline of this important segment of the building products market.

Modułowa konstrukcja w przemyśle motoryzacyjnym i budowlanym: eliminowanie systemowych wad użytkowych w zastosowaniu do fasad na bazie materiału drewnopodobnego

Słowa kluczowe: modularyzacja produktów, przemysł motoryzacyjny, budownictwo, budownictwo mieszkaniowe i handlowe, okładziny elewacyjne, produkty z drewna, farby, powłoki przezroczyste, trwałość farby, trwałość drewna.

Streszczenie: Kluczowe wymagania stawiane producentom na współczesnych zglobalizowanych rynkach to: (i) krótki cykl rozwoju, (ii) efektywność kosztowa, (iii) doskonała jakość produktu, oraz (iv) „wbudowana" zmienialność produktu i możliwość jego rozbudowy. Rozwój nowych produktów w tak dynamicznych warunkach rynkowych wymaga zintegrowanego podejścia do wszystkich etapów działalności firmy, w tym również projektowania produktu, prototypowania, produkcji, oraz rozszerzenia ww. również na okres użytkowania. Tak wysokie wymagania nie mogą być osiągnięte przez konwencjonalny, sekwencyjny model opracowania produktu i wymagają przejścia na podejście modułowe, co dodatkowo umożliwia efektywne dostosowanie rosnących potrzeb klientów do różnorodności produktów i ich natychmiastowej lub przyszłej personalizacji.

Artykuł ten dotyczy rozwoju produktów modułowych, w tym projektowania i montażu w zastosowaniach w przemyśle samochodowym, budownictwie i przemyśle budowlanym. Nacisk kładziony jest na wytyczenie drogi dla produktów nowej generacji o wysokiej jakości/wysokiej trwałości, takich jak modułowe elementy fasad dla niskich i wysokich budynków mieszkalnych i komercyjnych z naciskiem na trwałość produktu i długotrwałą estetykę. Artykuł rozważa również: (i) identyfikację głównych przyczyn zmniejszającego się udziału rynkowego drewnopodobnych elewacji budynków oraz (ii) podkreśla kluczowe aspekty rozwoju przełomowej technologii zapewniającej wysoką jakość wykończenia powierzchni o wysokiej trwałości dla produktów z drewna, oferującej doskonałą platformę do odwrócenia trwającego od dziesięcioleci spadku udziału tego ważnego segmentu rynku wyrobów budowlanych.

Introduction

To deal with customer-driven demands for product customisation manufacturers operating in the current market globalisation need to achieve: (i) short development cycle, (ii) cost effectiveness, (iii) excellent product quality, and (iv) in-built product variability and upgradability. Development of new products under such dynamic market conditions necessitates an integrated approach to all stages of company operations, including product design, prototyping, productionising and manufacture, and extending it to the lifetime serviceability.

The company's ability of to quickly respond to, and exploit rapid changes in technologies, market trends and variable customer preferences is an essential attribute of all winners in commercial markets, who recognise the strategic value of leveraging their capabilities, knowledge re *'know-how', 'know-why', 'know-what'* and *'know-who',* and restructured their processes into a multi-levelled "modularisation" of all operations. The principal means for this are:

Product modularisation: achieved through sub-division of the entire system into principal system platforms and independent functional or stylistic modules enabling identification of components which are: (i) common to an entire family of products, and (ii) those which facilitate product re-configuration and stylings. The latter are easily integrated into the final structure by mounting onto the principal system platform through interfaces facilitating rapid assembly and disassembly of the product,

Fixed asset parsimony approach: achieved by creating flexible 'modular business structures' through recognising that while focusing on core competency, the following issues become imperative: (i) strategic capabilities and resources in dynamic market conditions require 'structural flexibility' of entire business operations, (ii) rapid response to customer needs and variable market trends necessitates development of flexible intellectual assets, and (iii) companies cannot grow internally on short notice, necessitating the following →

Development of alliances and virtual R&D laboratories: achieved by interconnecting with other manufacturing and research establishments possessing complementary capabilities and various forms of intellectual property facilitating rapid creation of new products through outsourcing and utilising positive synergies instead of relying on own 'inflexible' capabilities and entering direct competition.

The overall structure of product family establishment process, as summarised by Jiao et. al in [1] is schematically illustrated in Figure 1.
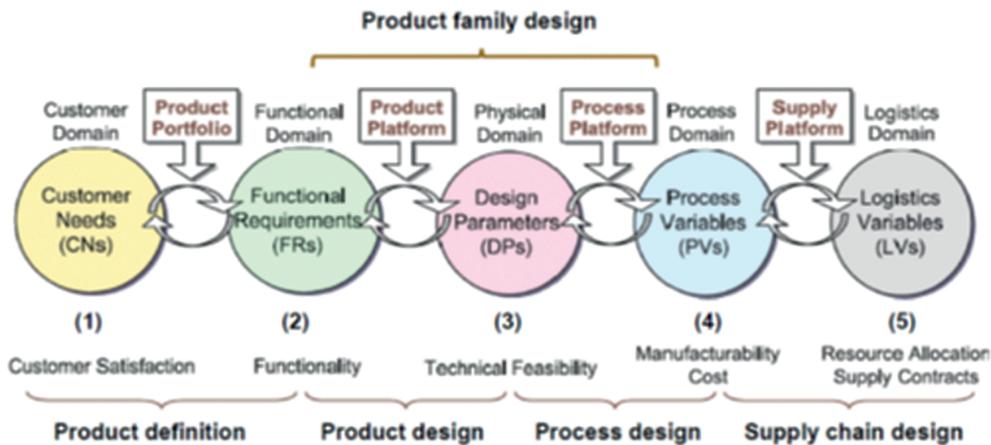
Fig. 1. **Schematic structure of product family establishment over the whole spectrum of issues associated with new product development and realisation: (1) customer needs, CNs, considering also market segmentation. These are analysed by designers from the viewpoint of engineering needs and concerns from the perspective of technologies available for the product realisation; (2) Functional requirements, FRs, involving translation of these into a set of key design parameters, DPs, which must satisfy the needs of the shared product platform, (3) Establishment of design parameters, DPs, from the viewpoint of satisfying the requirements of product functionality; (4) and (5), Logistics-related domains – Process variable, PV, are established by translating DPs (Design Parameters) with the aim of generating overall production planning involving utilisation of existing company process capabilities (logistics of repetitive use of machines, tools, rigs, etc, and routing) essential for configuring production process in the manner facilitating manufacture and assembly of variable versions of products within the same product family (adopted from Jiao et.al [1]**

Modular design and assembly are based on logical subdivision of products into smaller functional or decorative sub-units or building blocks which function, after their assembly, as integrated sets [3]. To achieve product functionality and upgradability, individual modules need to be inter-connected by appropriate interfaces, whose choice depends on the functional and stylistic complexity of the system [1]. Compatibility of modules is ascertained by "design rules" governing: (1) establishing the desirable product architecture and interfaces facilitating connectivity

and 'communication' between modules, (2) product architecture allowing flexible assembly, decomposition, standardization and exchangeability of modules [2], and (3) standardised tests of the system to ascertain the following: (i) designated performance of each module, and (ii) appropriate interaction of modules assembled into a system. Where needed, interfaces facilitate communication between inter-connected product sub-systems [3].

Appropriately designed modular architecture sub-divides the product into individual modules which can be readily re-arranged into desired configurations in the form of product variants. Individual modules in their original form, or re-styled modules can be assembled and dismantled 'on-demand' and replaced by new or alternative modules, thus facilitating availability of a *'morphing'* real or virtual product.

Individual components (modules) can be independently manufactured in various industrial manufacturing facilities as standardised, high quality and completely finished items which are transported to an assembly plant or construction site to be rapidly assembled into a designated structure.

Due to modular structures adaptability, some product categories: cars, aircraft, ships, buildings, weapons or infrastructure elements can be easily expanded, reduced or changed by adding or removing individual moduls without altering the principal platform structure, e.g. that of a vehicle or building. Such process facilitates easy change in appearance, functionality, and renovations depending on varying demands re product performance or longevity (e.g.: easy replacement of originally installed, but service-damaged or aged materials or surface finishes), or their architectural style and appeal requirements [3]. In this way new product families can be formed or extended using either: the initial, re-styled or newly developed modules without increasing the product complexity and manufacturing costs.

Overall, modularity facilitates easy generation of alternative product lines by utilising the original principal platform design which allows assembly of alternative modules exhibiting either, the originally designated or new functional and stylistic features of

the product in response to changing needs and desires of customers.

Through adoption of modularisation, the pivotal structure elements such as automotive framing systems or high-rise building's curtain wall framing and cladding can be quickly and cost effectively designed, re-designed when needed (for instance for re-styling or refurbishing) and cost-effectively reconfigured through assembly of a variety of re-designed or newly designed/developed sub-systems onto the principal system platform.

1. Modularity in Automotive Industry

Automotive OEMs (Original Equipment Manufacturers) vigorously pursue the concept of modular design and platform sharing to minimise their development and production costs due to the fact that the platform development costs account to approximately 50% of overall costs of a new model launch.

According to Dahmus et al [4] in 2001 alone Volkswagen saved $1.7 billion on development and production costs through developing effective product architecture and being able to share the platform and component commonality between its major brands: VW, Audi, Skoda, and Seat [5]. These included: front axles, rear axles, front ends, rear ends, exhaust systems, brake systems, and numerous other elements. Due to this Volkswagen was able to claim that all vehicles on this shared common platform are effectively differentiated in the eyes of customers.

The key structural component ascertaining structural integrity and stiffness of the vehicle is the under-body (see Figure 2) which forms the principal vehicle platform allowing integration of all vital car components, e.g. engine, transmission and suspension [5]. Any change to the shape of the under-body will affect all surrounding, interconnected components. Thus, as illustrated in Figure 2a, it limits the development of alternative designs, typically limiting production to a single vehicle variant manufactured at a dedicated assembly line due to its inherently inflexible architecture.
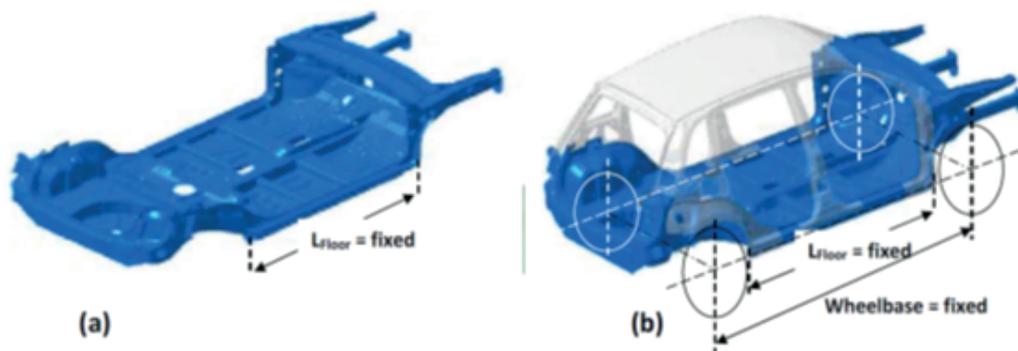
Fig. 2. a) Integral design of under-body assembly, and b) Body-in-White (BiW) with integral under-body (partially adopted from [6]

Any attempt to change the above type of platform is prohibitively costly, necessitating inefficient redesign requiring changes and additions to the existing inflexible manufacturing and assembly process.

Due to the above limitations, integral under-body systems are increasingly replaced by modular structures illustrated in Figure 3, which typically comprise the following modules: (i) The main floor (MF), (ii) Front-end module (FEM), (iii) Rear-end module (REM) and (iv) Motor (Engine) compartment (MC/EC).

The principles of modular approach to car design and assembly facilitating flexible configuration of alternative vehicle variants based on selection of appropriate modules are illustrated in Figure 3. The control of length and spatial configuration of individual modules enables fast and cost-effective customisation of vehicles in response to the market and recently, for higher-end vehicle brands, even to individual customer needs.
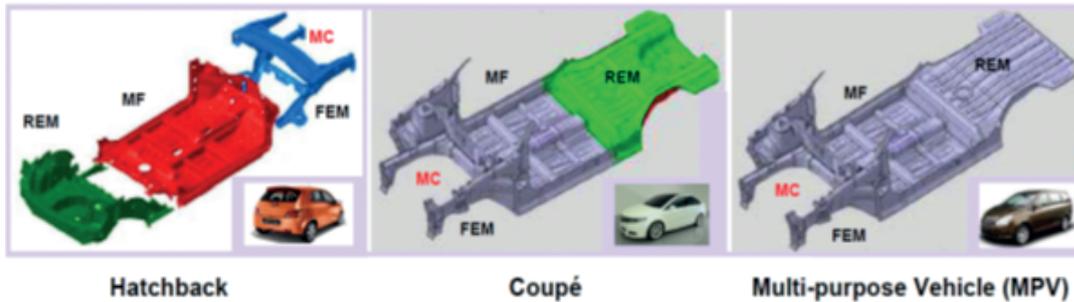
Fig. 3. Schematic illustration of car modular design regarding shared under-body platform common to a range of vehicle variants (Hatchback, Coupé, MPV) comprising flexible modules such as: (i) front-end module (FEM), (ii) motor compartment (MC), (iii) main floor (MF), (iv) rear-end module (REM). Practical examples of modular under-body platform in cars manufactured by Proton: Hatchback (Savvy), Coupé (Persona) and MPV (Exora). Note: under-body outlines adopted from [6] and [7]

The introduction of a variable main floor module facilitates the control of vehicle wheelbase, hence facilitating manufacture of diversified variants of vehicles: hatchback, coupé or multi-purpose vehicle. Additional incorporation of alternative stylised and functional modules of the body cladding or structure enables flexible adjustment of style variety and type of functionality of assembled vehicles, as demonstrated by photos in Figure 4 presenting modular body styling solutions achieved by Nissan in its EXA 1990 vehicles range.

Fig. 4. Flexible control of spatial body architecture and functionality through modular styling approach: Nissan EXA 1990 vehicles range

2. Modularity in Design and Assembly of Building Structures and Façades

2.1 Scope of Modular Concepts in Building Construction

Modular construction is becoming increasingly popular for residential and commercial buildings of up to four to eight storeys high. This mode of construction is carried out at two levels [8]:

1. On-site assembly of prefabricated room-sized volumetric (4-sided) units, and/or
2. On-site installation of fully finished individual panels (external cladding, partition walls, flooring panels, ceilings).

In this construction mode, fully prefabricated units and/or individual walls that are fully fitted out during in-factory

manufacture are installed on site as load-bearing 'building blocks', or their individual non-structural elements, such as wall panels, are installed into the building's structural frame. The current range of applications of modular construction is in cellular-type buildings, such as hotels, student residences, defence accommodation and social housing, where the module size is compatible with manufacturing and transportation requirements.

The primary advantages of modular construction are: (i) economy of scale in manufacturing of multiple repeated units, (ii) speed of on-site installation, and (iii) improved quality and accuracy in manufacture. Modular buildings and their integral sub-components can be potentially dismantled and reused, thereby effectively maintaining their asset value.

Figure 5 schematically illustrates the principles of modular design and construction at the level of complete multi-storey buildings with integrated individual wall panels, including definition of principal modular grids essential in modular design and construction (see an example in Fig. 5a), and 4-sided modular cells with timber cladding on wall panels (see Fig. 5b).

a)   b)
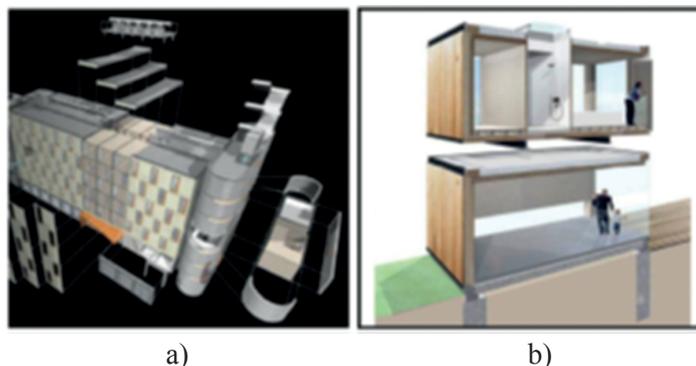
Fig. 5. Schematic illustration of modular design and construction principles: a) complete multi-storey building: adopted from [9], b) Individual modules with timber cladding on wall panels [10]

One of the largest areas of modular design and assembly in the building and construction sector are façades. Current literature in this domain has a focus on outdoor building materials such as aluminium, Alucobond® and Colorbond® to name a few. Very little has been done on timber use in architectural façades as an appearance element exhibiting insufficient longevity characteristics, i.e. suffering from poor durability on exterior exposure (excessive weathering, colour loss, etc).

The most commonly used façade systems utilise curtain walls schematically illustrated in Figure 6, which are widely used as exterior cladding systems in medium and high-rise buildings. They comprise of light-weight, typically aluminium-based framing structures enveloping the entire building. The underlying principal modular grid is based on a lattice configuration comprising mutually interconnected vertical mullions and horizontal transoms. The curtain wall grid is filled in by modular cladding panels utilising glass, metals, composites and thin stone veneers as the main categories of currently used surface finishing architectural materials.

a)   b)   c)
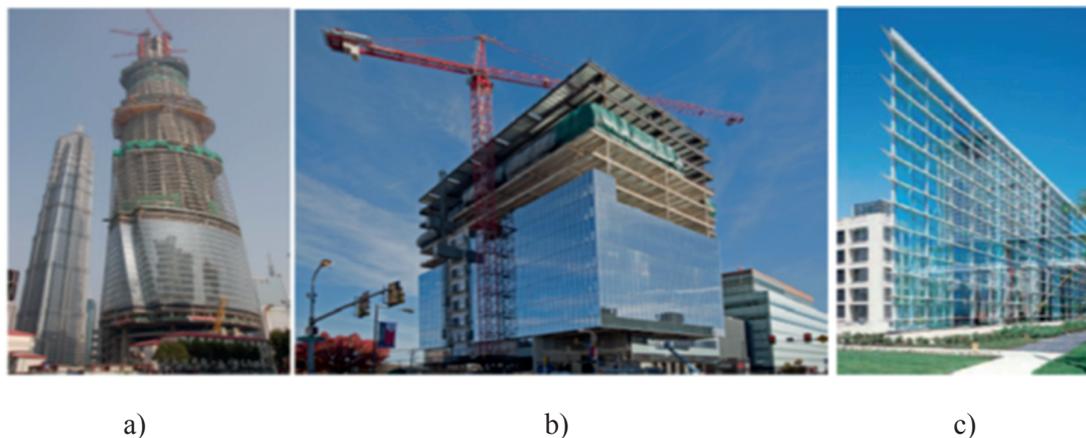
Fig. 6. Construction of curtain walls, architectural systems broadly utilise the principles of modular design, manufacture and on-site assembly: a) Shanghai Tower Curtain Wall (China), b) Science Research Centre, Wausau (Pennsylvania/US), c) Stick System curtain wall Reliance™ manufactured by Oldcastle [11].

As depicted in Figure 6(a) and (b), the curtain wall framing is mechanically attached to the main building structure and hence, does not transfer the floor loads, which are carried by the principal building structure. The only loads carried by curtain wall are those imposed through external wind pressure and cladding weight. These are transferred to the building structure typically at the individual floor levels.

The most commonly used cladding materials are: aluminium, glass, surface-coated metal panels (anodised or powder-coated) and composites including green materials such as Wood-Plastic Composites (WPC), which utilise plastic matrix and cellulose fibres as reinforcing materials. These are attached to the curtain wall framing by: (i) mechanical fixing, or (ii) adhesive bonding, see Figure 7 for details) utilising structural elastomeric adhesives (high-rise building curtain walls), or high-strength self-adhesive tapes (low-level residential or commercial buildings).
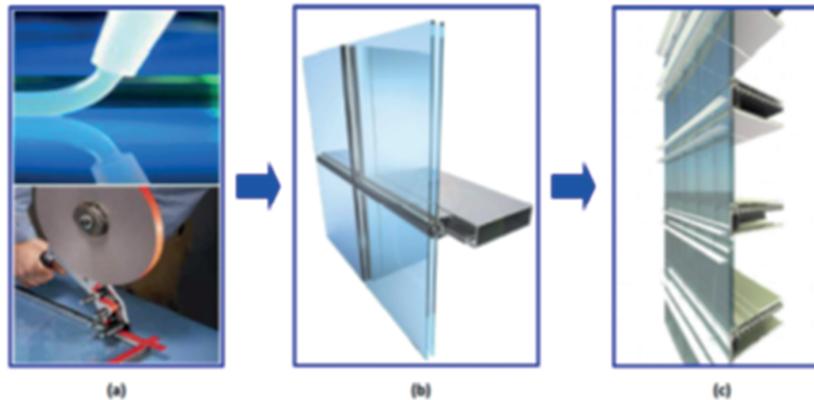
Fig. 7. Details of modular curtain wall manufacture and installation through structural glazing approach utilizing adhesive bonding of vision (glass) or solid decorative cladding panels to the framing system (mechanically attached to the building structural frame at each floor level): a) application of silicone adhesive or high-strength self-adhesive tape to the cladding panel; b) details of attachment of façade modular cladding panels to curtain wall framing by elastomeric adhesive; c) bonded cladding panels assembled in curtain wall system through aluminium framing mechanically fixed to building flooring panels [11]

2.2. Modular Approach in Timber Building Structures and Cladding

Designing and marketing exterior timber structures, including wooden façades presents inherent technical and practical challenges caused by this material's low durability and fast weathering, dimensional changes on external moisture variations, concerns with fire safety and related maintenance costs.

All of the above concerns form a platform for careful analysis of fundamental issues concerning manufacture and marketing of wood-based products family, as outlined and discussed in Figure 1 from the perspective of modularisation targeting construction of residential and commercial timber-based buildings, and in particular: wood-based cladding panels, i.e.

1) Customer needs (CNs) and perception regarding exterior decorative wood products, such as cladding panels, which would be able to have long-lasting (up to 20-30 years) appearance of natural, just-machined natural wood clearly showing wood texture and its natural colour. This issue needs to be analysed by designers from the viewpoint of engineering needs and concerns from the perspective of technologies available for ascertaining practical realisation of such long-lasting/low-maintenance product, and

2) Functional requirements (FRs) involving translation of CNs and FRs into a set of design parameters which must lead to a nearly-100% guaranteed ability of making the product satisfying the needs of the overall product platform in which wood-based façade panels will feature prominently, quickly exposing any potential deficiencies in long-term performance if and when the cladding surface would: (i) become discoloured on exposure to solar radiation, and/or (ii) suffer from undesirable peeling-off of the coating film from the wood surface (see Figure 14c demonstrating severity of these problems).

2.2.1. All-Timber High-Rise Modular Building

The design and construction of a 14-storey timber apartment building (the *'Treet'* Building) in Norway provides an excellent example of effective application of a modular approach to "all-timber" building structure in the building and construction sector [12].

The building, one of the tallest timber buildings in the world consists of load-carrying glulam trusses and two intermediate strengthened floor levels. Prefabricated building modules are stacked on top of the concrete garage and on top of the strengthened levels. Cross-Laminated Timber panels (CLT), which are not a part

of the main load bearing system, are used in the elevator shaft, internal walls and balconies. The structural timber elements: supporting columns, beams and trusses are protected from rain and sun by glass and metal cladding.

Illustrations in Figures 8 and 10 below provide comprehensive details regarding practical application of

modular approach to the design and construction of this building, highlighting a step-by-step assembly process ensuring that the building can be built correctly. As seen in Figure 10, the external cladding and glazing of the building are attached to the load bearing trusses and to the balconies.

Fig. 8.　a) 3-dimensional view of the completed "Treet" building: a 45-meter high building with laminated (Glulam) load-bearing structure, and b) details of Glulam-based building structure [adopted from [12]

The assembly of the "Treet" building involved an on-site installation of prefabricated elements using a tower crane, as well as a climbing scaffolding system during the building erection. Temporary roofs are used to protect apartments, joints and timber from moisture during the building process. All main load-bearing structures in the building are wooden: Glulam is used for the columns and trusses. Cross-laminated timber (CLT)

is used for the elevator shafts, staircases and internal walls. Timber framework is used in the construction of residential modules.

All glulam elements are connected by the use of slotted-in steel plates and dowels (see details in Figure 9). This is a high capacity connection commonly used in bridges and large buildings. Typically, 8 mm steel plates and stainless steel 12 mm dowels are used [12].
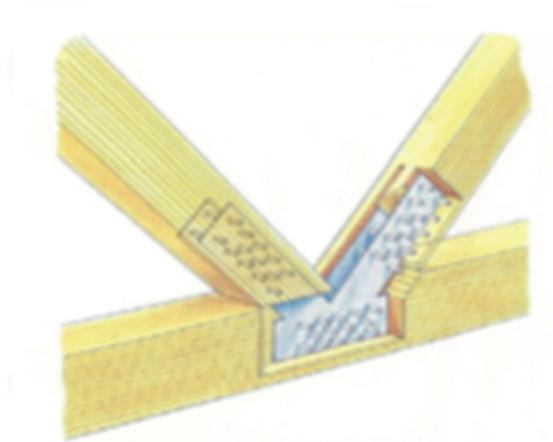
Fig. 9.　Details of slotted-in steel plates connecting all structural beams and columns in the "Treet" building structure [12]
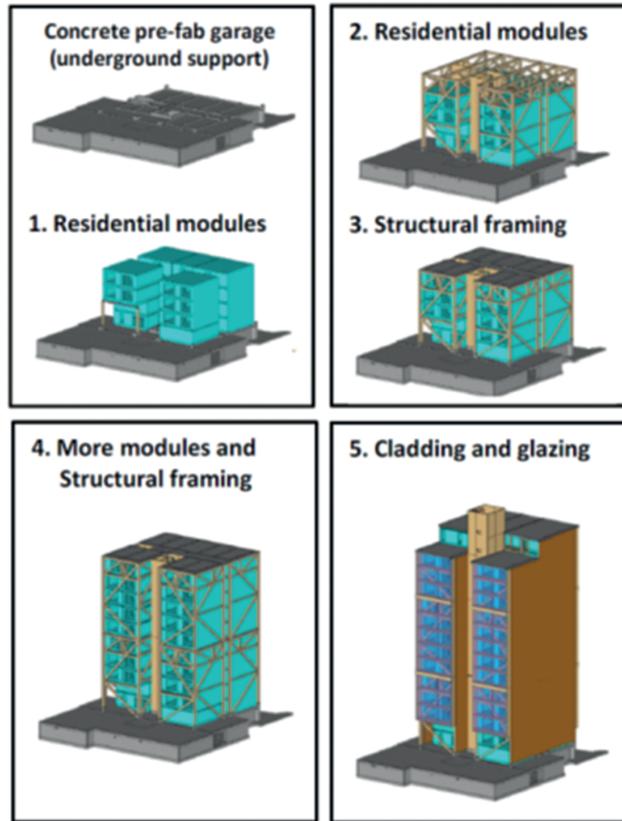
Fig. 10. Schematic visualization of the sequential (step-by-step) assembly of the "Treet" building (adopted from [12]

2.3. Addressing Critical Functional Requirements (FRs): Development of Technology Providing Durable Coatings Adhesion and Retention of Natural Wood Appearance

Issues No. 2(i) and 2(ii) outlined in Section 3.2 lead to rapid decline of market share of wood-based architectural products such as façade cladding, doors, windows and decking to their metallic or plastic equivalents regardless of the fact that these synthetic building materials do not have attributes of wood, such as attractive wood-grain aesthetics; eco-sustainability; excellent thermal insulation; fabrication ease and high strength. Regardless of all these advantageous attributes, while 20–25 years ago wooden products such as windows and doors represented 50% of the total market in Germany, USA and Australia, today's sales are about 25% or less of the overall numbers. Such huge market share loss is due to low durability of wood against low-maintenance substitutes made of metals, plastics and wood-plastic composites (WPCs) which offer up to 20–25 years of maintenance-free service performance.

The key problems with wood products, which have inadvertently lead to the collapse of market for wood as a popular architectural façade material are: (i) rapid surface discoloration and degradation upon solar exposure, and (ii) non-performing wood coating systems which frequently peel off from the painted surface and hence, require high-cost maintenance, i.e. 4–5 year cycles of re-painting.

The outcome of the above analysis and the assessment of current market trends lead to the formulation of key objective for the development of "winner-technology" which would facilitate the reversal of the current decline in the use of wood as an architectural finish material: it is the development of a breakthrough technology [22–26] able to ascertain elimination of paint delamination and facilitating the retention of wood's natural appearance for up to 15–20 years when painted with clear coatings.

2.3.1. Wood as Advanced Nano-Structured Composite Material

As schematically illustrated in Figure 11, wood cells present a characteristic pattern of honeycomb-like hollow micro-tubular structures in which the strong cellulose nano-fibrils act as a high-strength reinforcing material embedded in an amorphous matrix of lignin (see Fig. 11b) performing the role of a bio-based binder responsible for the overall integrity of the wood-based substrate.

The multi-layered cell walls comprise cellulose microfibrils angularly 'wound' in three consecutive layers (S_1, S_2 and S_3) distinguished from each other by different angles with respect to the cell axis (cellulose

microfibrillar angle, MFA). These tubular micro-fibrillar structures resemble those of high-strength, wound fibre hollow tubes fabricated from carbon or glass-fibre reinforced polymeric composites. The thickest layer, S2, constituting more than 80% of the wall, has the dominant influence on the wood mechanical properties.
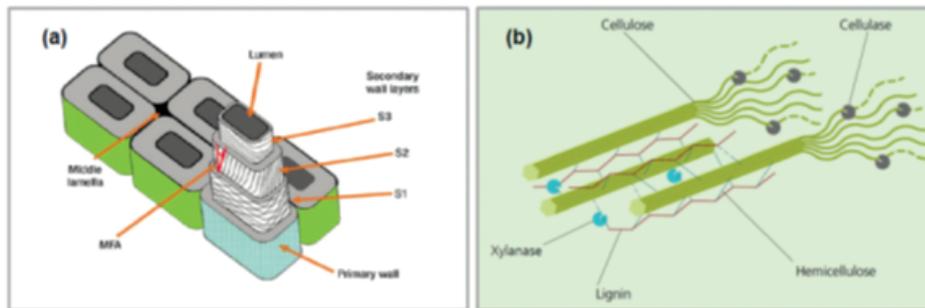
Fig. 11. a) Structure of wood fibres: S_1, S_2 and S_3: the sub-layers of cellulose micro and nano-fibrils resembling the structure of high-strength wound filament hollow profiles (e.g.: pipes) fabricated from carbon or glass-fibre reinforced polymeric composites; *MFA*: the microfibril angle – the angle between the cellulose fibrils and the longitudinal cell axis, which is a critical factor in determining the physical and mechanical properties of wood (adapted from [13]); b) Schematic structure of wood as a biomimetic composite, presenting orientation and interactions of its key constituents in the overall structure of wood cells including cellulose microfibrils, and the role and spatial orientation of polysaccharides and lignin within wood [14].

2.3.2. The Surface Properties of Wood

Wood is a natural composite material in which strong cellulose micro- and nano-fibrils and their aggregates are embedded in an amorphous matrix of lignin performing the role of binder providing the substrate integrity (see Figure 11). Various hydrophilic and hydrophobic extractives are also present in specific tissues of trees, typically not exceeding the level of 5 % in temperate zone woods. They are unattached to the ligno-cellulosic wood matrix. Due to their relatively low molecular weight they exhibit high mobility and gradually migrate to the surface of machined wood components, thus influencing the wood hygroscopic/hydrophobic properties and durability. As schematically illustrated in Figure 12, surface-bound extractives seriously hinder adhesion of wood. The non-polar (lipophilic) extractives such as free and esterified fatty acids and sterols form a weak boundary layer over the surface, which lowers the polarity of substrate thus reducing its wettability by polar adhesives and coatings. This phenomenon has adverse consequences demonstrated through sub-standard adhesion and long-term durability of all adhesives and surface coatings applied to the surface of timber products, particularly those made from hardwoods. Polar (hydrophilic) extractives such as tannins, other phenolic compounds and water-soluble carbohydrates contribute to long-term retention of moisture by wood surface.
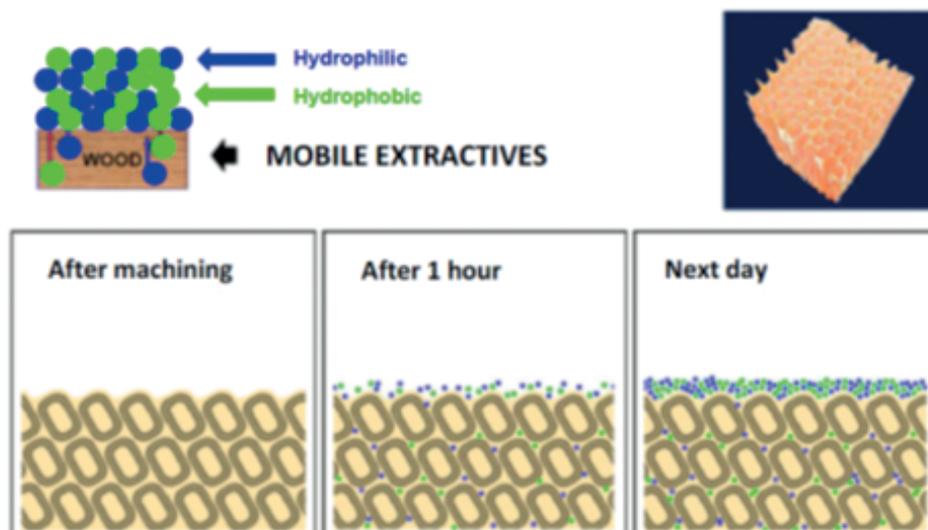
Fig. 12. Schematics of deleterious effect of wood extractives [27] progressively migrating from the bulk of a wood product to the surface (adopted from [15]).

2.3.3. Degradation of Wood Surface by UV and Moisture Exposure

An inherent poor durability of wood on exposure to UV radiation is a consequence of its chemical and morphological structure and properties of its principal polymeric constituents. Figure 13 provides schematic illustration of the uppermost surface of wood substrate subjected to solar radiation.

It is known that the UV and visible radiation penetrates the wood surface to a depth greater than 70μm, resulting in significant reduction of the tensile strength (50–75% loss) to a depth of 70 to 140μ. Experimental evidence shows that the strength changes may occur as far as to the depth of 280μm from the surface [16]. Discoloration of wood, demonstrated by darkening brown tint (see Figure 14a) turning into grey colour on long-term exposed wood occurs at UV radiation wavelengths range of 305–335 nm [16,18] due to the chromophoric centers in lignin (phenolic groups, double bonds, carbonyl groups, quinones, quinonemethides and biphenyls [17]) absorbing the UV light.
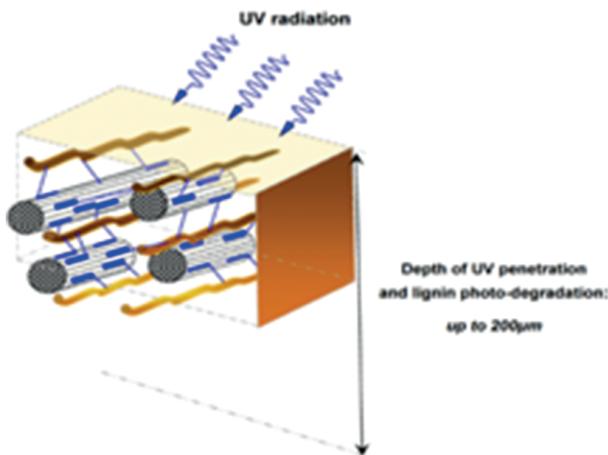
Fig. 13. Schematics of the uppermost surface of wood substrate subjected to solar radiation.

When exposed to the combination of external weather factors such as the UV- and visible light radiation, and the moisture/temperature fluctuations, the wood surface and sub-surface zone (particularly the uppermost zone, down to 85-90μm beneath the wood surface) are subjected to a variety of complex forms of photo-chemical and hydro-thermo-mechanical degradation, i.e:

1. Chain scission and subsequent loss of integrity of lignin acting as a binder within and between principal structural constituents of wood cells (cellulose nano- & micro-fibrills), and gradual discolouration of the lignin's decomposition products,
2. Cyclical water movement in wood cells.

3. Cyclical dimensional movements of the entire 3-dimensional network of wood structure, including the surface. This is stimulated by hydro-thermally controlled cyclic swelling and shrinkage due to moisture sorption/desorption cycles, and diurnal and seasonal temperature fluctuations including regular 24-hour cycles of solar heating. Swelling of wood cells upon moisture sorption additionally enhances light penetration deeper into the wood structure, hence broadening the depth of destructive effectiveness of UV and visible light.
4. Progressive surface checking and erosion leading to gradual displacement and detachment of loosened-up cellulose fibrils and splinters from the wood surface due to the combination of: (i) progressive decomposition of lignin by UV radiation, additionally assisted by the presence of oxygen, (ii) kinetic energy of rain precipitation, (iii) cyclical water movement and hydrothermal swelling-shrinking motion leading to the loss of integrity between friable fragments of wood no longer held by decomposed lignin.

As a consequence of the above mechanisms, for almost all exterior applications, the wood-based products require surface protection and surface-finishing for either: protection against the weather- and biologically-driven degradation, and for decorative and functional purposes. This is typically accomplished by the application of protective clear-coatings facilitating the retention of natural features of wood, e.g. surface colour and wood-grain appearance, or alternatively by solid colour painting, lamination with durable-species veneers, or other types of finishing materials such as decorative paper, plastic or metallic foils, stains, water-repellent materials, and others.

2.3.4. UV Degradation of Lignin: the Principal Cause of Wood Coatings Adhesion Failures

Photos in Figure 14(a) demonstrate progression of surface damage of wood panels apparent through gradually darker (brown) discolouration of their surface due to degradation of chromophoric constituents of lignin upon increased time of exposure to UV radiation [26].

Graphs in Fig. 14(b), in turn, demonstrate detrimental effects of real-time outdoor exposure of unpainted (machined only) wood, western red cedar (*Thuja Plicata*), to solar radiation before painting such pre-exposed uncoated cedar panels, on the resultant adhesion of acrylic latex (Dupont Lucide Wood Primer) and alkyd oil coating (Sherwin Williams AD-Primer); both applied after solar exposure of panels for the periods of 0 to 16 weeks.
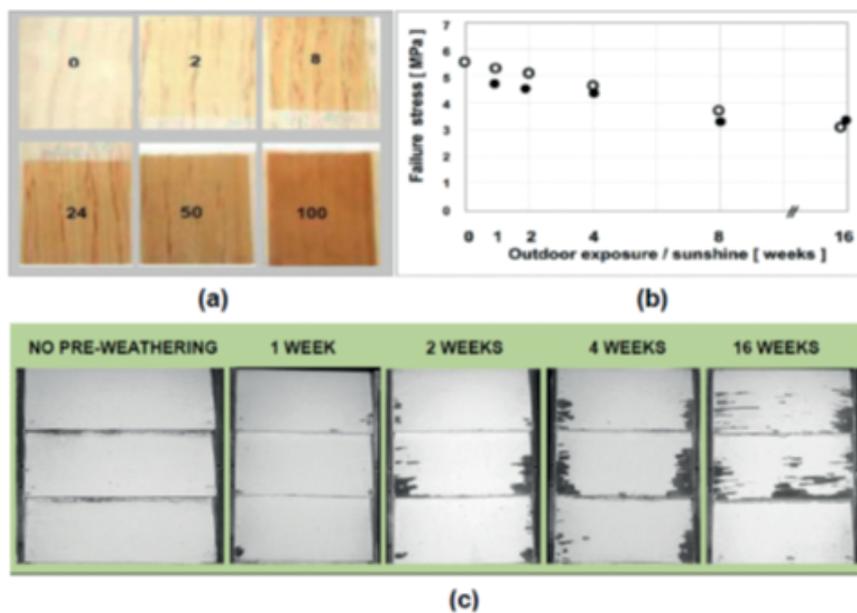
Fig. 14. (a) Progressive discolouration of *Pinus radiata* due to lignin photo-degradation on exposure (hours) to UV-B (303nm) [26]; **(b)** Influence of outdoor exposure to solar radiation of unpainted western red cedar on the adhesion of coatings applied after 1 to 16 weeks weathering (<u>open circles</u>: acrylic Dupont Lucide Wood Primer; <u>solid circles</u>: alkyd oil paint: Sherwin Williams AD-Primer) in comparison with unexposed surface (based on data in [19–21]), and **(c)** peeling-off of the poorly adhering coating film from the painted wood surface

As illustrated in Fig. 14b, it was observed [20, 21] that 4 weeks of cedar weathering prior to painting caused 25% reduction of coating adhesion which, surprisingly, was associated with 50% of specimens failing through coating delamination (paint peel-off effect). It needs highlighting that all specimens weathered for 8–16 weeks prior to painting failed by 100% coating delamination from wood. Photos in Fig. 14c illustrate the actual appearance of the same red ceder panels, showing extensive paint delamination of samples, which were exposed to UV prior to painting.

A clear conclusion from the above observations is that in order to provide effective protection of wood surface against environmental degradation by protective or decorative coatings, and in particular to alleviate the deleterious effects of degradation of lignin by the UV-driven photo-degradation, the following needs to be ascertained:

1. Coatings must be applied onto freshly machined wood which must not be exposed to solar radiation prior to painting,
2. Coatings must provide effective barrier against UV transmission through the coating,
3. Excellent coating adhesion to the underlying substrate must be ascertained.

2.3.5. Industrial Technology for Improving Adhesion to Solid Wood or Wood-Based Products

The principles of novel technology [22–25] for improving adhesion of coatings and adhesives to solid wood are schematically illustrated in Figure 15. It utilises a water-based solution of appropriate macromolecules [28] of specifically controlled length, such as polyethyleneimines (PEIs) and does not require any pre-treatment of wood before application of the primer solution.
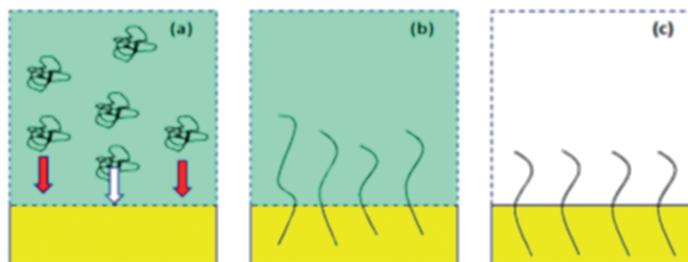
Fig. 15. Schematic principles of a novel, single-step CSIRO process for improving adhesion of coatings and adhesives to wood-based products [22–25, 28]: **(a)** solution of graft chemicals (PEI) in water, **(b)** chains of graft chemicals penetrating into the sub-surface of the treated wood-based product and chemically bonding to the wood cells; **(c)** treated wood surface ready for bonding.

A set of photographs in Figure 16 depicts the laboratory treatment unit for an on-line treatment of flat timber components. The photos provide good insight into the simplicity of this technology. All treated components (e.g. machined wood components) are placed on a conveyor moving at controlled speed (2–10 m/minute)

synchronized with the requirements of the manufacturing process. These are subsequently passed under the spray-head (Figure 16b) of the primer delivery system. Immediately after the spray, the treated components are flashed-off under infra-red (IR) driers and are ready for painting, bonding or any other intended use.
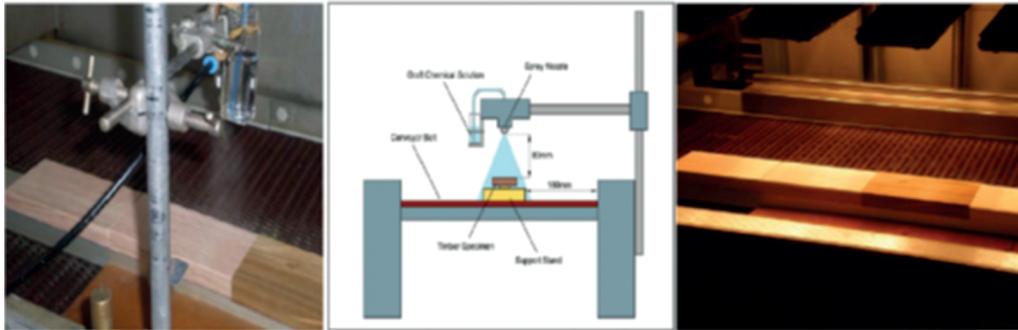
Fig. 16. Laboratory treatment unit for an on-line treatment of flat timber components for improved adhesion: (a) spray application of graft chemicals; (b) overall schematics of surface treatment, (c) Infra-red (I-R) lamps for evaporating residual water film after the spray [15].

Photos in Figure 17 illustrate the influence of alternative methods of wood surface preparation on the quality of adhesion of various high-quality architectural

coatings to the surface of European Redwood (*Pinus sylvestris*) commonly used in European window manufacturing.
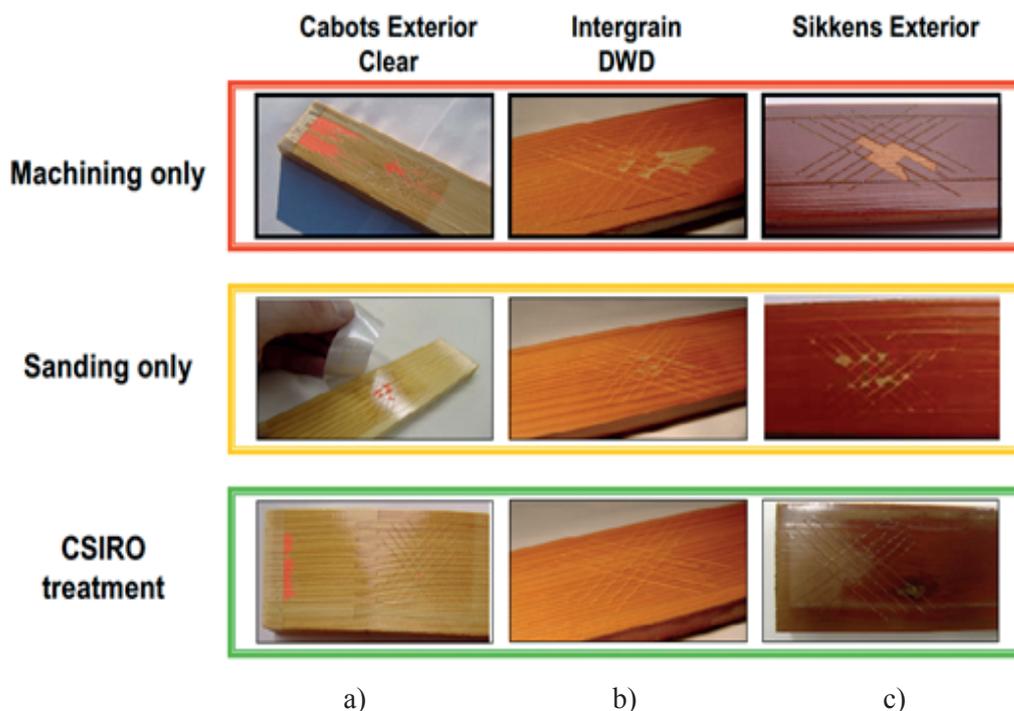
Fig. 17. Quality of adhesion of architectural coatings: Cabots Clear; Intergrain DWD; Sikkens to the surface of European Redwood (*Pinus sylvestris*): (i) machined only, (i) machined and sanded (80 and 150 grit); (iii) molecular brush on machined surface; after 600 hours UV exposure (QUV-B; 303 nm) and 10 days immersion in 40°C water prior to paint adhesion testing (ASTM D 3359 – 95a). Data from [15].

It is clearly seen in photos presented in Figure 15 that wood surface modified by surface grafted molecular

brushes (denoted: CSIRO Treatment) completely eliminates delamination of all 3 coatings investigated in this work.

4. REFERENCES

1. Jiao J.R., Simpson T.W., Siddique Z.: Product family design and platform-based product development: a state-of-the-art review. *Journal of intelligent Manufacturing*, 2007, 18, pp. 5–29.

2. Huang C.C.: Overview of Modular Product Development. *Proceedings of the National Science Council, Republic of China, Part A (Physical Science and Engineering)*, 2000, 24(3), pp. 149–165.

3. Baldwin C.Y., Clark K.B.: *Modularity in the Design of Complex Engineering Systems*. In: Braha D., Minai A.A., Bar-Yam Y. (eds): *Complex Engineered Systems*. Springer, 2006, pp. 175–205.

4. Dahmus J.B., Gonzalez-Zugasti J.P., Otto K.N.: Modular product architecture. *Design studies*, 2001, 22(5), pp. 409–424.

5. Bremner R.: Cutting edge platforms. *Financial Times Automotive World*, 1999, September, pp. 30–38.

6. Paralikas J., Fysikopoulos A., Pandremenos J., Chryssolouris G.: Product modularity and assembly systems: An automotive case study. *CIRP Annals – Manufacturing Technology*, 2011, 60, pp. 165–168.

7. Proton Exora: *Malaysia's first MPV: Exora Platform – spin-off strategy*, 2009.

8. Lawson R.M., Richards J.: Modular design for high-rise buildings. *Proc. Inst. Civil Eng.*, 2010, 163(3), pp. 151–164.

9. *Visuals for limited competition scheme for RBH new Headquarters Building*. Oxford Brooks University, Unite Modular Solutions and KKK Architects, Studio Guide: modular construction, Preliminary Flier, 2012.

10. Welch A.: *House in Ulcombe, English Residence*. [Online]. 2017. [Accessed 1 September 2019]. Available from: https://www.e-architect.co.uk/england/ulcombe-house

11. Kuys B., Gutowski M., Li S., Gutowski W.S., Cerra A.: Modular design and assembly of automotive and architectural structures: product integration through adhesive bonding. *Advances in Manufacturing Science and Technology*, 2016, 40(3), pp. 5–28, DOI: 10.2478/amst-2016-0013.

12. Abrahamsen R.B., Malo K.A.: Structural Design and Assembly of TREET – A 14-Storey Timber Residential Building in Norway. In: *World Conference on Timber Engineering, Quebec City (Canada), 10–14 August 2014*. Proceedings, 2014, pp. 2035–2043.

13. Tabet T.A., Aziz F.A.: *Cellulose microfibril angle in wood and its dynamic mechanical significance*. In: van de Ven T., Godbout L. (eds.): *Cellulose – Fundamental Aspects*. InTech, 2013, pp. 113–142.

14. Fraunhofer-Instituts für Angewandte Polymerforschung IAP: Annual Report, 2012, p. 40.

15. Kuys B.: *Science and design: surface modification for timber window frames*. [PhD Thesis]. Swinburne University of Technology, Faculty of Design, 2010.

16. Jirous-Rajkovic V., Turkulin H., Miller E.R.: Depth profile of UV-induced surface degradation. *Surf. Coat. Int., Part B*, 2004, 87, pp. 241–247.

17. Kataoka Y., Kiguchi M.: Depth profiling of photo-induced degradation in wood by FTIR microspectroscopy. *J. Wood Science*, 2001, 47(4), pp. 325–327.

18. Bamber R.K., Summerville R.: Microscopic studies of the weathering of radiata pine sapwood. *Journal of the Institute of Wood Science*, 1981, 9(2), pp. 84–88.

19. Williams R.S., Feist W.C.: Duration of wood preweathering: Effect on the service life of subsequently applied paint. *Journal of Coatings Technology*, 2001, 73(920), pp. 65–72.

20. Williams R.S., Winandy J.E., Feist W.C.: Correlation of Adhesive Strength with Service Life of Paint Applied to Weathered Wood. In: *9th Durability of Building Materials and Components Conference, Brisbane (Australia), 17–20 Mar 2002*. Proceedings, paper 161, pp. 1–11.

21. Williams R.S.: Don't get (sun) burned: exposing exterior wood to the weather prior to painting contributes to finish failure. *Journal of Architectural Coatings*, 2005, pp. 56–60.

22. Li S., Yang W., Gutowski W., Molenaar S., Spicer M.: *Method and Composition for Priming Wood and Natural Polymers*. US Patent No. US 8,449,668 B2, 28 May 2014.

23. Gutowski W.S., Russell L., Bilyk A., Hoobin L.P., Li S., Filippou C., Spicer M.: *Treatment of Natural Polymer Materials and the Products Based Thereon*. US patent 6,830,784, 2004

24. Gutowski W.S., Russell L., Bilyk A., Hoobin L.P., Li S., Filippou C., Spicer M.: Treatment of Natural Polymer Materials and the Products Based Thereon. European Patent EP1253999, 2004.

25. Gutowski W.S., Russell L.J., Bilyk A., Hoobin P.M., Li S., Filippou C., Spicer M.: *Treatment of natural polymer based materials and the products based thereon*. US Patent 7,459,185, 2008.

26. Gutowski W.S., Li S., Bilyk A., Spicer M.: *Treatment of Natural Polymer Based Materials*. US Patent No 6,830,784, 2007.

27. Gutowski W., Li S., Kuys B., Filippou C., Russell L.: Chemical grafting improves adhesion of coatings on façade materials. *European Coatings Journal*, 2015, 2, pp. 18–22.

28. Widsten P., Gutowski W., Li S., Cerra T., Molenaar S., Spicer M.: Unwelcome Migrants on Surface of Adhesively Bonded Wood. *International Forestry Review*, 2005, 7(5), p. 110.

29. Gutowski W.S., Li S., Russell L., Filippou C., Hoobin P., Petinakis S.: Theoretical and Technological Aspects of Surface-Engineered Interface-Interphase Systems for Adhesion Enhancement. *Journal of Adhesion*, 2003, 79, pp. 483–519.

Piotr CZAJKA*, Wojciech MIZAK
Łukasiewicz Research Network – Institute for Sustainable Technologies, Radom, Poland
* Corresponding author: piotr.czajka@itee.radom.pl

A METHOD FOR MONITORING GLASS MELT SURFACE IN A GLASS FURNACE

Keywords: glass industry, glass smelting process, vision monitoring

Abstract: This article describes a method for vision monitoring of the glass surface inside a glass furnace with its main advantages and limitations. It presents the structure of a vision monitoring system developed by the authors with a dedicated vision head and the operator's stand. The elements of this monitoring system have been installed in a glass factory. The experimental research which has been conducted confirmed the proper functioning of the system. The registered images of the furnace interior are a foundation for further work on the development of a programme module for automated image analysis and selected parameter measurements of the process. The authors of the article have reviewed publications on the processing and analysis of glass furnace images. This monitoring system constitutes a very important source of information on the condition of the glass melt surface inside the furnace as a support for the operators in charge of the glass melting process.

Metoda monitorowania lustra szkła w piecu szklarskim

Słowa kluczowe: przemysł szklarski, proces wytopu szkła, lustro szkła, monitoring wizyjny

Streszczenie: W artykule zaprezentowano koncepcję wizyjnej metody monitorowania lustra szkła w piecu. Przedstawiono podstawowe możliwości i ograniczenia metody. Zaprezentowano strukturę wizyjnego systemu monitorowania z opracowaną przez autorów dedykowaną głowicą wizyjną i stanowiskiem operatora. Elementy systemu monitorowania zostały zainstalowane w hucie szkła. Przeprowadzone badania eksperymentalne potwierdziły poprawność działania systemu. Zarejestrowane obrazy wnętrza pieca są podstawą do planowanych dalszych prac związanych z opracowaniem modułu oprogramowania do automatycznej analizy obrazów i pomiaru wybranych parametrów procesu. Autorzy artykułu dokonali przeglądu literatury odnośnie do metod przetwarzania i analizy obrazów dla pieców szklarskich. Opracowywany system monitorowania stanowi bardzo istotne źródło informacji o stanie lustra szkła wewnątrz pieca, wspomagając operatorów kontrolujących proces wytopu szkła.

Introduction

The increase in demand for utility glass products and progress in manufacturing have contributed to the automation of the manufacture in the glass works, which, in turn, has influenced the introduction of large output, continuous operation furnaces [1, 2, 3, 4]. In automated manufacture plants, the daily requirement for raw glass material can be as large as several hundred tons [3]. The image of the inside of the melting tank provided by the camera mounted in the vision head in the upper part of the furnace is an supplemental source of information for the operator managing glass melting. Even though there have been a number of vision systems introduced in the glass industry, which serve as an optical inspection tool for the manufactured glass [5], at the stage of melting, the visual evaluation of glass surface in most of the installed systems is conducted by humans [6, 7]. If the temperature is set too low, the resulting product may be of inferior quality, causing considerable losses. If the maintained temperature is too high, it results in an increased energy consumption, which plays a substantial part in manufacturing costs [8] and in increased output of pollutant (mainly nitrogen oxides and greenhouse gases). The automated measurement of the process parameters based on the analysis of the glass surface images can ensure the repeatability and optimisation of melting process [6].

The work presented in this article is financed by *Operational Program: Intelligent Development* as part

of the project "The development and implementation of integrated, multifunctional system for increasing manufacturing effectiveness and product quality in glass industry by applying innovative technology".

The glass works Trend Glass has applied for and is the recipient of the system, while the Łukasiewicz Research Network – The Institute for Sustainable

Technologies is carrying out the research and development work. Each specific module of the system (Fig. 1) carries out its assigned task consisting in monitoring different stages of the production process and product quality inspection, including the preparation of the tools for product forming, monitoring the melting process, and quality inspection of glass products.
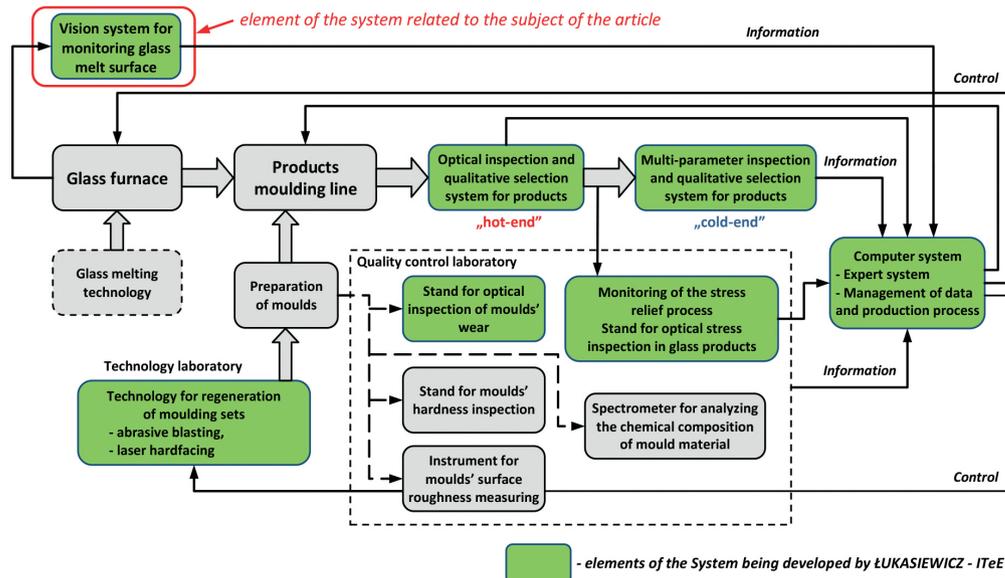
Fig. 1.   An integrated, multifunctional system for increasing manufacturing effectiveness and product quality – general structure (developed by Łukasiewicz Research Network – The Institute for Sustainable Technologies ITeE)

This article focuses on the module which provides a vision monitoring system of the glass melt surface in the furnace.

1. The structure of a glass furnace

Tank furnaces work on a continuous shift basis where all the stages and processes of glass melting are taking place simultaneously in various parts of the tank. From one end, the tank is loaded with a mix of raw materials, i.e. glass melting set, which on contact with the hot flame melts. The molten glass filling the tank flows to the other

end where it is transferred to the forming machine, and the decrease in the glass melt is filled as the other end the tank is charged with another batch of mix [2]. Glass furnaces can be fuelled by natural gas, generated gas, or heating oil. The burning of these fuels takes place using burners which create long flames touching the surface of the bath across a large area [4]. Depending on how the burners are situated, the furnaces are divided into side-port and end-port furnaces. In side-port furnaces (Fig. 2a) the burners are situated in the side walls perpendicularly to the glass flow in the bath. In end-port furnaces, the burners are placed in the back wall, and the flame from the burner curves into a U when firing (Fig. 2b).
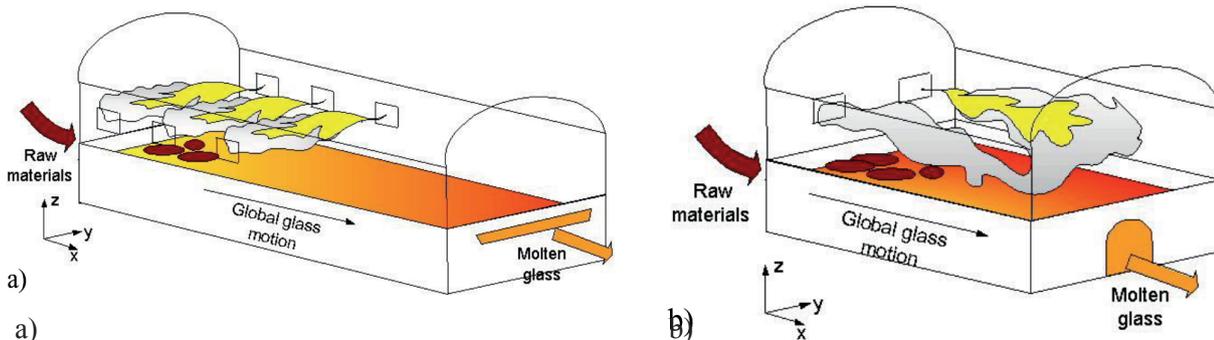
Fig. 2. Diagrams of glass furnaces with different flame paths [1]: a) a side-port furnace, b) an end-port furnace

Moreover, the furnaces are equipped with heat regenerator systems, which improve thermal efficiency for the glass melting process. In the regenerator chamber, the supplied air is pre-heated using the outgoing hot flue gas. Regenerators work cyclically. In the first cycle, hot flue gas is run through the chamber, and in the next cycle, the intake of air, going in the opposite direction, absorbs the heat accumulated in the chamber [4]. Figure 3 shows an example of a cross-section of an end-port regenerative glass furnace with a bath (melting tank).
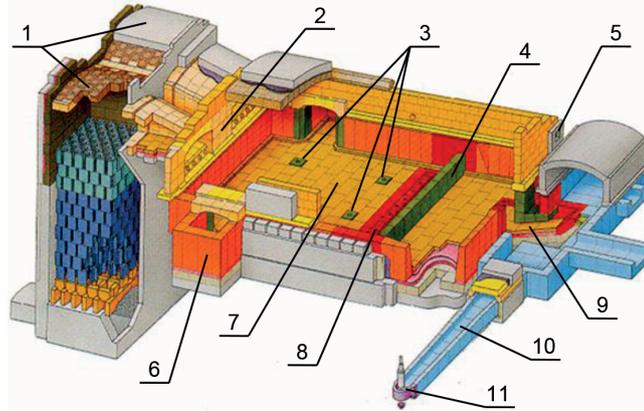
Fig. 3. **A cross-section of a regenerative, end-port furnace [9]: 1 – regeneration chambers, 2 – burner wall, 3 – electrodes, 4 – weir, 5 – inspection viewer, 6 – doghouse, 7 – tank, 8 – bubblers, 9 – flow, 10 – distribution feeder, 11 – gob feed spout**

The cross-section of the furnace shows the typical elements, such as the doghouse where the new batches of glass material are supplied, the openings for electrodes which enable electric, supplementary heating, and the bubblers. Bubbling is a process of blowing compressed air into the glass bath through the vents placed in a row in front of the weir. Its purpose is to prevent the flow of unmolten particles into the fining zone. The molten glass flows through the channel to the feeders, and there to the gob spout, where it is fed to the machines which make glass products.

2. The glass melting process in the furnace

Figure 4a shows a diagram of the glass melting process in a tank furnace. The raw materials for glass production include quartz sand, cullet, soda (glass mix) [3] and are supplied at one end of the tank. These elements float on the surface of the molten glass, and as a result of firing, these elements melt and sink into the glass melt. The glass melt creates convection currents which allow the melt to mix. Additionally, the heating electrodes cause the creation of vertical convection currents. The weir and the bubblers create return currents and further equalise the temperature in the melt and extend the minimal path that the mass must travel before reaching the other side of the bath [1, 2].
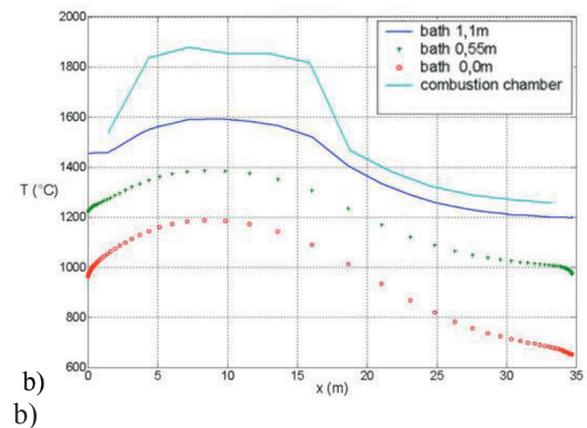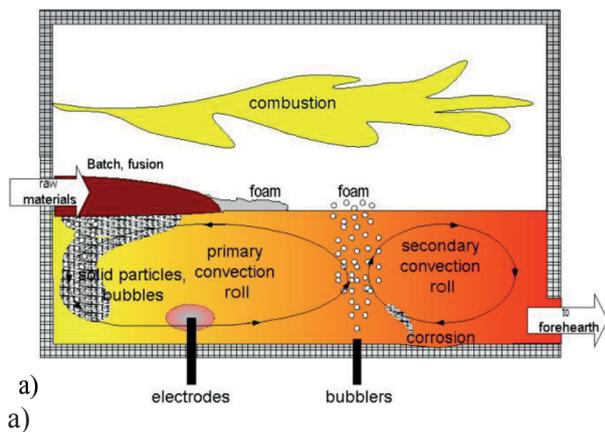
Fig. 4. **A presentation of glass melting process [1]: a) a diagram showing the process in the glass melt with the currents b) a temperature chart for different levels of the melt and in the flaming zone**

Figures 4b show the chart for temperature distribution at different levels of the glass melt along the entire length of the bath and additionally at the flame level above the surface of the melt.

3. The concept of a vision monitoring method

A simplified model of a glass furnace bath is shown in Figure 5. In the front wall, from the working end, there is an opening for inserting the vision head. Due to extreme temperatures inside the furnace of 1,500°C, only an endoscope is inserted through the opening. It contains an internal system for image transmission and a water jacket cooling system. The forced circulation of the cooling medium and the cooling generator of sufficient power provide continuous monitoring the operation. Figure 5 shows

sample images of the inside of an end-port glass furnace registered by a thermal imaging camera [11] and a visible light camera [12]. The images show the surface of the melted glass, the unmelted fragments of the glass mix floating on the surface, the back wall with burners, parts of the side walls, and the furnace roof. The application of a thermal imaging camera provides the measurements of the temperature distribution on the surface of the glass melt and the visible for the camera part of the internal furnace structure, while the application of the visible light camera provides images of the furnace interior with a greater resolution. The monitoring system with the visible light camera is cheaper than the one with the thermal imaging camera. The lower price is related to the the camera itself and to the image transmission system. It is important in the monitoring system that the lens in the vision head is wide-angle and includes as large an area of the furnace as possible.
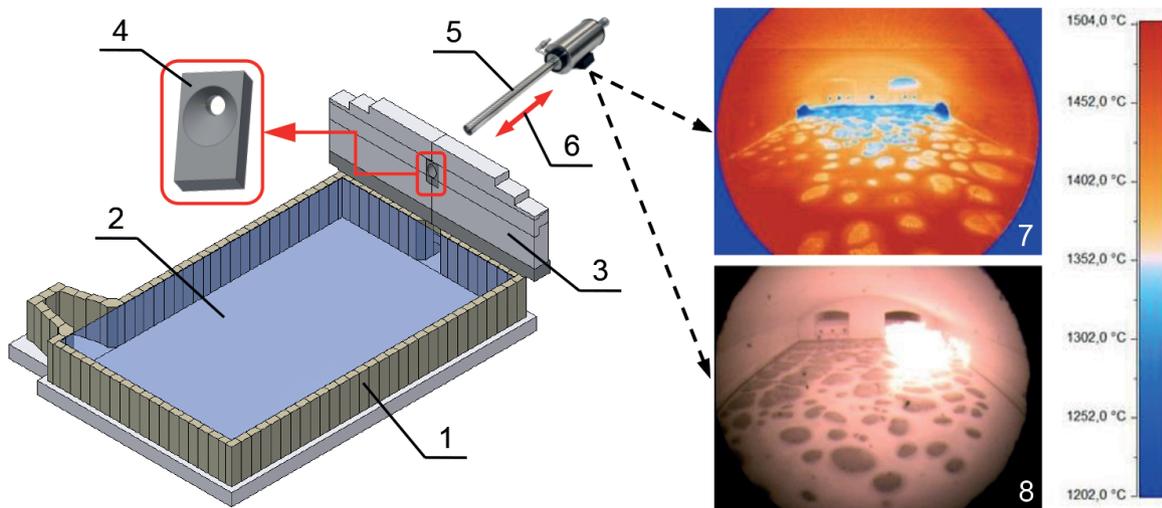
Fig. 5.   A concept of vision monitoring system inside a glass furnace, originally developed based on [10, 11, 12]: 1 – a simplified model of glass melt tank, 2 – glass melt bath, 3 – furnace front wall, 4 – fitting with an opening for the vision head, 5 – an example of a vision head with a furnace endoscope [10], 6 – retraction system for the endoscope, 7 – the image of the furnace interior obtained from the thermal imaging camera with colour scale for temperature changes [11], 8 – the image of the furnace interior obtained from the visible light camera [12]

The system presented in Figure 5 is intended for continuous on-line inspection of the condition of the glass melt surface via a vision method. An important element of the system, which influences the operation safety, is the retraction system of the endoscope. If the temperature limit is exceeded, or water flow or air compression is decreased, the control system ensures an automatic retraction of the endoscope from the aperture in the furnace.

Table 1 presents basic capabilities and limitations of the vision monitoring method for the glass furnace interior. The surface of the glass melt can be used for the observation of level of the glass melt in the bath, the size and location of unmelted fragments of the glass mix, and whether the bubbling process is taking place properly. In addition to the observation of the glass melt surface, this method also enables the observation of the shape and location of the flame from the burners, the burner wall, and fragments of side walls and the roof.

Table 1. The main capabilities and limitations of the vision monitoring method for a glass furnace (based on authors' work)

Capabilities (advantages) of the method	Limitations (disadvantages) of the method
– A contact-free measurement method – The observation of the location and size of the glass mix batch – The observation of the shape and location of the flame issuing from the burners – The observation of the bubbling process – The measurement of the temperature distribution of the glass melt surface and the structure of the interior of the furnace (requires thermal imaging camera) – The observation of the melt glass level in the bath – The improvement in the stability of the glass melting process – The decrease in energy consumption and the nitrogen oxide and greenhouse gasses emissions	– A limited area of monitoring when only one camera is installed – A limited resolution of images in thermal imaging camera – A limited resolution of optics systems used in furnace endoscopes (including visible light as well as thermovision in infrared) – The effect of the flames from the burners on the measurements (the necessity to conduct some of the measurements during a reversal) – A limited precision of the measured temperature when using thermal imaging camera

4. The construction of the vision head

Figure 6 shows key construction elements of the vision head for monitoring the interior of a glass furnace as follows: protective casing with the camera placed inside, and the furnace endoscope in the form of a water jacket cooling system enclosing the optical tube for image transmission. The endoscope is inserted into the furnace, while the camera in its casing remains outside of the furnace.
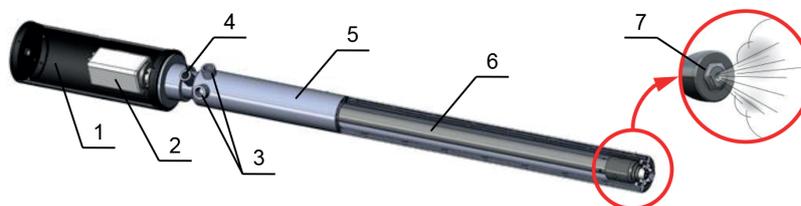
Fig. 6.   An illustrative diagram of vision head structure [13]: 1 – protective casing of the camera, 2 – camera, 3 – water supply points, 4 – compressed air supply point, 5 – cooler with a water jacket, 6 – optical tube, 7 – air flow arount head lens

As a support for the cooling process, the water inside the cooler is additionally set into a swirling motion (Vortex effect) [13]. There are two basic structures of the coolers, i.e. with one or with two water jackets (Fig. 7). Using a double water jacket provides better protection and a more uniform temperature distribution on the surface of the cooler.
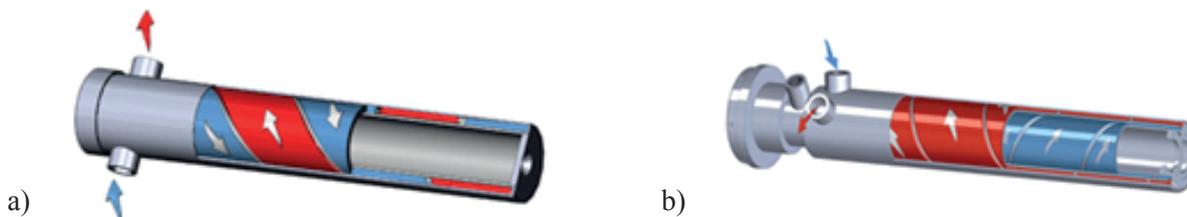
Fig. 7.   Basic constructions of water coolers used for monitoring high temperature processes [13]: a) with one water jacket, b) with a double jacket

The front lens, as the most forward element of the vision system, is most exposed to the temperature inside the furnace and thus exposed to thermal damage; therefore, in addition to closed system water cooling, the endoscope is equipped with open system air flow (Fig. 6). The compressed air cleans the lens and also cools it using the Venturi effect [13].

Inside the cooler with a water jacket, there is an image transmission system from the interior of the furnace. There are two main ways of image transmission.

The first solution (Fig. 8a) applies an optical tube with an internal system of lenses, which cooperate with the camera placed in the outer protective casing. The second solution (Fig. 8b) uses a comprehensive vision system including a camera and a lens placed inside the cooler. In this case, the range of applications is limited to a small camera due to the small inside diameter of the cooler, and its distinguishing characteristic is a lack of external protective casing for the camera. This solution is used mainly for visible light cameras.
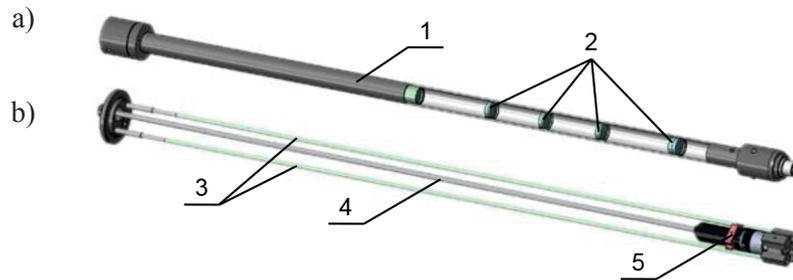
Fig. 8. **Modes of transmission inside the the vision head [13]: a) optical tube with a system of lenses, b) comprehensive viewing system including the camera and the lens (1 – optical tube, 2 – lens system, 3 – mounting brackets, 4 – image transmission cable, 5 – vision system (camera + lens)**

As a result of tests done on the demonstration vision heads (using thermal imaging and visible light cameras), a monitoring system of glass melt surface was selected using visible light colour camera, which also met the industry partner's requirements. The available systems with visible light camera (by SVA Industrie Fernseh) work with the monitor for viewing the interior of the furnace and an optional image recorder. The monitoring system for a glass furnace is shown in Figure 9. In the SVA design, the complete viewing system, including the camera and the lens, is placed inside the cooler [14].
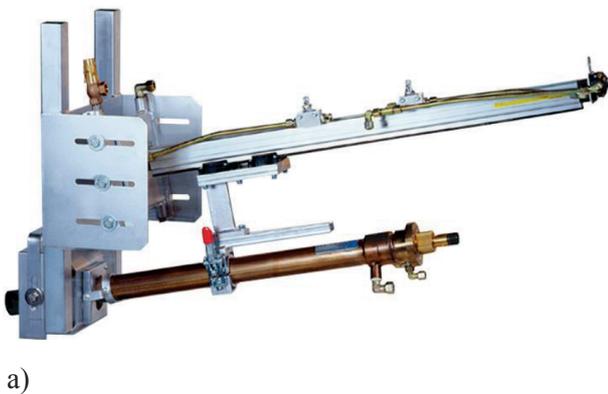
Fig. 9. **A general view of the standard version of the monitoring system for glass melt surface using visible light camera [14]: a) vision head with the coupling system and with the endoscope retraction b) a control system for endoscope retraction with the media connection box**

The standard solutions do not have the functionality required in the project related to the analysis of the recorded images and the transfer of the results to the IT system. The authors proposed a dedicated monitoring system for the glass melt surface adapted for industrial settings. The main differences in comparison with the available solutions include the use of a high resolution camera with the capability to transfer digital signal (Gigabit Ethernet) and an operator stand with a computer system, which analyses the images and sends the results to the primary IT system.

The elements selected for the vision system are a digital visible light camera and a wide angle pinhole lens. The selection of the pinhole lens was determined by the small diameter of the front lens (a few millimetres), and because it minimises the negative effect of heat on the optical elements of the lens. The C-mount type was selected, which is commonly used in industrial cameras. Among available small and compact cameras, the standard case size was selected of 29 mm by 29 mm. It is a size for a large selection of cameras available from different manufacturers including JAI, Basler, Flir, Allied Vision, and it will allow for easy selection of replacement parts. Mounting of these types of camera (a diagonal of ca. 41 mm) is possible inside a cooler with the inside diameter of 50 mm. The main specifications of the vision system of the camera and the lens are presented in Tables 2 and 3 below.

Table 2. Main parameters for the camera

Manufacturer	Allied Vision
Sensor resolution	1.9Mpx (1600x1200px)
Sensor type	CMOS, colour
Sensor size	1/1.8"
Interface	GigE PoE
Mounting type	C-mount
Working temperature	+5°C – +45°C

Table 3. Main parameters for the lens

Manufacturer	CBC (Computar)
Focal length	4 mm
View angle	76.3° (H), 61.6° (V)
Working with the sensor	1/2"
Aperture	F2.5 – F32C
Mounting type	C-mount
Working temperature	-20°C – +50°C

The cooler manufactured by SVA with a water jacket, 100 cm long, and an inside diameter of 50 mm is shown in Figure 10a. The photograph of the image transmission system, developed by the authors, which is placed inside the cooler, is shown in Figure 10b. The view of the whole head with the cooler and the vision system mounted inside is shown in Figure 10c.
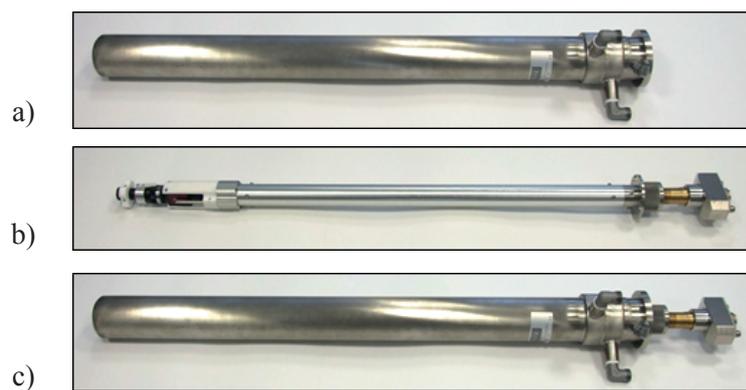
Fig. 10. The elements of the dedicated version of the vision head (authors' work): a) a cooler with a water jacket, b) the developed image transmission system, c) a vision system mounted in the cooler

A detailed view of the front and the back of the image transmission system is shown in Figure 11. The front part (Fig. 11a) has a vision system consisting of a visible light camera with a pinhole lens. At the end of the lens, there is a bracket which sets the location of the lens inside the cooler. Behind the bracket, there is a lens lock, which is to block any accidental change of settings. The photographs show one of the two Pt100 type temperature sensors placed on each side of the camera, which provide data for monitoring the temperature inside the cooler by the retraction system and by the operator's stand in the control room. The aluminium conduit contains cables which provide the transmission of the image from the camera, supply electricity, and the reading of the signals from the temperature sensors.
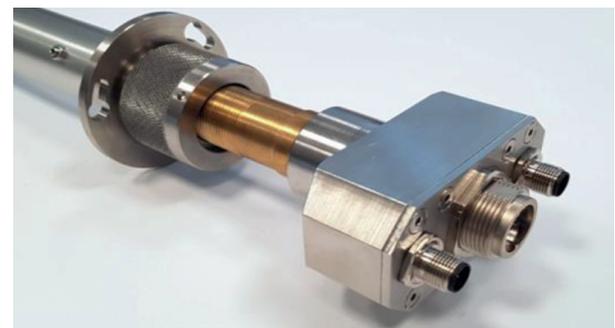
Fig. 11. A detailed view of the image transmission system (authors' work): a) a detailed view of the vision system, b) a detailed view of the electric connector module

Electric cables from the subcomponents of the vision system are connected to the connector module located at the back of the vision head (Fig. 11b). The photo also shows the flange, which enables the installation of the vision system inside the cooler.

5. The structure of the vision monitoring system

Figure 12 shows the general structure of the monitoring system for the glass melt surface inside a furnace with all of the necessary modifications. In the high temperature zone by the furnace, there is a dedicated vision head, which has a pneumatic system for emergency retraction of the endoscope from the furnace. Near the furnace, there is a control system for endoscope retraction and the media connection box. The system has an independent container with compressed air for emergency retraction of the vision head in case when there is a lack of compressed air in the system. In this area, there is also a cooling generator (chiller), which ensures the cooling of the vision head. The cooling agent is demineralised water. For the control room, the operator's stand was designed for conducting the observations of the inside of the furnace.

Figure 13 shows the vision head with the mounting system to the structure of the furnace and the head retraction using pneumatic actuator system.
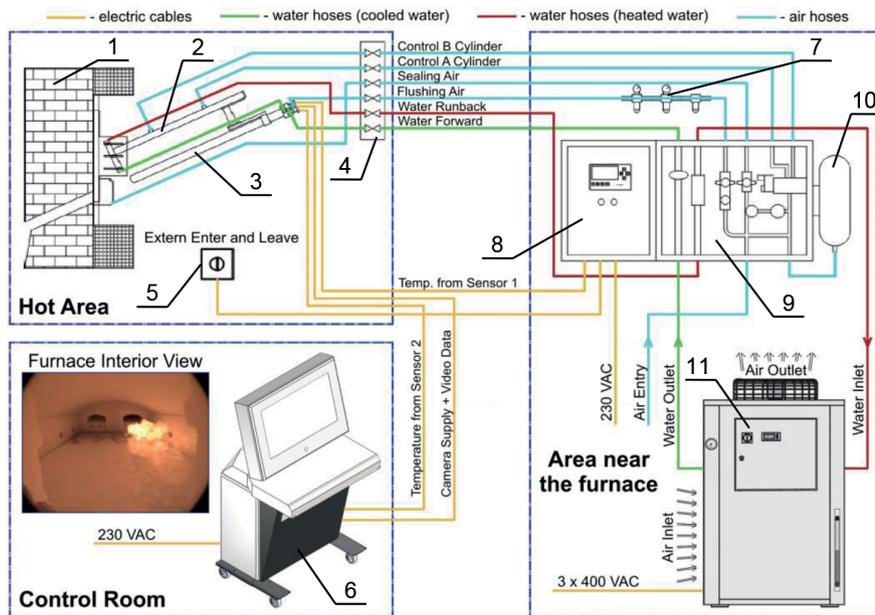
Fig. 12. The structure of the vision monitoring system of glass melt surface (authors' work based on [15]): 1 – furnace wall, 2 – the system for vision head retraction, 3 – vision head, 4 – terminal with valves, 5 – manual control of head retraction, 6 – operator's stand in the control room, 7 – air filter set, 8 – control system box for vision head retraction, 9 – media connection box, 10 – reserve air container, 11 – cooling generator (chiller)

a)   b)

Fig. 13. Photographs of the mounting system of the vision head to the structure of the furnace with the the endoscope retraction system (installation location: high temperature zone – directly next to the glass furnace), (authors' work): a) dismounted vision head, b) vision head mounted in the clamp

Photographs of the remaining elements of the system, including the cooling generator and the control system of the head retraction with the media connection box, are presented in Figure 14. These elements were installed under the furnace's glass tank.
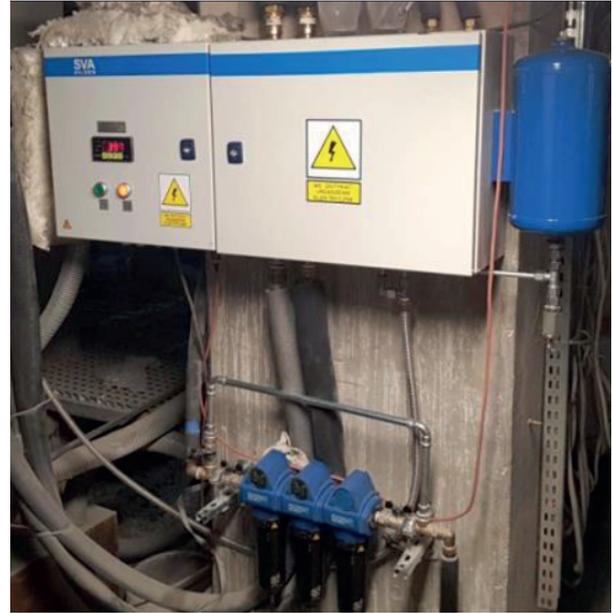
a)   b)

Fig. 14. Photographs of the remaining elements of the system for monitoring glass melt surface (location of installation: under the glass-melt tank (authors' work): a) cooling generator, b) control system box for the retraction of the vision head, with the media connection box and a set of air filters

The operator's stand for a glass melt surface monitoring system was developed and manufactured (Fig. 15). The dedicated industrial casing protects the following elements placed inside: an industrial computer, an LCD monitor, programmable PLC controller, and emergency UPS power supply. It protects those elements from the negative effects of external conditions including dust, dirt, or splashing. The stand is placed on wheels with a stop lock, so it can be placed wherever needed.

a)   b)   c)

Fig. 15. A view of the developed operator's stand for monitoring the surface of glass melt in a furnace (location: furnace control room), (authors' work): a) a photo with the keyboard retracted, b) a photo with the keyboard extended, c) screenshot of the operator's interface

The operator's stand is equipped with a pull-out shelf with a water and dust proof keyboard (Fig. 15b). The keyboard comes with a touchpad. After the operator sets the appropriate parameters, the shelf can be retracted (Fig. 15a). Using the developed software installed in the operator's stand (Fig. 15c), the monitor can display the images of the furnace interior and register video sequences on demand.

6. Experimental research

First, the images of the inside of the furnace were recorded using the developed vision head. After the effectiveness of the cooling system was ascertained and the endoscope was placed properly in relation to the opening in the fitting, several sequences of furnace images were registered. Sample images for different stages of furnace firing are shown in Figure 16. The

registered images encompass a large portion of the glass melt surface, the back wall with burners, the doghouse, the furnace roof, and portions of the side walls. On the surface of the glass melt, there are unmelted fragments of the glass mix batch, shown as darker areas near the rear wall of the furnace with light areas of the flames from the burners. During this study, the bubblers were turned off, which is why the process is not visible in the images.

a)

b)

c)

d)

Fig. 16. A sample of registered images of the furnace interior (authors' work): a) initial testing and setting the correct placing of the vision head (the aperture in the fitting for vision head is visible), b) burners turned on, on the right, c) burners turned off during reversion, d) burners turned on, on the left

The testing confirmed the correct functioning of each the elements in the monitoring system, the effectiveness cooling of the vision head, the satisfactory quality of the registered imaged, the large field of view, and the correct placing of the vision head in the aperture.

7. The system's potential for further development

One of the functionality requirements of the monitoring system for glass melt surface is the transfer of the measurement information to the primary IT system. The data will be obtained based on the analysis

of the registered images of the furnace interior by the vision head directed towards the surface of the glass melt. The planned analysis includes the calculation of the percentage of the glass mix content, the detection of the limits of the mix, the analysis of the bubbler system functioning, the measurement of the glass melt surface level (optional), the analysis of the shape, and the angle of the flames from the burners.

The authors have reviewed the publications related to the methods of image processing and analysis of glass furnaces [6, 7, 16], and their one common denominator is the necessity to take into account the point of view of the images. The camera is placed in the chamber of the furnace at an angle, so the image is

a two dimensional, homographic transformation of the surface of the glass melt. By identifying the parameters of this transformation, we can conduct a reverse transformation and obtain the image of the glass melt surface as seen from above [6, 7]. Another common feature of the applied algorithms is conducting the segmentation of the glass melt image based on the image brightness. The purpose of this operation is to delimit areas with unmelted fragments of the mix

in order to calculate the percentage of the glass melt surface coverage by glass mix and borders of the glass mix batch.

Sample stages of image processing based on [6] are shown in Figure 17. The resultant image (Fig. 17c) shows the surface of the glass melt surface in a projection form above. The black shows the glass mix, dark grey shows clear glass melt, and the light grey is the area beyond the field of view of the camera.

a)   b)   c)
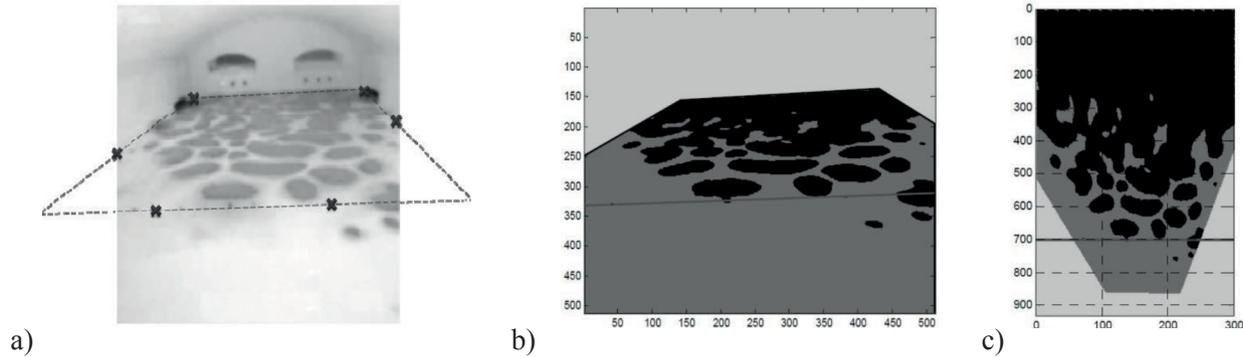
Fig. 17. The stages of image processing for glass melt surface (one-camera system) [6]: a) the image obtained from the vision head with the glass melt surface marked and delimited by the bubblers, b) glass melt surface after the segmentation of the glass mix (the scale on the axes is in the camera pixels), c) the image after perspective processing showing the projection from above (the scale on the axes is in centimetres)

In order to limit the dead zones of the system, the single camera system can be replaced with two cameras

placed on both sides of the front wall of the furnace (Fig. 18) [16].

a)   b)   c)
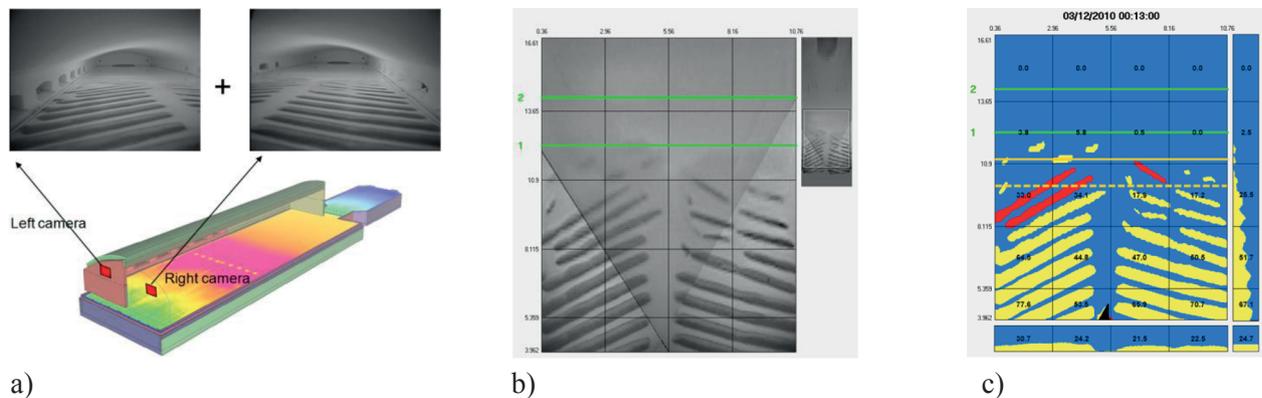
Fig. 18. The stages of image processing for glass melt surface (two-camera system) [16]: a) the image obtained from the left and the right camera, b) the image after perspective processing showing the projection from above (data from both cameras), c) the image after the segmentation of the glass mix

The literature analysis shows that the methods for processing and analysis of images of furnace interior relate to the glass melt surface and allow: the detection of glass mix limits, the determination of the percentage of glass mix coverage, the delineation of the asymmetry of the glass mix distribution, the control of the bubbling process, and others. The planned development of authors' software for automated analysis of the interior of the furnace, in addition to monitoring the glass melt surface, will

include the analysis of the flame issued from the burners located above the surface of the glass melt.

Conclusions

The system which is being developed is intended for continuous on-line monitoring of the condition of the glass melt surface using the vision method. It constitutes a very important source of information for

the operators in charge of the process of glass melting. Until now, the information on the process was based solely on the sensors (e.g., thermo-elements) placed in the selected areas of the furnace. Additionally, at set intervals, the operator would conduct visual inspection of the melting process by observing the interior of the furnace through the side inspection holes using special glasses with optical filters. The visual inspection carried out by humans in the proximity of the furnace is not safe and causes fatigue due to the high temperature, noise, and dust. The possibility of the remote monitoring of the glass melt surface will greatly improve working conditions for the operator. Moreover, so far, there has been no system for archiving the images of the furnace interior, e.g., in an atypical situations where the parameters are exceeded, or if there is an emergency situation; however, the periodic registration of the images can determine the range of fluctuation of the processes inside the furnace. The planned development of the software module for an automated analysis of the images of the furnace interior will offer the advantage of eliminating the human factor related to a lack of repeatability, fatigue, subjectivity, etc. In a majority of systems for monitoring the interior of the furnace, the evaluation of the condition of the glass melt surface is still done by a person. This system, at this stage of development, does not ensure an automation of the flame control process or the work of the doghouse directly based on the image analysis. This monitoring system plays the support role, increasing the operator's capabilities of real-time control of the process based on the condition of the glass melt surface inside the furnace.

References

1. Auchet O., Riedinger P., Malasse O., Iung C.: First-principles simplified modeling of glass furnaces combustion chambers. *Control Engineering Practice*, 2008, 16(12), pp. 1443–1456.
2. Piech J.: *Piece ceramiczne i szklarskie*. Kraków: AGH Uczelniane Wydawnictwa Naukowo-Dydaktyczne, 2001 [in Polish].
3. Ziomek M.: Technologia działań podczas awarii pieca hutniczego do wytopu szkła. *W akcji*, 2018, (3), pp. 8–13 [in Polish].
4. Czajka P., Garbacz P.: Diagnostyka eksploatacyjna pieca szklarskiego z zastosowaniem hybrydowego systemu wizyjnego. *Studia i Materiały Polskiego Stowarzyszenia Zarządzania Wiedzą*, 2014, 68, pp. 45–57 [in Polish].
5. Nishu, Agrawal S.: Glass Defect Detection Techniques using Digital Image Processing -A Review. *IP Multimedia Communications*, 2011, pp. 65–67.
6. Rotter P., Skowiniak A.: Metoda komputerowej analizy obrazu dla pieców szklarskich. *Wydawnictwo PAK*, 2013, 59(7), pp. 684–687 [in Polish].
7. Rotter P., Skowiniak A.: Image-based analysis of the symmetry of the glass melting process. *Glass Technology: European Journal of Glass Science and Technology Part A*, 2013, 54(3), pp. 119–131.
8. Ross C.P., Tincher G.L.: *Glass melting technology: A technical and economic assessment*. Glass Manufacturing Industry Council, U.S. Department of Energy Industrial Technologies Program, 2004.
9. Glass global consulting: *Glass Melting Furnaces*. [Online]. [Accessed 09 December 2019]. Available from:https://www.glassglobal.com/consulting/reports/technology/
10. Advanced Energy Industries: *Temperature Measurement Products FurnaceSpection*. [Online]. [Accessed 20 December 2019]. Available from: https://www.advancedenergy.com/products/temperature-measurement/thermal-imagers-and-systems/furnacespection/
11. DIAS Infrared Systems: *Glass industry*. [Online]. [Accessed 09 December 2019]. Available from: https://www.dias-infrared.com/applications/glass-industry
12. Clive Ward: *Heat up CCTV furnace viewing system*. [Online]. [Accessed 09 December 2019]. Available from: http://heat-up.co.uk/UK.html
13. Cesyco: *How does it work?* [Online]. [Accessed 20 December 2019]. Available from: http://www.cesyco.com/en/generalities
14. SVA Industrie Fernseh: *Furnace Monitoring System*. [Online]. [Accessed 09 December 2019]. Available from: https://www.furnace-monitoring.com/index.php?article_id=6
15. SVA Industrie Fernseh: *Instrukcja obsługi kamery piecowej PL*. Hilden: SVA, 2017.
16. Glass Service: *Batch monitoring*. [Online]. [Accessed 09 December 2019]. Available from: https://www.gsl.cz/services-products/smart-process-control/advanced-control-expert-system-es-iii/batch-monitoring/

Piotr GARBACZ*, Mirosław MROZEK
Łukasiewicz Research Network – Institute for Sustainable Technologies, Radom, Poland
* Corresponding author: piotr.garbacz@itee.radom.pl

INSPECTION OF TABLEWARE GLASS PRODUCTS WITH USE OF STRUCTURAL BACKLIGHT

Key words: machine vision, quality inspection, glassware, structural backlight.

Abstract: The paper presents a method for defect detection in tableware glass products using a structural backlight system. In the first part of the article, the designing of the imaging system is described. Furthermore a real-time system for generating pattern images is presented. Finally, laboratory tests carried out using the developed system and algorithms for image processing and analysis are described.

Inspekcja wyrobów szklanych z wykorzystaniem tylnego oświetlenia strukturalnego

Słowa kluczowe: wizja maszynowa, kontrola jakości, produkty szklane, oświetlenie strukturalne.

Streszczenie: W pracy przedstawiono metodę detekcji wad w wyrobach szklanych przy wykorzystaniu tylnego oświetlenia strukturalnego. W pierwszej części artykułu zaprezentowana została struktura opracowanego systemu obrazowania. Następnie opisano system czasu rzeczywistego do generowania obrazów z wzorcami. Zaprezentowano opracowane algorytmy przetwarzania i analizy obrazów oraz przedstawiono rezultaty testów wykonanych za pomocą proponowanego systemu.

Introduction

The glass manufacturing process consists of several stages in which a number of monitoring and inspection techniques can be used [1]. The final product quality control is made before the packaging process at the end of production line. A high transmissivity of glass products in the range of visible light spectrum can be used for simultaneous detection of surface and internal structure defects. Most of the flaws such as cracks, inclusions, or bubbles cause a high contrast on images acquired with use of a standard backlight system (Fig. 1) which ensures reliable detection.
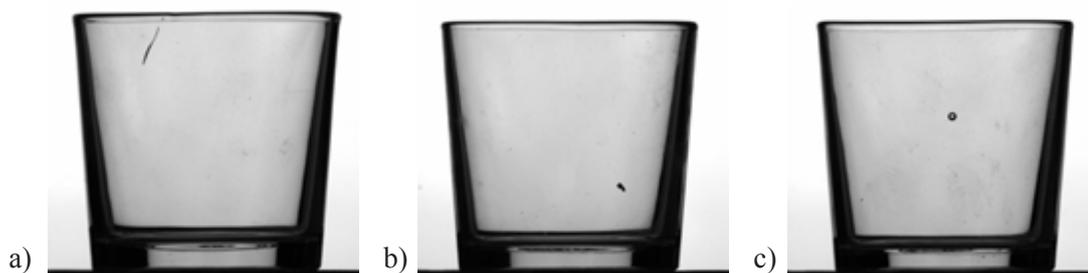
Fig. 1. Images of example defects acquired with use of standard back light system: a) crack, b) inclusion, c) bubble

However, defects occurring by the presence of local distortions (Fig. 2a) of surface geometry cannot be easily detected on a production line with use of a standard backlight setup (Fig. 2b).
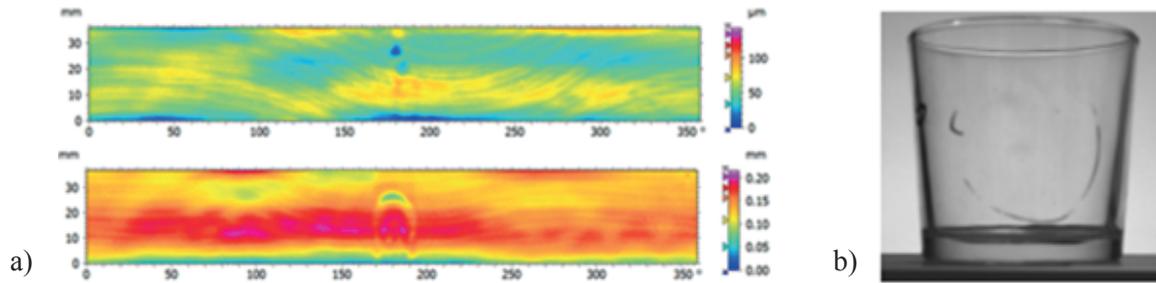
Fig. 2.   Geometric deformation defects of glass products [2]: a) Examples of results of the scan side surface, b) backlight image

This defect arises as a result of accidental disturbances in the technological process. It is the result of air closure between the moulds on the wall of the glass product during the pressing process. Even a good process operator cannot completely prevent this defect. It can happen accidentally and be unnoticed in mass production. Only automatic inspection of each article can eliminate this defect from the batch sent to the customer. Fortunately, it is possible to recognize this type of defect with use of backlight deflectometry [3]. This method involves the analysis images of a known pattern that is emitted by source and passed through the transparent object which allows emphasizing possible geometry distortions (Fig. 3).

Fig. 3.   Transparent objects and phase measuring deflectometry [3]

One of the possible solutions is to use commercially available LED illuminators with one type of pattern printed on the surface [4]. However, due to the random nature of geometric defects and a large variety of shapes of glass products, this solution does not guarantee reliable detection. In order to increase the effectiveness of the inspection system, it is necessary to apply a solution enabling the generation of various types of patterns depending on the shape of the product and the type of defects expected.

1. Inspection systems structure

Preliminary laboratory tests carried out in stationary conditions allowed determining general assumptions for the inspection system. In accordance with the adopted concept, the proposed system consist of two imaging setups placed perpendicular to each other [Fig 4a.]. In order to improve the repeatability of the system, telecentric lenses [5] have been used. Furthermore, to reduce the size of the imaging system in the final system, classical telecentric lenses have been replaced with a compact solution design by Opto Engineering [6] [Fig. 4b].
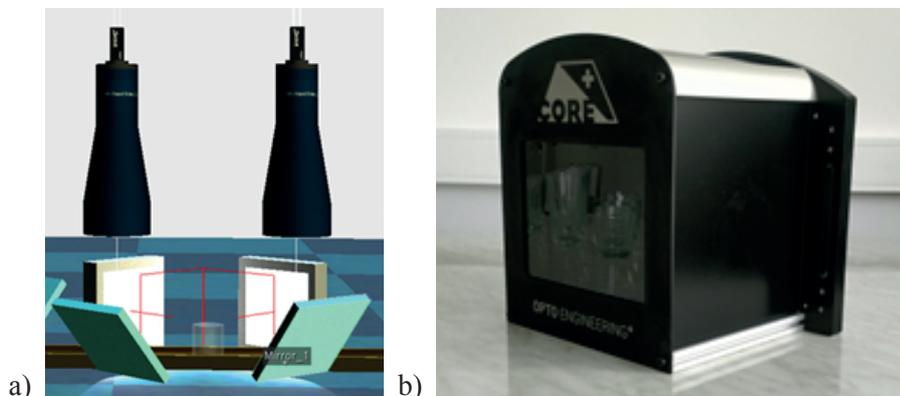
Fig. 4.   Inspection module for geometric flaws detection: a) concept of imaging system with classical telecentric lenses and mirrors, b) compact telecentric lens.

Due to construction size limitations and requirements for obtaining the appropriate imaging resolution, the field of view of lens must be chosen. It is worth noting that one of the disadvantages of telecentric lenses is that they must be larger than the maximum observed scene [7]. Depending on the number of images to be used for analysis and the acquisition rate of the entire system, the size of the lens field of view should be chosen accordingly. In the proposed system, a TCCP23144 lens from Opto Engineering was used which has a maximum field of view 145x121 mm.
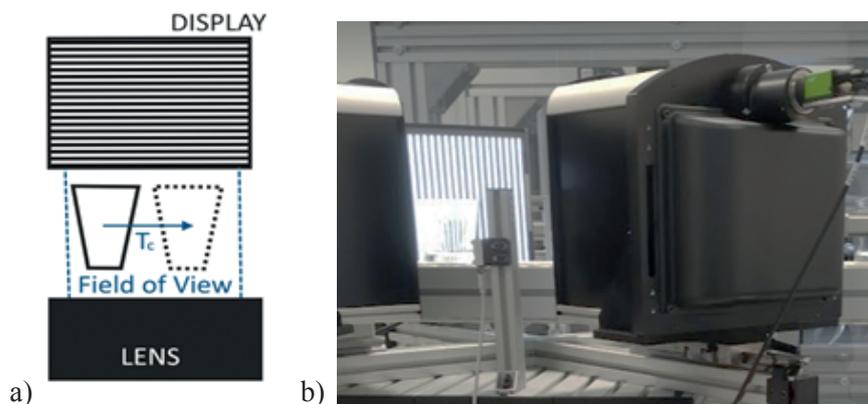
Fig. 5.   Imaging setup for multi-image acquisition [own elaboration]: a) concept, b) laboratory stand

A very important issue during the development of the system was to select a reliable system for generating sequences of different patterns. In the target manufacturing line, products that are inspected are transported on the production line at a speed above 0.5 m/s. Therefore, the basic criterion for the pattern display system was shortening the response and pattern visualization time and guaranteeing its repeatability. In general, the complete image acquisition cycle time T_c should be less than time needed to move the inspected product outside of the lens field of view (Fig. 5a). Another critical issue was the selection of appropriate display, which was due to the fact that the inspected articles move at high speeds on production line. It has become important to select a high-brightness display that would allow the use of the shortest exposure time and thus reduce the blur effect [8] on the analysed images. Standard displays have a brightness of approx. 350 cd/m2, which is not enough to use short exposure times. In the designed system, a Litemax DLH1568 [9] display was used that has basic parameters that are as follows: brightness is 2000 cd/m2, the response time is 8ms, resolution is 1024x768, and the display area is (mm) 304.13(H) x 228.1(V) mm. To control the acquisition process of a series of images, a dedicated system has been developed to work in real time (RT). The RT controller monitors signals from the LED through-beam photoelectric sensor responsible for detecting the presence of the object and generates structured images to the display and synchronizes the camera frames acquisition (Fig. 5b). The generated images are black and white with vertical, horizontal, or diagonal stripes (optional) with a specific width and angle (for diagonal stripes). Images are vector generated, so no extra memory is required to store them. The generated images are saved on a special, fast RAM memory for graphics. Time charts of individual signals of the acquisition system are shown on Figure 6. Image 1 is displayed until the signal (We1) from the trigger system is activated (Fig. 6). This signal informs the system that the object has appeared in the field of view of the camera. When the appropriate signal appears, the microcomputer sends a signal to the camera (Wy2). Then it waits for the falling edge of the confirmation signal that the camera has finished the acquisition process of Image 1 (We3). Image 2 is displayed after the confirmation signal. After that, the confirmation signal of Image 1 is displayed again, and the microcomputer waits for the next signal from photoelectric sensor. In the developed system, when using two types of strip patterns, the cycle time is below 50 ms.
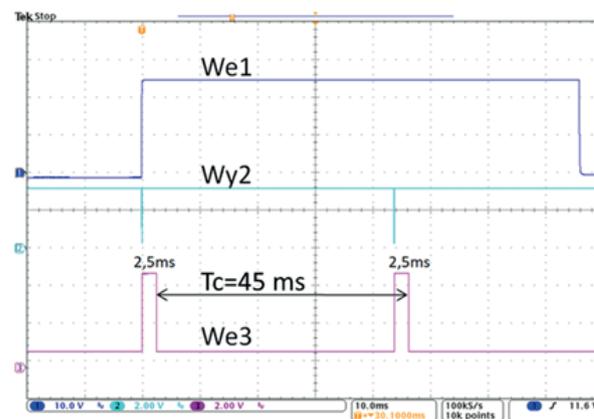
Fig. 6.   Time charts of individual signals-image acquisition system

2. Image processing and analysis

The developed inspection algorithm is implemented on a Matrox 4Sight EV6 [10] vision controller. In the presented case, the general inspection procedure can be grouped into the following stages:

1. Region of Interest adjustment,
2. Detection of stripe edges on sub-regions,
3. Global distortion analysis, and
4. Final decision.

In the first stage of the inspection procedure, the exact position of tableware glass is determined. For this purpose, the outer edges of the glass are detected and its centre is calculated (Fig. 7a). Then the inspection window is positioned relative to calculated value (Fig. 7b).
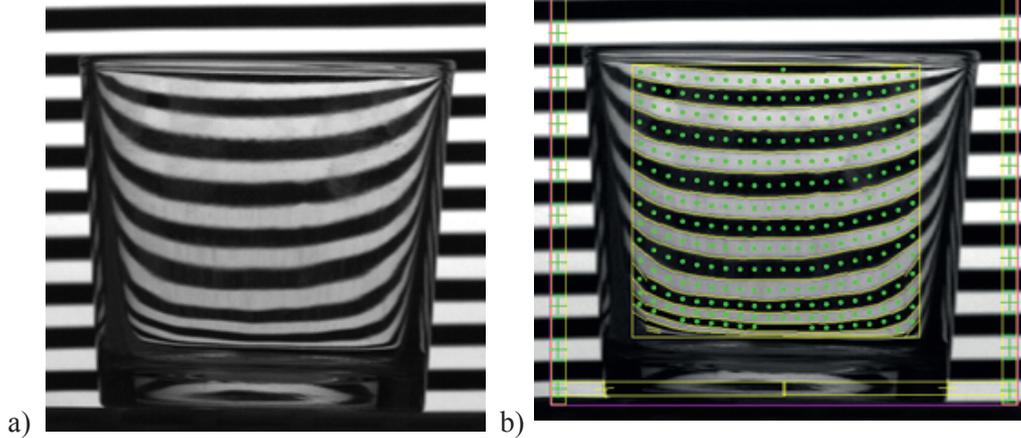
Fig. 7. **Example image of inspected article: a) camera raw image, b) positioning algorithm for inspection window (yellow rectangle)**

In the second step of the algorithm, sub-regions are created in the inspection window in which the positions of the black and white stripe edges are detected. The sub-regions are in the form of a rectangle with the long side perpendicular to the direction of the stripes in the background (Fig. 8a). Based on the determined positions of the stripe edges, areas are then identified in which the angles of a single stripe edges are different from each other beyond the accepted tolerance (Fig. 8b). In addition, in areas where the edge angles are accepted, the width of stripe is also checked to determine if it complies with accepted range (Fig 8c).
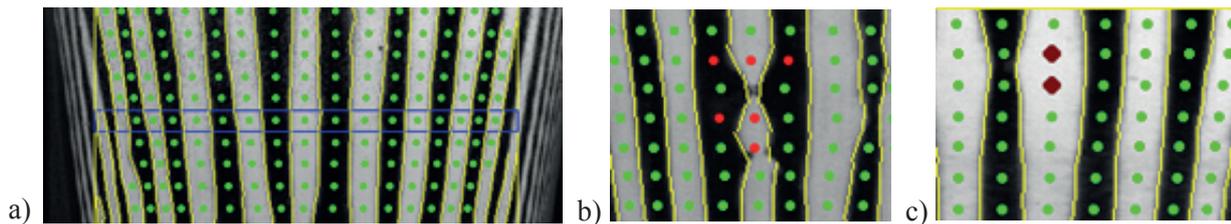
Fig. 8. **Example image: a) detection of edges in the sub-region (blue rectangle), b) stripe angle defect (light red circle), c) stripe width out of range (dark red circle)**

In the next stage, global analysis of the controlled area is performed on the basis of local inspection results from sub-regions. The final decision is made on the basis of the number of areas with small defects and their distribution or the occurrence of a critical defect in the local sub-region.

3. Experimental results

The conducted tests where made with use of a laboratory stand (Fig. 9) developed at Łukasiewicz-ITeE within the project "Creation of the Intelligent Specialisation Centre in the Field of Innovative Industrial Technologies and Technical and Environmental Safety" financed from the Regional Operational Programme of the Mazowieckie Voivodeship 2014–2020. The main objective was to check the effectiveness of the developed detection algorithms in conditions close to industrial reality. The products were transported in a closed loop at the speed corresponding to the maximum production capacity of the target glassworks. For this reason, camera exposure times were reduced below 3ms to avoid blur on the images being analysed. However, due to the low contrast in the images during the image acquisition, the binning technique was used, which solved this problem but simultaneously reduced the image resolution to 1280x1024 pixels.
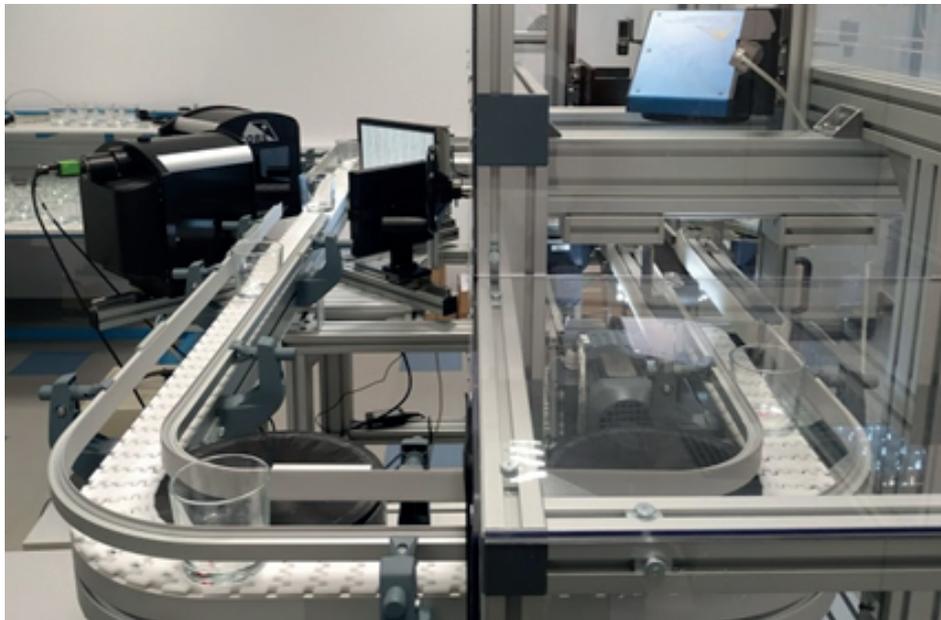
Fig. 9. Closed-loop laboratory test stand

During the tests, a system using two types of stripes patterns was evaluated. Based on the results obtained, it should be stated that this is the minimum number of patterns that provides an acceptable level of defect detection.   Due to the different deformation of the surface, some defects are more pronounced when using vertical rather than horizontal (Fig. 10) stripes and some defects are more pronounced when using horizontal rather than vertical stripes. It is also worth noting that typical defects are visible in the same way when rotated 180 degrees. Therefore, the preliminary assumption about the use of two optical paths is correct.
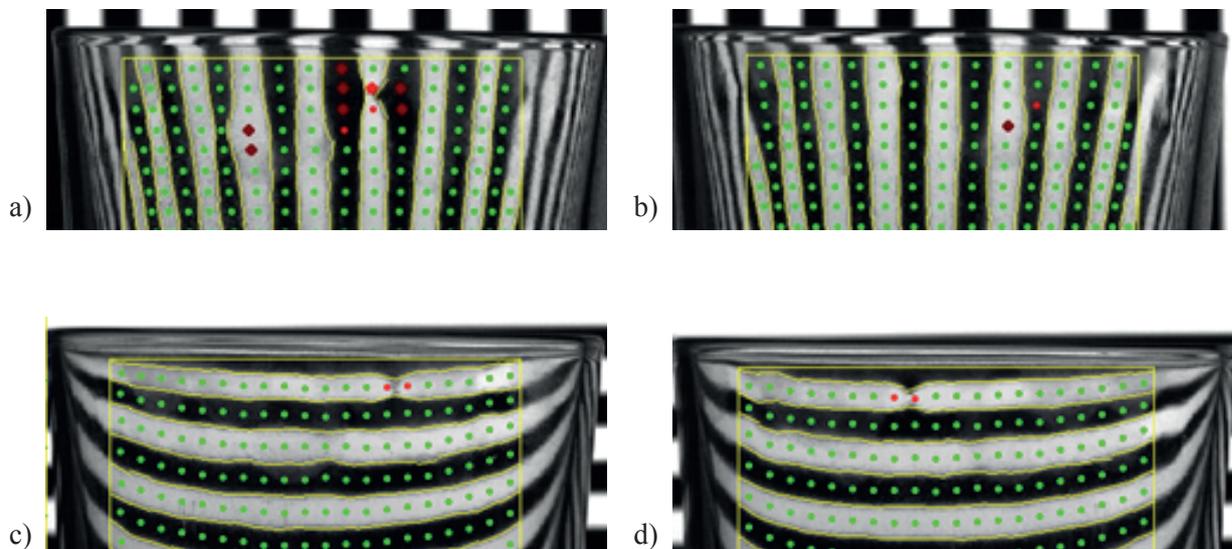
Fig. 10. Example images of tableware glass product at different rotary position and patterns: a) vertical stripe – 0°, b) vertical stripe – 180°, c) horizontal stripes – 0°, d) horizontal stripes – 180°

In the 100 articles tested, there were 40 defective products that were 100% correctly classified. However, a significant percentage of false identifications (approx. 5%) were also observed. A large number of these identifications can be caused by a subjective assessment of the glassworks quality control department stuff. Therefore, the level of system sensitivity must be determined in the future in order to achieve the highest level of productivity while eliminating significant flaws.

Conclusions

The growing demand for better and more reliable inspection systems for many manufacturing industries leads to the development of more sophisticated solutions. The costs of inspection system installations are not only considered in terms of return on investment but also in terms of the company's reputation and achieving quality above the standard level present on the market. Although the defect for which the presented detection system is dedicated is not critical in terms of product safety, the large number of articles it can inspect justifies its use to reduce the number of entire batches of glass products being returned to the glassworks. This is also associated with high costs of customer complaints.

The presented method is characterized by the high efficiency of optical distortion detection. However, it can cause a significant level of false-positive identification. For this reason, proper parameterization of detection algorithms by system operators is very important. In addition, it allows one to detect other types of defects such as cracks or inclusions, which further increases the reliability of the entire inspection system. A limitation of the proposed method may be the increase in dimensions of the cold-end inspector, which, in many cases, can prevent installation at the end of the production line.

Future work will be focused on building a prototype system to be tested on the production line. Tests carried out under real conditions will allow the verification of the proposed method. Another direction of research will be implementation of additional types of stripe patterns in the designed imaging system.

References

1. Garbacz P.: Inspection of Tableware Glass Products at the Hot End of Production Line. *Journal of Machine Construction and Maintenance,* 2019, 112(1), pp. 77-84.
2. Garbacz P., Czajka P.: Vision Techniques For The Inspection Of Tableware Glass Products. *Problemy Eksploatacji – Maintenance Problems,* 2016, 4, pp. 17–29.
3. Brodersen J.: *Phase Measuring Deflectometry for Machine Vision*. [Online]. 2019. [Accessed 20 December 2019]. Available from: http://smartvisionlights.com/blog/phase-measuring-deflectometry-for-machine-vision
4. Fermum L.: *Inspecting Transparent Objects*. [Online]. 2019. [Accessed 20 December 2019]. Available from: www.stemmer-imaging.com
5. Opto Eingeering: *Telecentric Lens Tutorial*. [Online]. 2019. [Accessed 20 December 2019]. Available from: www.opto-e.com
6. Opto Engineering: *TC CORE PLUS series*. [Online]. 2019. [Accessed 20 December 2019]. Available from: www.opto-e.com/products/TCCORE-PLUS-ultra-compact-bi-telecentric-lenses#Insight
7. Hollows G.: *Eliminate Image Distortion*. [Online]. 2007. [Accessed 20 December 2019]. Available from: https://www.qualitymag.com/articles/89447-eliminate-image-distortion
8. West P.C.: *High Speed, Real-Time Machine Vision*. [Online]. CyberOptics, 2001. [Accessed 20 December 2019]. Available from: http://www.imagenation.com/pdf/highspeed.pdf
9. Litemax: *Main website*. [Online]. 2019. [Accessed 20 December 2019]. Available from: www.litemax.com
10. Matrox Imaging: *Matrox 4Sight EV6*. [Online]. 2019. [Accessed 20 December 2019]. Available from: www.matrox.com/imaging/en/products/vision_systems/4sight_ev6

Jarosław MOLENDA, Bernadetta KAŹMIERCZAK*
ŁUKASIEWICZ Research Network – Institute for Sustainable Technologies, Radom, Poland
* Corresponding author: bernadetta.kazmierczak@itee.radom.pl

THE USE OF SPECTRAL METHODS TO IDENTIFY THE MICROSTRUCTURE AND CHEMICAL STRUCTURE OF BIOCARBONS USED IN THE PROCESSES OF THE EXPLOITATION OF TECHNOLOGICAL LIQUIDS

Key words: biocarbons, biocarbon structure, X–ray energy dispersion spectroscopy (EDS), infrared spectrophotometry (FTIR), the Raman spectroscopy.

Abstract: In the dynamic development work in the use of plant waste to produce biocarbons, the assumed sorption capacity resulting from the chemical structure of the surface determines the need to adapt the advanced spectral methods to test the quality of newly-manufactured materials. In this paper, the usefulness of X-ray energy dispersion spectroscopy (EDS), infrared spectrophotometry (FTIR), and Raman spectroscopy techniques to determine the chemical composition and identification of functional groups and the ordering of the biocarbon crystal structure were determined. In particular, examples of the interpretation of obtained spectra are presented. The EDS technique allows the determination of changes in the chemical composition occurring during pyrolysis under certain thermal conditions. Thanks to infrared spectrophotometry (FTIR), information was obtained about functional groups present on the surface of biocarbon, as well as directions of structural changes occurring in cellulose waste due to pyrolysis, which are dependent on temperature conditions. The Raman spectroscopy allowed the assessment of the degree of ordering of biocarbon structures based on the identification of the intensity of spectral signals corresponding to the D band, characteristic for the amorphousity of carbon structures and the G band, indicating the ordering of carbon structures. These techniques are a package of complementary analytical methods that allow for a comprehensive study of the chemical structure of biochar, which is a product of the pyrolysis of waste of plant origin, which is used, among others, in processes of the exploitation of technological fluids, particularly for purifying industrial waters.

Zastosowanie metod spektralnych do identyfikacji mikrostruktury i budowy chemicznej biowęgli wykorzystywanych w procesach eksploatacji cieczy technologicznych

Słowa kluczowe: biowęgle, budowa biowęgli, rentgenowska spektroskopia dyspersji energii (EDS), spektrofotometria w podczerwieni (FTIR), spektroskopia Ramana.

Streszczenie: Dynamiczny rozwój prac w zakresie wykorzystania odpadów roślinnych do produkcji biowęgli o założonych zdolnościach sorpcyjnych, wynikających m.in. ze struktury chemicznej powierzchni, determinuje konieczność adaptacji zaawansowanych metod spektralnych do badania jakości nowo wytwarzanych materiałów. W niniejszej pracy określono przydatność techniki spektroskopii rentgenowskiej z dyspersją energii (EDS), spektrofotometrii w podczerwieni (FTIR) i spektroskopii Ramana do określenia składu chemicznego oraz identyfikacji grup funkcyjnych oraz uporządkowania struktury krystalicznej biowęgli. W szczególności przedstawiono przykładowe sposoby interpretacji uzyskiwanych widm. Technika EDS pozwala na określenie zmian w składzie chemicznym zachodzących podczas pirolizy w określonych warunkach termicznych. Dzięki spektrofotometrii w podczerwieni (FTIR) uzyskano informacje o grupach funkcyjnych obecnych na powierzchni biowęgli, a także o kierunkach przemian strukturalnych zachodzących w odpadach celulozowych na skutek pirolizy, które są zależne od warunków temperaturowych. Natomiast spektroskopia Ramana pozwoliła na ocenę stopnia uporządkowania struktur biowęglowych na podstawie identyfikacji intensywności sygnałów spektralnych odpowiadających pasmu D, charakterystycznemu dla amorficzności struktur węglowych i pasmu G, świadczącym o uporządkowaniu struktur węglowych. Wymienione techniki stanowią pakiet uzupełniających się metod analitycznych, pozwalających na kompleksowe zbadanie struktury chemicznej biowęgli, stanowiących produkt pirolizy odpadów pochodzenia roślinnego, znajdujący zastosowanie m.in. w procesach eksploatacji cieczy technologicznych, w szczególności do oczyszczania wód przemysłowych.

Introduction

Currently, a significant increase in interest in biocarbons is observed, including their specific surface, properties, and the possibility of their application in environmental protection [1]. The biocarbon is similar in structure to charcoal. The developed specific surface, microporosity, or the presence of functional groups make biocarbon an increasingly popular sorbent, and thus encourage researchers to carry out more and more extensive work on their properties and practical application [1]. The chemical structure of the surface of coals significantly affects its adsorption, acid-base, oxidation-reduction, as well as catalytic and electrochemical properties. These properties depend to a large extent on the occurrence of function groups (mainly oxygen and nitrogen) on the surface, arising directly at the pyrolysis stage or introduced during the physical or chemical activation of carbon precursors [2–6]. A characteristic feature of biocarbon is their very well-developed porous structure [7]. However, the structure and physicochemical properties of biocarbon differ depending on the biomass from which they were obtained, as well as the thermal parameters of pyrolysis [8].

The knowledge of the structure and, above all, the chemical composition of biocarbon and the presence of functional groups formed on their surfaces determines the areas of the application of this type of products as effective sorbents intended for removing pollution from sewage and industrial oils, removing toxins and odours from the air, improving the quality of produced pharmaceutical, petrochemical and food products, as well as drinking water treatment [9–14].

The correct selection of biocarbon for specific applications requires knowledge of their structural features, including their chemical structure. Therefore, checking the impact of their production technology on the chemical structure is essential in forming the physicochemical properties of the biocarbon at the stage of their production. Thus, it is necessary to use advanced analytical techniques enabling comprehensive analysis of biocarbon quality. The spectral techniques are very useful in this area. To determine the physicochemical properties of biocarbon, i.e. the structure, chemical composition or the presence of functional groups on their surface, it is necessary to use advanced spectral analysis techniques, in particular, infrared spectrophotometry (FTIR), X-ray energy dispersion spectroscopy (EDS), and Raman spectroscopy [15–18]. The analysis of biocarbons using these techniques allows obtaining information on their microstructure, the presence of functional groups on their surface, and their chemical composition.

The aim of the work was to present a comprehensive approach to the determination of the microstructure and chemical structure of biocarbon, obtained pyrolytically from plant biomass, using spectral analysis methods.

The paper presents sample results illustrating the scope of information obtained from spectral analyses carried out using the FTIR method, Raman spectroscopy, and the EDS technique.

Materials and method

The characteristics of research objects

The vegetable waste, i.e. cherry stones and biocarbon obtained during the pyrolysis of cherry stones at temperatures up to 500°C and up to 700°C were used as demonstrative materials used in spectral tests. The waste plant that was used during laboratory work was dried and characterized by a moisture content not exceeding 10%. The procedure for preparing and carrying out cherry stones pyrolysis was described in an earlier work [19]. Infrared spectrophotometry (FTIR), X-ray energy dispersion spectroscopy (EDS), and Raman spectroscopy were used to study the microstructure of biochar obtained from cherry seeds and to identify their elemental composition.

FTIR infrared spectrophotometry

The FTIR technique is used to identify the structure of biochar functional groups. By using the FTIR technique, it is possible to identify the types of bonds, and the effects of the vibration of ions and molecules in crystal lattices in the tested material. The most important groups that can be analysed by the FTIR technique include carbonyl groups, -OH groups, C-H bonds, double and triple bonds (C=C, C≡C). The shape of the spectrum depends on the rotation and oscillation of chemical bonds [20]. In the FTIR spectrum, several ranges of key wave numbers can be distinguished for identifying the chemical structure of the material being tested. For example, the range 4000–2500 cm^{-1} corresponds to the valence vibrations of O–H, N–H, C–H, S–H, CH_2 and CH_3 bonds. The range of 2500–2000 cm^{-1} is the valence vibrations of the C=C=C system and the triple bonds C≡N and C≡C. The 2000–1500 cm^{-1} range includes valence vibrations of C=C, C=O, C=N, N=N double bonds, deformation vibrations of N–H and O–H bonds from water. The range of 1500–650 cm^{-1} is a dactyloscopic area, which is difficult to interpret, and contains mainly valence vibrations of C–C, C–N, C–O bonds and C–H deformation vibrations [21]. Due to the above, spectrum analysis allows the identification of emerging functional groups during radical reactions occurring during pyrolysis, and also allows the destruction of bonds, e.g., glycosidic, which is present in waste cellulosic products.

The FTIR spectra of biocarbons were obtained using a FTIR 6200 spectrometer (from Jasco) in reflection mode. For recording spectra of biocarbon, a Pike type diamond

crystal attachment was used. The following parameters were used during spectral measurements: spectral range: 4000–600 cm^{-1}, spectral resolution: 4 cm^{-1}, TGS detector, and averaging the spectrum from 30 scans.

The Raman spectroscopy

The Raman spectroscopy is used to determine the biocarbon structure. This technique involves measuring inelastic radiation of photon scattering. Very strong radiation sources are used for excitation, currently only lasers. The Nd: YAG (yttrium-aluminium), XeF or KrF lasers are most commonly used. The Raman spectroscopy gives spectra containing oscillatory bands corresponding to the normal vibrations of the molecules. The intensity of Raman bands is determined by the change in polarizability during normal vibration, not the change in the electric dipole moment, as for infrared bands. Using this technique, it is possible to determine the crystal form, chemical composition, intermolecular interactions, the degree of ordering, and the spatial distribution of stresses in the tested material [22–26].

The Raman spectra were taken at room temperature using an NRS-5100 spectrometer from Jasco (Japan), using green laser excitation with a wavelength of 532 nm and an exposure time of 100 seconds. The spectra were recorded in the Raman range from 260 cm^{-1} to 3900 cm^{-1} with a resolution of 3.2 cm^{-1}.

The X-ray energy dispersion spectroscopy (EDS)

The X-ray energy dispersion spectroscopy (EDS) is used to determine the chemical composition of biocarbon. This technique is usually connected with scanning electron microscopy (SEM) enabling the selection of x-ray examination sites in the microstructure. The EDS is a technique that uses the measurement of X-rays emitted by the material under study as a result of its excitation with an electron beam. In the EDS technique, the energy of individual x-ray photons produces a current charge in a semiconductor detector, where it is converted into a voltage pulse. The content of elements is determined by the proportional dependence of the number of characteristic X-ray pulses emitted on the concentration of elements in the tested sample [27]. The EDS technique allows for elemental qualitative and quantitative analysis of the tested material, which consequently allows the verification of the presence of molecular structures identified by other spectral techniques.

A Hitachi SU-70 scanning electron microscope equipped with EDS x-ray microanalyser was used to identify the biocarbon elemental composition. The analyses were carried out under the following conditions: magnification x500, x1000, and x2000, accelerating voltage 15 kV, receiving angle 30°, and vacuum 10^{-8} Pa.

Results and discussion

Evaluation of surface chemistry of biocarbon

The approach to the interpretation of FTIR spectra enabling the determination of functional groups was presented on the basis of a comparative analysis of spectra obtained for biocarbons obtained from cherry stones (Fig. 1).
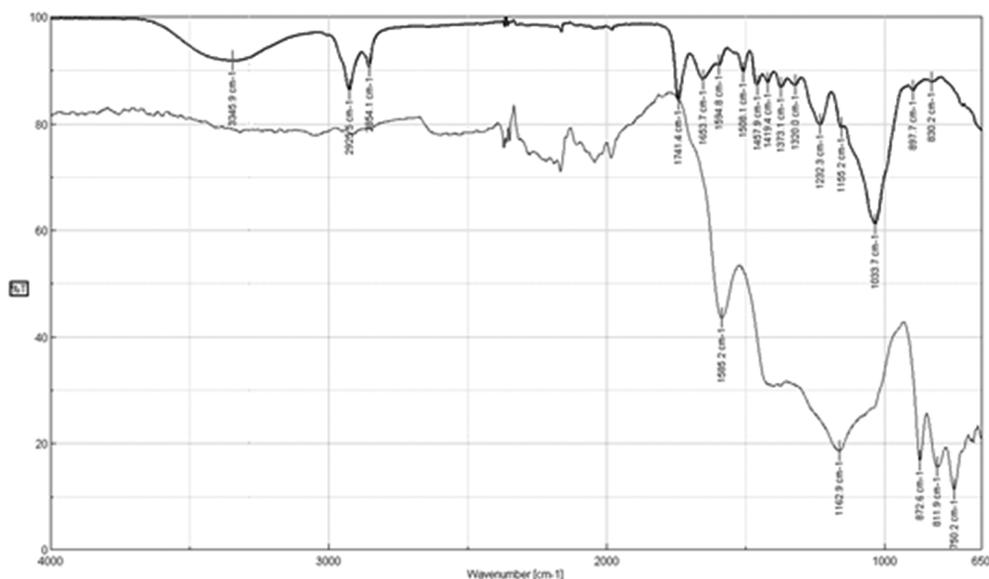
Fig. 1.   The comparison of FTIR spectra of cherry stones (a) before and (b) after pyrolysis at 500°C

The analysis of recorded infrared spectra indicates the lack of vibration signals stretching the oxygen-hydrogen bond in hydroxyl groups, which were recorded in the spectra of plant waste before pyrolysis. In the spectrum obtained for cherry stones, the extreme spectral band was located at approx. 3346 cm⁻¹. This means that the hydroxyl group present in cellulose is destroyed by pyrolysis. Therefore, hydroxyl, optionally hydrogen and oxygen radicals can be generated. It should also be noted that hydrocarbon functional groups also undergo structural conversion during pyrolysis, which is manifested by the disappearance of spectral bands in the 3000–2800 cm⁻¹ wave number range (valence vibrations of C-H structures in methyl, methylene and methine groups) in FTIR biocarbon spectra compared to the waste spectra before pyrolysis. The binding of glycoside in cellulose is also destroyed, as evidenced by

the lack of bands in the biocarbon spectra corresponding to the -C-O-C- group, i.e. located at a wavelength of about 1034 cm⁻¹. A detailed analysis of the biocarbon spectra obtained during pyrolysis allows us to conclude that structural products containing oxygen and nitrogen are present in the obtained products. In particular, in the spectra of biocarbon from cherry stones obtained, a clear signal is observed located at a wave number of 1585 cm⁻¹. These bands are located in the vibration region of coupled C=C and C=O bond systems, and thus aromatic ring structures with a ketone group may be formed.

The presented comparative analysis clearly shows that the FTIR technique allows the description of chemical changes occurring during pyrolysis. In addition, this technique allows the assessment of the impact of technological parameters on the chemical structure of pyrolysates. Exemplary results are shown in Fig. 2.
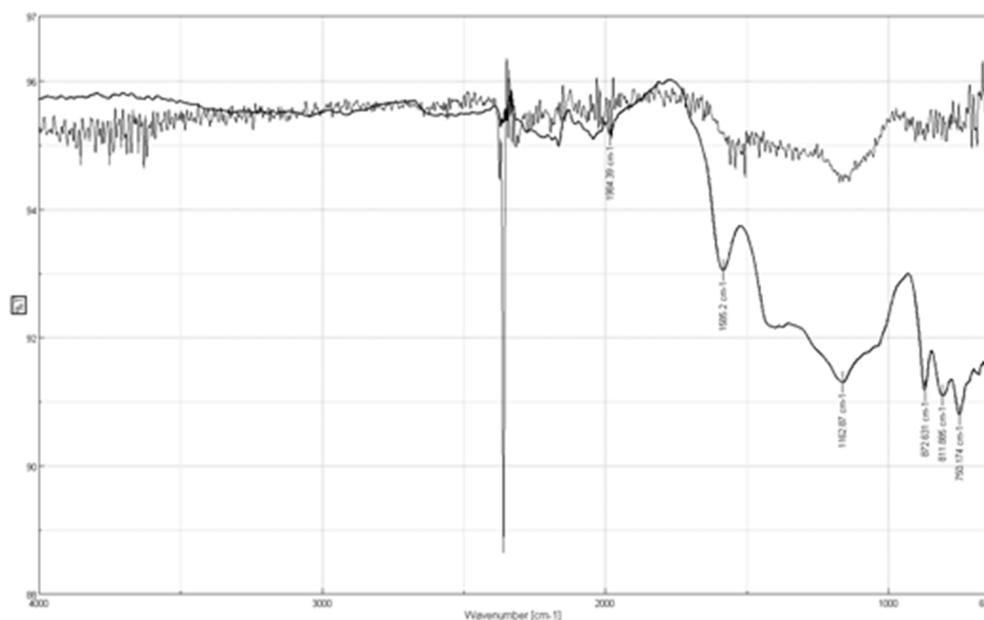
Fig. 2.   The comparison of FTIR spectra of biocarbon obtained from cherry stones under the following thermal conditions: a) up to 500°C, b) up to 700°C

The analysis of recorded infrared spectra indicates that the temperature conditions of pyrolysis determine the chemical structure of the products obtained. Under thermal conditions up to a temperature of 500°C, carbon products are formed, containing organo-oxygen structural groups in their structure coupled with carbon-carbon double bonds in aromatic rings. This is evidenced by spectral bands located in the biocarbons spectra obtained from cherry stones at a wave number of 1585 cm⁻¹ [15]. Increasing the pyrolysis temperature to 700°C leads to the disappearance of the abovementioned bands in the FTIR spectra of the biocarbon. High-temperature pyrolysis reduces the possibility of the formation of active organo-oxygen structures on the biocarbons

surface. Biocarbons obtained from cherry stones when heated to 700°C do not contain functional groups such as carbonyl or quinone group independently occurring on the carbon surfaces of oxygen, identifiable by means of infrared spectrophotometry. The C=O bond vibration band in quinones occurs at a wave number of 1657 cm⁻¹. However, the band at the wave number 1617 cm⁻¹ corresponds to the vibrations of the aromatic ring. The confirmation of the occurrence of the mentioned molecular structures is the band discussed earlier at the wave number 1576 cm⁻¹, associated with the vibrations of the C=C moiety in the aromatic ring, connected with the C=O carbonyl group. However, the incorporation of oxygen into carbon cyclic structures in the form of ether bridges is likely, which

can be indicated by spectral bands present in the spectra of products obtained at higher temperatures, whose maxima are in the range of 1020-1075 cm^{-1} (aromatic ethers) or 1060-1150 cm^{-1} (aliphatic ethers). However, the lack of clear signals from the aromatic rings in the spectra obtained indicates that, in carbon structures, C=C bonds are only a small remainder

of the originally occurring structures rebuilt during thermal treatment [28–31].

Considering the above observations, it can be concluded that the FTIR analyses carried out allow the identification of functional groups on the surface of biocarbon, which can be active centres particularly useful in sorption operations.

The identification of elemental biocarbons structure (EDS)

a)

b)
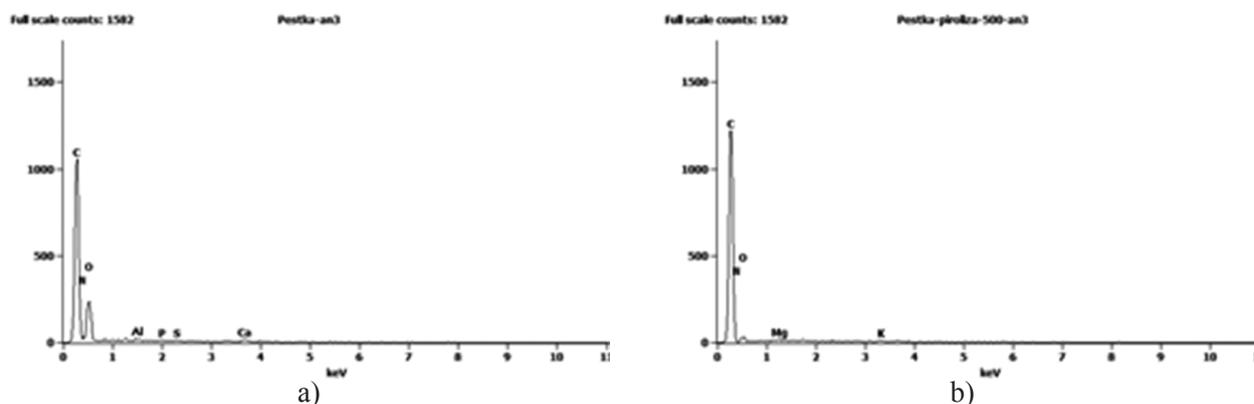
Fig. 3. The EDS spectra recorded during cherry stones testing: a) before pyrolysis, b) after pyrolysis at 500 ° C

In the tested material before and after pyrolysis, the presence of carbon, oxygen and nitrogen, i.e. elements that are part of the building material, is observed, and additionally signals from magnesium, phosphorus, calcium and potassium, i.e. elements that could be absorbed by plants from artificial fertilizers [14]. However, the current sulphur in cherry stones before pyrolysis comes from chemical compounds that create resin-oil substances. After the heat

treatment of cherry stones, sulphur is not observed in the pyrolysates, which indicates that sulphur compounds were removed along with pyrolysis oil or in gas products.

Based on EDS analyses, it is also possible to compare the percentages of the main building elements in waste materials before pyrolysis and in biocarbons obtained by pyrolysis. The examples of the results are summarized in Table 1.

Table 1. The comparison of the relative percentages of carbon and oxygen in the material before and after the pyrolysis of cherry stones

Component	The content of the component in the tested material [% mass]		
	waste before pyrolysis	biocarbon after pyrolysis to temperature 500°C	biocarbon after pyrolysis to temperature 700°C
Carbon	44.91	58.54	69.18
Oxygen	43.60	24.84	6.12

The results obtained (Table 1) indicate that in biocarbons obtained for different process conditions, a carbon content increase is observed compared to the content in the original natural waste. The highest increase in carbon content was observed for products obtained during pyrolysis carried out to a temperature of 700°C (10.64% m/m) compared to pyrolysis carried out to a temperature of 500°C. The observed changes indicate the destruction of hydrocarbon chains and the removal during the pyrolysis of elements other than carbon in the form of low-molecular chemical compounds, e.g., in the form of low-molecular hydrocarbons, sulphur oxides, carbon oxides, and others. With the increase in carbon

content, a decrease in oxygen content was observed. The greatest oxygen decrease for biocarbons was observed during pyrolysis carried out to a temperature of 700°C. The reduction of oxygen content in post-pyrolysis products indicates the breaking of carbon-oxygen bonds in the structures of hydroxyl and glycoside cellulosic wastes, followed by conversion to low-molecular products removed from the pyrolysis chamber. The oxygen determined in biocarbons can come from both the oxygen radicals released during the destruction of plant waste and then built into the biocarbons structure. The resulting functional groups associated with the biocarbons surface can be active centres in selective sorption processes.

The use of X-ray energy dispersion spectroscopy (EDS) as a modern analytical method enables a closer understanding of the surface structure of solids, as well as some of the basic phenomena occurring on them. Therefore, X-ray energy dispersion spectroscopy (EDS) is undoubtedly one of the most important tools used in biocarbon characteristics. The X-ray energy dispersion spectroscopy (EDS) spectra can be used to identify the chemical composition of small sample fragments.

Research on crystalline and amorphous biocarbon structures

The analysis of the structure of the obtained biocarbon, including the evaluation of the ordering of the crystal structure was possible thanks to research using the Raman spectroscopy. The examples of spectra allowing a comparison of the characteristics of biocarbon obtained at different temperatures are shown in Figure 4.
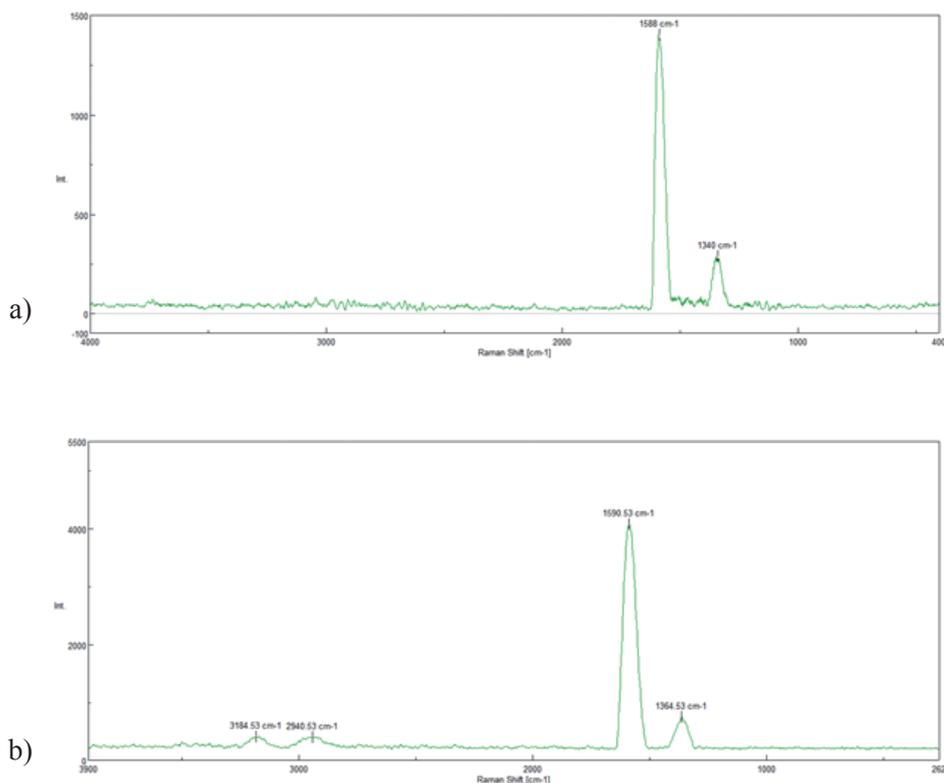
Fig. 4. The comparison of Raman spectra of biocarbon obtained during pyrolysis of cherry stones conducted at the temperature of: a) Stone 700°C, b) Stone 500°C

The spectra of the studied biocarbon contain bands directly related to the vibrations of carbon and hydrocarbon structures. In the case of analysis of the Raman spectra obtained for biocarbon from cherry stones by pyrolysis at 500°C and 700°C, a band size of 1580 cm^{-1}, otherwise known as the G band, is observed. This band corresponds to stretching vibrations with E_{2g} symmetry. It comes from tensile vibrations of the sp^2 hybridization of the carbon bond pairs occurring in ring structures. This band occurs in the case of graphite with an ordered structure. An additional band located at the Raman shift above 1340 cm^{-1} and 1364 cm^{-1} characterizes the level of amorphousness of carbon structures and indicates a highly disordered biocarbon structure. This band is usually called the D1 defect band. It corresponds to A1g symmetry and is associated with plane imperfections, e.g., defects and heteroatoms [19, 24, 32].

The Raman spectroscopy is a new technique that has recently been used in many analytical areas. The use of this technique in biocarbons analysis is a new, intensively developed issue. Raman spectroscopy, like infrared spectroscopy, provides information about the structure of the molecule, the interatomic bonds that make it up, as well as about their polarizability. Thus, it can be concluded that Raman spectroscopy is complementary to FTIR spectroscopy and vice versa.

Conclusion

By using such techniques as X-ray energy dispersion spectroscopy (EDS), infrared spectrophotometry (FTIR), and Raman spectroscopy, one can determine the microstructure, chemical composition, and degree

of ordering of the structure of biocarbons obtained from vegetable waste, which was demonstrated by the example of testing products made from cherry stones on by pyrolysis in two temperature ranges of 500°C and 700°C. The analysis of biocarbons obtained during pyrolysis up to 500°C by infrared spectrophotometry (FTIR) allowed the determination of the occurrence of organo-oxygen groups that may be useful during physicochemical sorbing of polar compounds or chelating metal ions. The biocarbons obtained up to a maximum value not exceeding 700°C, on the other hand, have ether moieties embedded mainly in aliphatic cyclic moieties. By using the X-ray energy dispersion spectroscopy (EDS), it is possible to analyse the elemental composition of biocarbons. Analysis of the obtained charts and tables showed a decrease in oxygen content and an increase in carbon content in biocarbons. The reduction of oxygen content is a result of increasing the temperature of the pyrolysis process. This indicates the possibility of conversion of oxygen functional groups and oxygen removal, e.g., in gaseous products generated during pyrolysis. On the other hand, an increase in the carbon content of pyrolysis products indicates the destruction of hydrocarbon chains and the removal of low-molecular chemical elements during pyrolysis. The Raman spectroscopy analysis helped to obtain information on the degree of biocarbons structure ordering. For the obtained biocarbons, two bands are most characteristic: the G band and the D band. The G band that comes from the stretching vibrations of carbon bond pairs of sp^2 hybridization occurring in ring structures and is closely related to the occurrence of ordered carbon structures. The D band characterizes the level of the amorphousity of carbon structures. The conclusions of the study are complementary and allow one to determine the structure of biocarbons obtained from vegetable waste. The obtained results of the analyses can be used during quality control of commercial products used in various types of process fluids exploitation, in particular, for purifying industrial waters.

References

1. Malińska K., Dach J.: Biowęgiel jako materiał pomocniczy w procesie produkcji biogazu. *Inżynieria Ekologiczna*, 2015, 41, pp. 117–124 [in Polish].

2. Choma J., Kloske M.: Otrzymywanie i właściwości impregnowanych węgli aktywnych. *Ochrona Środowiska*, 1999, 2(73), pp. 3–17 [in Polish].

3. Jaramillo J., Alvarez P.M., Gomez-serrano V.: Oxidation of activated carbon by dry and wet methods. *Surface chemistry and textural modifications. Fuel Prcessing Technology*, 2010, 91, pp. 1768–1775.

4. Figueiredo J.L., Pereira M.F.R., Freitas M.M.A., Orfao J.J.M.: Modification of the surface chemistry of activated carbons. *Carbon*, 1999, 37, pp. 1379–1389.

5. Figueiredo J.L., Pereira M.F.R.: The role of surface chemistry in catalysis with carbons. *Catalysis Today*, 2010, 150, pp. 2–7.

6. Jansen J.J., Van Bekkum H.: Amination and amoxidation of activated carbons. *Carbon*, 1994, 32, pp. 1507–1516.

7. Weisser P., Malińska K.: Od biomasy do biowęgla – pomysł na biznes. *Biomasa*, 2016, 1(19), pp. 42–45 [in Polish].

8. Malińska K.: Biowęgiel odpowiedzią na aktualne problemy ochrony środowiska. *Inżynieria i Ochrona Środowiska*, 2012, 15(4), pp. 387–403 [in Polish].

9. Kobyłka A.: Zastosowanie adsorpcji na węglu aktywnym w różnych układach technologicznych oczyszczalni ścieków. *Technical Issues*, 2016, 4, pp. 27–34 [in Polish].

10. Chwiałkowski W.: Zastosowanie mieszaniny węgli aktywnych o różnym charakterze powierzchni do oczyszczania oleju posmażalniczego. *Inżynieria i Ochrona Środowiska*, 2016, 16(3), pp. 361–371 [in Polish].

11. Kaleta J., Kida M., Koszelnik P., Papciak D., Puszkarewicz A., Tchórzewska-Cieślak B.: The use of activated carbons for removing organic master from groundwater. *Archives of Environmental Protection*, 2017, 43(3), pp. 32–41.

12. Kuśmierek K., Świątkowski A.: Wpływ chemii powierzchni węgli aktywnych na adsorpcję kwasu 2,4-dichlorofenoksyoctowego. *Inżynieria i Ochrona Środowiska*, 2016, 19(2), pp. 255–263 [in Polish].

13. Lach J., Ociepa E.: Wpływ wysokotemperaturowej modyfikacji węgla aktywnego na sorpcję anionów Cr(VI) i kationów Cr(III) z roztworów wodnych. *Ochrona Środowiska*, 2003, 25(3), pp. 57–60 [in Polish].

14. Hofman M., Pietrzak R.: Adsorpcja fenolu z roztworów wodnych na modyfikowanych azotem adsorbentach otrzymanych z pestek śliwek. *Przemysł Chemiczny*, 2012, 91(12), pp. 2461–2466 [in Polish].

15. Ouhammou M., Lahnine L., Mghazli S., Hidar N., Bouchdoug M., Jaouad A., Mandi L., Mahrouz M.: Valorisation of cellulosic waste basic cactus to prepare activated carbon. *Journal of the Saudi Society of Agricultural Sciences*, 2019, 18, pp. 133–140.

16. Chen Y., Zhu Y., Wang Z., Li Y., Wang L., Ding L., Gao X., Ma Y., Guo Y.: Application studies of activated carbon derived from rice husks produced by chemical-thermal process – A review. *Advances in Colloid and Interface Science*, 2011, 163, pp. 39–52.

17. Valente Nabais J.M., Laginhas C.E.C., Carrott P.J.M., Ribeiro Carrott M.M.L.: Production of activated carbons from almond shell. *Fuel Processing Technology*, 2011, 92, pp. 234–240.

18. Sobiesiak M., Gawdzik B., Puziy A.M., Poddubnaya O.I.: Analysis of structure and properties of active carbons and their copolymeric precursors. *Applied Surface Science*, 2010, 256, pp. 5355–5360.

19. Molenda J.: The influence of the protective pyrolysis atmosphere of vegetable waste on biocarbon construction. *Journal of Machine Construction and Maintenance*, 2018, 4, pp. 99–104.

20. Zofka A., Maliszewska D., Maliszewski M.: Zastosowanie techniki FT–IR w badaniach materiałów asfaltowych. *Budownictwo i Architektura*, 2014, 13(4), pp. 317–324 [in Polish].

21. Dudkiewicz M., Berłowska J., Kręgiel D.: Oznaczanie białek metodą FTIR w produktach spożywczych i biotechnologicznych – cz. II. *Laboratorium Przemysłowe*, 2015, 9–10, pp. 44–49 [in Polish].

22. Szurgot M., Tszydel I.: Zastosowanie spektroskopii Ramana do identyfikacji minerałów meteorytu NWA 4967. *Acta Societatis Metheoriticae Polonorum, Rocznik Polskiego Towarzystwa Meteorytowego*, 2011, 2, pp. 158–170 [in Polish].

23. Merlen A., Buijnsters J.G., Pardanaud C.: A Guide to and Review of the Use of Multiwavelength Raman Spectroscopy for Characterizing Defective Aromatic Carbon Solids: from Graphene to Amorphous Carbons. *Coatings*, 2017, 7, 153, pp. 2–55.

24. Grodecki K.: Spektroskopia ramanowska grafenu. *Materiały Elektroniczne*, 2013, 41(1), pp. 47–53 [in Polish].

25. Nykiel P.: Spektroskopia Ramana: nowoczesna technika w diagnostyce medycznej i analizie biochemicznej. *Biul. Wydz. Farm. WUM*, 2013, 4, pp. 27–36 [in Polish].

26. Smith M.W., Dallmeyer I., Johnson T.J., Brauer C.S., McEwen J.S., Espinal J.F., Garcia-Perez M.: Structural analysis of char by Raman spectroscopy: Improving band assignments through computational calculations from first principles. *Carbon*, 2016, 100, pp. 678–692.

27. Słowik G.: Podstawy mikroskopii elektronowej i jej wybrane zastosowania w charakterystyce katalizatorów nośnikowych. In: Ryczkowski J. (ed.): *Adsorbenty i katalizatory. Wybrane technologie a środowisko*. Uniwersytet Rzeszowski, pp. 219–243 [in Polish].

28. Wang X., Chi Q., Liu X., Wang Y.: Influence of pyrolysis temperature on characteristics and environmental risk of heavy metals in pyrolyzed biochar made from hydrothermally treated sewage sludge. *Chemosphere*, 2019, 216, pp. 698–706.

29. Zhang G., Guo X, Zhao Z., He Q., Wang S., Zhu Y., Yan Y., Liu X., Sun K., Zhao Y., Qian T.: Effects of biochars on the availability of heavy metals to ryegrass in an alkaline contaminated soil. *Environmental Pollution*, 2016, 218, pp. 513–522.

30. Valente Nabais J.M., Laginhas C.E.C, Carrott P.J.M., Ribeiro Carrott M.M.L.: Production of activated carbons from almond Shell. *Fuel Processing Technology*, 2011, 92, pp. 234–240.

31. Molenda J., Swat M., Wolszczak M.: Budowa chemiczna i mikrostrukturalna biowęgli otrzymanych pirolitycznie z odpadów roślinnych. *Przemysł Chemiczny*, 2018, 97, pp. 1380–1386 [in Polish].

32. Ferrari A.C., Robertson J.: Interpretation of Raman spectra of disordered and amorphus carbon. *Phys. Rev. B.*, 2000, 61, pp. 14096–14107.

Anna KOWALIK-KLIMCZAK *, Monika MAKOWSKA, Ewa WOSKOWICZ, Karolina DZIOSA

Łukasiewicz Research Network – Institute for Sustainable Technologies, Radom, Poland
* Corresponding author: anna.kowalik-klimczak@itee.radom.pl

DAIRY WASTEWATER TREATMENT USING MEMBRANE FILTRATION SUPPORTED BY BIOLOGICAL PROCESSES

Key words: wastewater treatment, dairy wastewater, membrane filtration, bioaugmentation, Microalgae.

Abstract: This paper presents efficient treatment methods for dairy wastewater using membrane techniques and applying the biological utilization of secondary wastes. The influence of ultrafiltration (UF) and both ultra- and nanofiltration (UF/NF) systems on the removal efficiency of the contaminants was determined. It has been found that the UF enables the removal of larger organic compounds, whose presence on the NF membrane surface would reduce its efficiency. The recovery of water from these processes is associated with the generation of retentate, which is difficult to treat. For the utilization of the retentate, biological methods based on bioaugmentation process and microalgal culture were used. The combination of both these methods contributed to the significant reduction in the content of nutrients in the regenerated water (the total nitrogen <1.0 mg/dm^3, the total phosphorus <0.1 mg/dm^3). Furthermore, it was possible to obtain a microalgae biomass, which becomes more commonly used, e.g., as renewable energy resources. These studies are part of the prospective trends in the development of the bioeconomy, especially in a closed circuit.

Oczyszczanie ścieków mleczarskich przy użyciu filtracji membranowej wspomaganej procesami biologicznymi

Słowa kluczowe: oczyszczanie ścieków, ścieki mleczarskie, filtracja membranowa, bioaugmentacja, mikroalgi.

Streszczenie: W pracy przedstawiono metody efektywnego oczyszczania ścieków mleczarskich z zastosowaniem technik membranowych i procesów biologicznych. Zbadano wpływ ultrafiltracji (UF) oraz zintegrowanych procesów ultra- i nanofiltracji (UF/NF) na skuteczność usuwania zanieczyszczeń. Stwierdzono, że UF umożliwia usuwanie większych cząstek organicznych, których obecność na powierzchni membrany NF pogorszyłaby jej wydajność. Odzyskiwanie wody z zastosowaniem tych procesów wiąże się z powstawaniem retentatu, który jest trudny do uzdatnienia. Do tego celu w pracy wykorzystano metody biologiczne, oparte na bioaugmentacji i hodowli mikroalg. Połączenie obu tych metod przyczyniło się do znacznego zmniejszenia zawartości związków biogennych w wodzie regenerowanej (azot ogólny <1,0 mg/dm^3, fosfor ogólny <0,1 mg/dm^3). Ponadto uzyskano biomasę alg, która może znaleźć zastosowanie m.in. jako odnawialny surowiec energetyczny. Podjęte badania wpisują się w perspektywiczne trendy rozwoju biogospodarki, w szczególności w obiegu zamkniętym.

Introduction

The food industry is one of the most important and fastest growing sectors of the economy. The share in the sales value of the food industry among industries in Poland is about 24%, and it is one of the highest in Europe [1]. The dairy industry, considered the largest source of food processing waste, is also one of the largest in the food industry, both in terms of total raw material and water consumption. It is estimated that 1 dm^3 of processed milk consumes 1.44 dm^3 of water, while the production of cheese, butter or curd cheese is even more water-consuming (1.6–4.0 dm^3 of water per 1 dm^3 of milk), while milk powder requires yet more water (15−20 dm^3 water per 1 dm^3 of milk) [2]. Approximately 80−90% of used water becomes wastewater, which forces the needs for economical water management [3]. The effective use of water resources in production processes requires counteracting the wastage of water, which means the necessity to reduce the amount of industrial wastewater and to recover as much water as possible for reuse.

Modern technologies of wastewater treatment that permit closed water circuits involve processes of membrane filtration, which have already found numerous applications in the dairy industry [4–7]. Appropriately selected membrane techniques provide the opportunities to fractionate industrial wastewater mixtures into groups of approximately defined composition, thereby facilitating further use or utilization. In practice, membrane filtrations have some limitations. Thus, wastewater requires an appropriate pre-treatment step before it is directed into the filtration system. A no less important problem, requiring an urgent solution, is the utilization of retentate, which is a concentration of pollutants that did not pass through the filtration membrane. The separation of high molecular weight organic substances (fats, proteins, polysaccharides) from minerals would enable the reuse of retained compounds as components of culture media for the production of high value-added biotechnological products. One example assumes the use of food industry wastewater for fungal culture *Rhizopus oryzae* [8] or xanthan production [9]. Wastewater from the dairy industry, owing to the high water content and nutrients, is essential for microorganism growth including algae, which might be used for the production of bioenergy [10,11].

For the treatment of dairy wastewater, biological methods are also used, among which, due to its high efficiency and relatively low costs, the most common is activated sludge process [12]. This method uses activated sludge flocs that form as a result of combining heterotrophic bacteria with organic and inorganic particles. Enzymes produced by these bacteria are capable of decomposing macromolecules such as proteins, lipids, and fats into more assimilable forms, while inorganic compounds are assimilated immediately. As a result of the biochemical processes which occur, the pollutants are removed from the wastewater. The use of biological methods for the treatment of wastewater from the food industry has already been widely described in the literature [13–16]. Dairy wastewaters can be treated using systems of aerated lagoons, trickling filters, sequencing batch reactor (SBR), upflow anaerobic sludge blanket (UASB) reactors, and anaerobic filters. In some cases, anaerobic, aerobic, and anoxic series of processes are used [16]. Owing to the limitations of prolonging activated sludge processes, there is an increasing need to enhance these methods by commercially available bioactivators of selected strains of microorganisms, which are capable of oxidizing specific types of pollutants such as proteins, fats, and oils [17–20]. Bioaugmented inocula should meet specific requirements of ability to degrade pollutants and contaminants *in situ*, and after inoculation, to be durable and competitive. The result of bioaugmentation carried out by bacteria depends on the relationship between them and the

environment they occupy in terms of survival, activity, and migration [19]. Therefore, the production of such inocula involves the selection of bacteria from the same ecological niche.

An alternative treatment for wastewaters as well as secondary wastes generated during membrane filtration is to use them as media for the culture of single-celled algae [21]. Microalgae (among others, *Chlorella sp.)* are the most promising organisms due to their fast growth rate, low culturing requirements, high photosynthetic yield, and the ability to accumulate large amounts of lipids (some algae species contain even 75% of lipids in the dry residue [22]). Therefore, their valuable biomass is a renewable source of chemicals for many industrial applications [23, 24]. The ability to rapid reproduction has made them more desirable substrates than edible grains. In particular, microalgal lipids have become a promising energy source for biofuels, since the use of edible oil plants for this purpose had raised concerns about food safety [25, 26]. An industrial scale of algal lipids production is limited by high costs. Thus, different strategies are being developed to increase biomass productivity, especially desirable metabolites, reducing the costs of the culture medium, (through simplifying the way it is prepared, using low cost synthetic substitutes, and reducing energy consumption) [27].

The promising sources of nutrients for microalgae are municipal and industrial wastewater (dairy wastewater in particular), and effluents resulting from the biological decomposition of organic matter rich in easily absorbed nitrogen and phosphorus compounds [28]. Wastewater treated in anaerobic conditions is subjected to further technological processes until acceptable and safe levels of nutrients for the environment are achieved. According to the literature, the content of nutrients such as nitrogen and phosphorus in dairy wastewater is sufficient for effective algal biomass production [21]. Microalgae can be used in bioremediation of polluted waters, thus contributing to the protection of water reservoirs against the eutrophication [29,30]. The natural biosorption properties of algae can also be used to limit heavy metal ions from wastewaters and to recover valuable ones [31].

The aim of the study was to investigate the possibility of the effective treatment of dairy wastewater using membrane techniques along with the utilization of the secondary wastes. To achieve this goal, it was necessary to study the influence of the proposed membrane filtration processes on the efficiency of removal of pollutants from raw dairy wastewater and the use of biological methods, based on the bacterial and microalgal culture, in order to utilize the retentates. This proposed method of dairy wastewater treatment is a part of the strategy for sustainable development by saving water resources and minimizing environmental emissions resulting from wastewater and secondary wastes from industrial sources.

1. Materials and methods

1.1. Dairy wastewater

The object of the research was the raw dairy wastewater generated during the cleaning of the technological line in the production plant. The experiment included the analyses of raw wastewater, permeate, and retentate after ultra- (UF) and nanofiltration (NF), as well as samples after biological wastewater treatment using bacterial and microalgal culture. Due to the presence of suspended solids, it was necessary to pre-treat the dairy wastewater before the membrane filtration processes. For this purpose, a polypropylene filter bag (removal rating 5 μm) was used. The values of the physico-chemical parameters of raw and filtered dairy wastewater are listed in Table 1.

Table 1. Physico-chemical properties of dairy wastewater

Parameter	Value	
	Raw wastewater	Filtered wastewater
Total nitrogen, mg/dm^3	51.7	40.5
Total phosphorus, mg/dm^3	9.7	8.7
Chemical oxygen demand, mg/dm^3	2 430	1 090
Volatile fatty acids, mg/dm^3	139	136
Total organic carbon, mg/dm^3	1 551	571
pH	8.9	8.7
Conductivity, μS/cm	840	933
Dry residue, mg/dm^3	1 980	1440
Turbidity, NTU	844	400
Total suspended solids, mg/dm^3	1 092	426
Sulphates, mg/dm^3	210	143
Calcium, mg/dm^3	22.8	23.0

1.2. Membrane filtration

The membrane processes (UF and NF) were carried out using laboratory scale set-up (Fig. 1) with detailed description given in the previous work [32]. The ultra- and nanofiltrations were performed under transmembrane pressure: 6 and 14 bar, respectively. The retentate flow rate was 0.23 m^3/h for both processes. The values of transmembrane pressures were determined based on the previous studies on the dairy products and dairy wastewater [33–35], and the retentate flow rate depended on the construction of the laboratory scale membrane set-up. During the membrane processes, the temperature in the feed tank was constant and equal to 25±1°C. The ultra- and nanofiltration were carried out in the batch mode. A permeate was collected in a separate tank and a retentate was recycled to the feed tank.
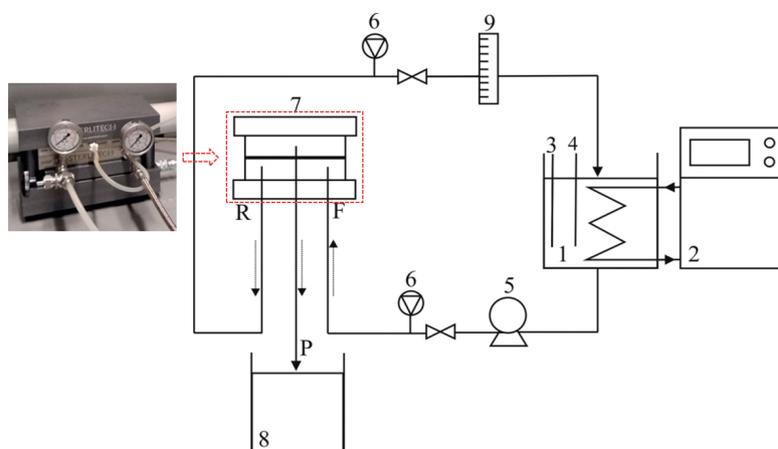
Fig. 1. Schematic diagram of the membrane system set-up: 1 – feed/retentate tank, 2 – thermostat, 3 – thermometer, 4 – pH-meter, 5 – pump, 6 – manometer, 7 – SEPA CF membrane cross-flow cell, 8 – permeate tank, 9 – flow-meter, P – permeate, F – feed, R – retentate

The flat sheet ultra- and nanofiltration membranes dedicated for protein-contaminated wastewaters were used in the experiments. The total active membrane area was 0.0140 m^2. The characteristics of the membranes used in experiments were shown in the Table 2.

Table 2. Characteristics of the membranes used in experiments

Characteristics	Manufacturer's data	
	UF membrane	NF membrane
Manufacturer	Synder	GE Osmonics
Material	PVDF*	PPZ/PSU**
Cut-off, g/mol	50 000	150-300
pH of feed	3-10	2-11
Process temperature, °C	<60	<50

*PVDF – POLYVINYLIDENE FLUORIDE, **PPZ – POLY(PIPERAZINE-AMIDE), PSU – POLYSULFONE

1.3. Calculated parameters

The efficiency of the membrane processes of dairy wastewater were determined with permeate flux (J_p, $dm^3m^{-2}h^{-1}$):

$$J_p = V_p/(A \cdot t), \qquad (1)$$

where

V_p – permeate volume, dm^3;

A – membrane area, m^2;

t – time needed to collect a defined volume of permeate, h.

The effectiveness of dairy wastewater treatment, using membrane filtration and biological methods, were evaluated based on weight-to-volume percentage reduction in solution contamination (R, % w/v):

$$R = (1 - C_1/C_2) \cdot 100, \qquad (2)$$

where

C_1 – the concentration of the component in the solution after the treatment, mg/dm^3;

C_2 – the concentration of the component in the solution before the treatment, mg/dm^3.

In the membrane terminology, R is called the retention.

1.4. Bacterial culture

The UF retentate was utilized using biological processes via an inoculum of bioaugmented bacteria. The experiments were conducted in a laboratory bioreactor with an active capacity of 1 dm^3 which were equipped with magnetic stirring elements and aeration system. The bacterial activators which were used (SK-BIOACTIV-05) in the study were comprised of the specialized, highly efficient aerobic, anaerobic, and facultative anaerobic microorganisms capable of degrading pollutants in dairy wastewaters. In addition to bioaugmented bacteria, the bio-product also contains specific micro- and macroelements (trace metals, vitamins, amino acids, and metabolic stimulants) necessary for their sustainable development. In order to maintain the environment suitable for the microorganisms, the pH of the retentate was adjusted to 7.5 with 1M hydrochloric acid. The biological treatment of the UF retentate was carried out in a 24-hour bioreactor cycle at 20°C. The process duration depended on the dynamics of the stabilization of the organic and nutrients content and was 11 days.

1.5. Microalgal culture

The UF retentate and the same after the treatment with bacteria were used as culture media for growth of microalgae biomass. The selection of algae species for the experiments was mainly based on the ability of the species to adapt to the specific environmental conditions, resistance to the contaminants, and rapid cell growth. The most commonly found (in both freshwater and the marine environment) species of algae from the green algae group is *Chlorella vulgaris*.

The laboratory culture was inoculated with *Chlorella sp.* (inoculum volume was 20 cm3), which was derived from our own culture, initiated by the inoculum obtained from Culture Collection of Baltic Algae (Institute of Oceanography of the University of Gdańsk). The experiments were performed in the Erlenmeyer flasks with a capacity of 1 dm3. The volume of each suspension was 700 cm3. The cellulose plugs provided free gas exchange between the culture medium and the environment. The source of the artificial light with the selected wavelength (characteristic for chlorophyll) was 30 W LED lamp (*Neonica Growy LED 118*) placed in a horizontal position within 20 cm of the flasks. The lighting conditions of the culture were changed periodically – photoperiod of 16h/8h (light/dark). The culture was conducted at room temperature (25±1oC) with a forced stirring (160 rpm) using a *Heidolph Unimax 2010* orbital shaker. The appropriate circulation of the medium facilitated the maintenance of algal cells in a suspension and their flows to the best lit areas, the transport of CO_2, as well as the distribution of nutrients.

The experiment was continued until the total phosphorus content in the culture medium decreased below 1 mg/dm^3. The UF retentate required 25 days, while UF retentate after biological treatment using bacteria needed 16 days.

1.6. Physico-chemical analysis

The total suspended solids (TSS) in water solutions (25-cm^3 sample volume) was determined by a *HACH DR6000* UV-VIS Spectrophotometer (accuracy +/-1 nm, resolution +/-0.1 nm, optical path 1"). Furthermore, chemical oxygen demand (COD), total nitrogen bound (TNb), total phosphorus (TP), volatile fatty acids (VFAs), total organic carbon (TOC) and sulphates, using appropriate LCK cuvette tests, were identified in the samples. The instrument automatically averages 10 measurements for each sample and eliminates outliers. The samples of retentates after biological treatment (with both bacterial and algal culture) were taken every few days, and before the physico-chemical analysis, they were filtered with a paper filter (0.17 mm, 75 g/mm^2), since a suspended biomass may be the reason of measurement errors.

Measurements of pH and conductivity were carried out using a *Mettler Toledo Seven Multi* pH/Conductivity Meter. The concentrations of calcium ions were determined by means of *Mettler Toledo* ion selective electrodes. The turbidity measurements were performed using a *HACH 2100Q is* Portable Turbidimeter.

The dry residue content was determined by weight method. The samples (~5 cm^3) were placed on aluminium disposable weighing pans inside a Radwag MAC 50/1 Moisture Analyser. During analysis, a standard drying profile was used (no change in weight of 0.001 g over 60 s at 105°C).

2. Results and discussion

2.1. Membrane filtration performance

In the first step of the experiments, the possibility of using UF for the treatment of dairy wastewater was investigated (Fig. 2a). During the UF process, a permeate flux was reduced by 13% compared to the initial value of permeate flux 25 dm^3/(m^2·h). It was found that the UF membrane used was able to completely remove total solid suspensions in the dairy wastewater, and it also contributed to a significant reduction in the concentration of nutrients such as total nitrogen (68%) and total phosphorus (56%) (Fig. 2a). It was also found that the only 22% of organic compounds were retained in the UF (Fig. 2a). This suggests that the predominant organic substances in the wastewater constituted lactose, organic acids, and peptides, which, like mineral salts, penetrate the pores of the UF membrane. The retention of calcium ions at 50% (Fig. 2a) was likely due to the presence of casein micelles containing calcium phosphates. Nevertheless, the treatment of dairy wastewater in the UF was not efficient. Since the dairy wastewater primarily had contained organic compounds of low molecular weight, it was necessary to use a membrane with a much lower cut-off limit. In order to remove low molecular weight organic compounds from the dairy wastewater, the NF was used, whose separation capabilities have been widely described in the literature [33–36]. However, during the NF of dairy wastewater, a 60% decrease in permeate flux was observed compared to the initial value of 67 dm^3/(m^2·h). It was caused by the deposition of dairy components on the surface of the NF membrane. The dominant components of the filter cake on polymer membranes used for whey and milk filtration are proteins, but lactose and minerals have also been identified [37]. The same composition of the filter cake on the NF polymeric membranes during dairy wastewater treatment was most likely. For economic reasons, direct treatment of dairy wastewater in the NF is not highly recommended. Therefore, the dairy wastewater was subjected to treatment in an integrated system consisting of UF and NF membranes.


a)
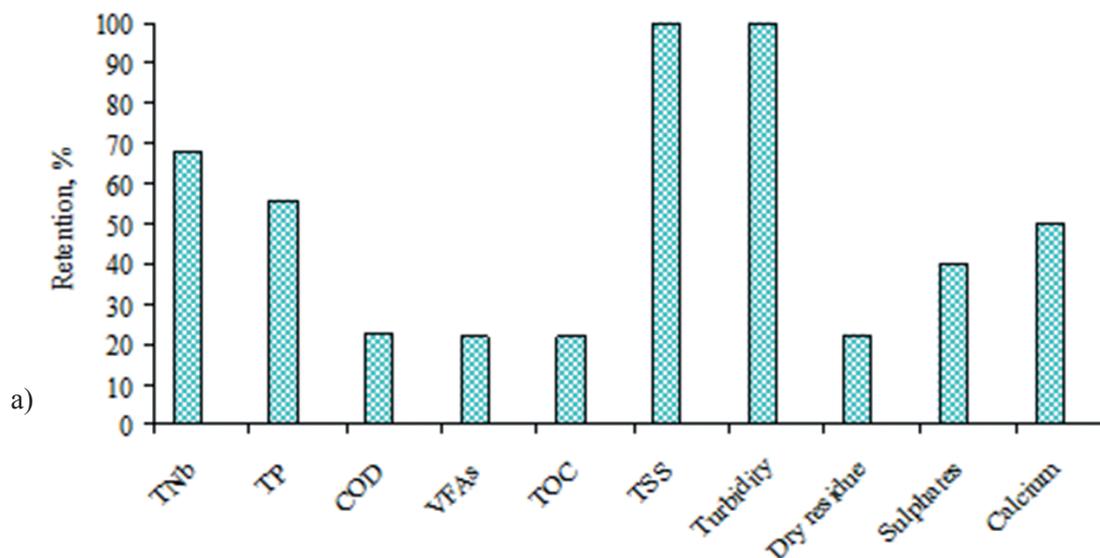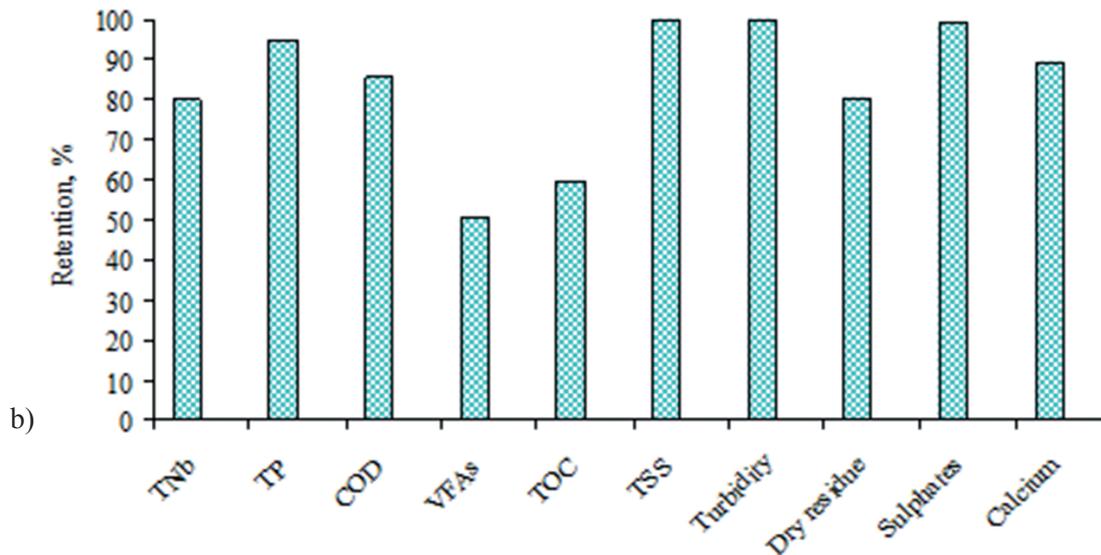
Fig. 2. Retention of individual components of dairy wastewater in the process of: (a) UF and (b) UF/NF

The ultrafiltration made it possible to remove the larger molecular organic compounds, which would reduce the efficiency of the process by adsorption on the surface of the NF membrane. In the case of the nanofiltration of dairy wastewater pre-treated via ultrafiltration, only a 4% decrease in permeate flux was noted compared to the initial value 117 $dm^3/(m^2 \cdot h)$. It was found that the system consisting of UF and NF allowed a very high degree of the removal of organic matter from the dairy wastewater (Fig. 2b). The NF membrane also allowed a significant depletion of the sulphate and calcium ions concentrations (Fig. 2b).

Based on the obtained results, it has been found that the pre-filtration through 5μm pores filter bag followed by integrated system of UF/NF is a rational way to treat dairy wastewater. These key steps enable the efficient regeneration of water from dairy wastewater. However, the recovery of water from dairy wastewater through membrane filtration is related to the waste stream in the form of a retentate, which is a concentrated mixture of pollutants retained by a membrane. In the system of UF/NF proposed for dairy wastewater treatment, there was a retentate generated in UF process, which was characterized by high molecular weight organic compounds and nutrients. The obtained results were compared to the acceptable parameters, which, according to the current regulations (in Poland and in the EU), should be met by wastewater discharged into water or soil. Significant exceeding of these parameters necessitates the need to develop methods of effective utilization of the retentate. The organic and inorganic compounds present in wastewater should not be discharged into water and soil without appropriate pre-treatment. Otherwise these might contribute to undesirable interferences in the aquatic ecosystems of living organisms as well as deterioration of water quality [33]. Therefore, wastewater with high nutrient content is usually directed towards further technological processes (including biotechnological processes) aimed at achieving the levels of contaminants which are safe for the environment.

In the next step of the experiment, the possibility of utilization of the UF retentate was investigated using bacteria as well as algae for which wastewater could be a source of valuable nutrients.

2.2. Efficiency of bacterial treatment

The retentate which was a concentrate of pollutants retained by the UF membrane was subjected to bioaugmentation process with the aid of a bioactivator consisting of bacterial cells. The effectiveness of the method applied was evaluated based on the degree of removal of individual pollutants. It has been found that the bacterial process allowed over 90% removal of organic matter (COD) from the UF retentate (Table 3). Similar COD removal efficiencies have been obtained in another studies on dairy wastewater treatment using bacteria [12, 38]. The effectiveness of biological treatment method was lower for nutrients (nitrogen and phosphorus compounds) (Fig. 3). The content of TNb and TP was reduced by 63% and 50%, respectively.

Denitrification is a process of the reduction of inorganic nitrogen forms such as nitrates. This process requires the presence of readily biodegradable carbon compounds as electron donors for denitrifying bacteria and anoxic conditions [39]. Its efficiency is directly dependent on the ratio of COD to TNb [38, 40]. The effectiveness of nitrogen removal using denitrification bacteria increases with an increasing COD/TNb ratio and a minimum COD/TNb ratio of 10 is required for total nitrogen reduction in dairy wastewater [41]. Denitrifying bacteria belong to the group of facultative anaerobes. In the UF retentate,

the initial COD/TNb ratio was ~35, and the total nitrogen was reduced by only 63%. The reason for relatively low reduction of total nitrogen at high COD/TNb ratio might be the poor or lack of the process of ammonification performed by the microbes,

which conduct mineralization to utilize the organic molecules of nitrogen as electron donors, acquiring energy and producing ammonium under both aerobic and anaerobic conditions. Thus, the subsequent nitrification and denitrification processes are limited.

Table 3. Physico-chemical properties of the UF retentate treated with bacteria

Parameter	Value
Total nitrogen, mg/dm^3	12.2
Total phosphorus, mg/dm^3	2.67
Chemical oxygen demand, mg/dm^3	74.6
pH	8.7
Total suspended solids, mg/dm^3	12
Turbidity, NTU	6.5
Conductivity, μS/cm	1 574
Dry residue, mg/dm^3	1 060

Fig. 3.   Changes in the total nitrogen (TNb) and phosphorus (TP) content in the UF retentate during bacterial treatment
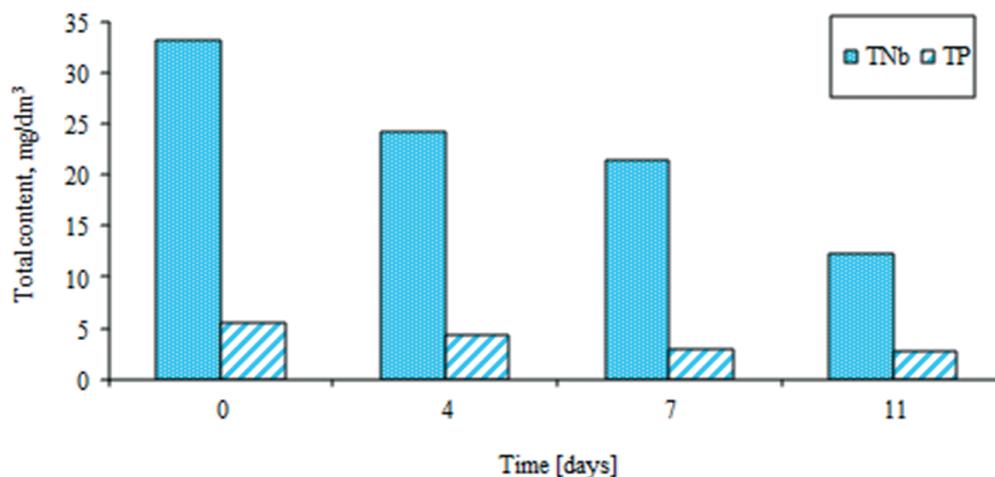
The efficiency of phosphorus removal by the microbes is also the COD/TP ratio-dependent. The best

efficiency of biological dephosphorylation is observed at COD/TP >50 [42]. The ratio of organic matter to the TP in the retentate after UF was 213, which seems to be favourable to ensure the required depletion of phosphorus from wastewater. On the other hand, not only is the COD/TP ratio important for the reduction of total phosphorus, but parameters such as pH and the oxygen content are important [42]. There are also publications with data [43] indicating difficulties with the simultaneous removal of nitrogen and phosphorus in bioreactors. This is conditioned by the oxygen content in the bioreactor. The biological dephosphorylation process requires alternating anaerobic-aerobic and anaerobic-anoxic conditions to select and develop specific microorganisms that exhibit the ability to store greater amount of phosphorus within the cells than they require in normal physiological demands [44]. Most of the

plants removing phosphorus thus far utilize chemical precipitation using aluminium and lime [42]. In dairy wastewater, for this purpose, lanthanum-modified bentonites have been already tested [45]. Another types of bioreactor or modification of their operating times might also be helpful, taking into account both aerobic and anaerobic phases.

The physico-chemical parameters of the UF retentate treated by bacteria (Table 3) were compared to the values to be met by wastewater discharged into water or soil. It was found that bacterial treatment allowed the effective removal of pollutants. Most of the parameters are within the acceptable limits in Poland and other EU countries. However, the limit for the TP content, according to the EU Directive, was slightly exceeded. It is possible that the treatment using algae might be a suitable method for its complete removal.

2.3. Efficiency of the microalgae treatment

Both the UF retentate and the same after subsequent treatment with bacteria were proposed to be used as the media for microalgae cultivation. The control of the process primarily consisted in the study of changes in the total nutrients (nitrogen and phosphorus) content in culture media, which resulted from the metabolism of algae. Based on the studies, it was also possible to determine the efficiency of microalgae biomass production. The cultivation was continued until the phosphorus content in the culture medium drastically decreased, since its deficiency is a limiting factor for the growth of algae [46].

Figure 4 shows the changes in the total nitrogen and phosphorus content in the culture medium during the experiments. The algal cultivation based on the UF retentate was inoculated with *Chlorella sp.* in an aqueous solution of BG-11 medium [47].
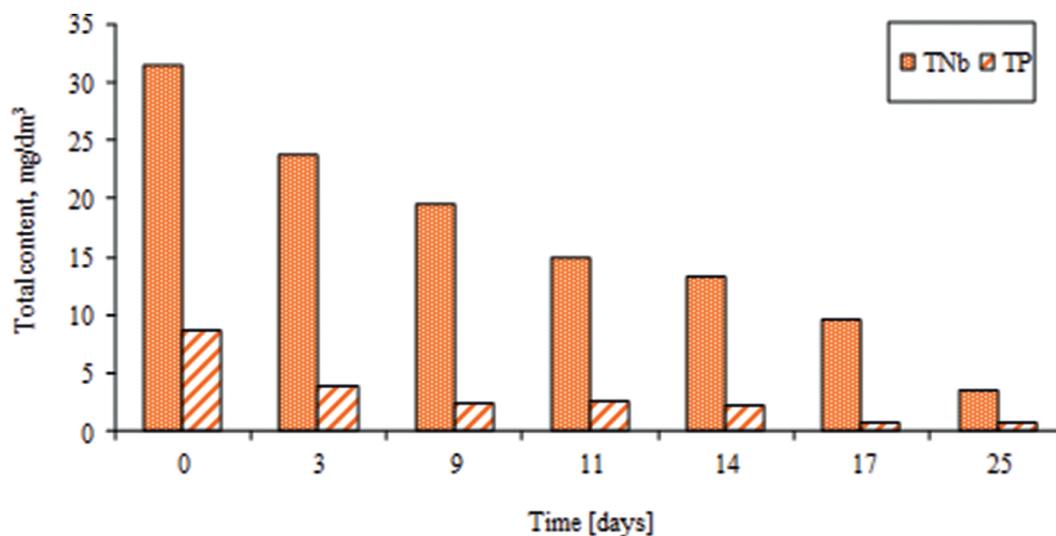

Fig. 4. Changes in the total nitrogen (TNb) and phosphorus (TP) content in the UF retentate used as a medium for the cultivation of microalgae

The total phosphorus content in the culture medium decreased by more than half within the first 3 days, and the total nitrogen decreased by more than half within 11 days. The initial intensive reduction in the phosphorus concentration (about 1.6 mg/dm^3 per day), despite the small populations of growing algae, was probably due to over assimilation of the elements. It is believed that the phosphorus is stored in algae cells and used when its content in the medium becomes insufficient [48]. This also demonstrates that the adaptation of algae to the new environmental conditions was very rapid. An average daily assimilation of nutrients from the retentate within 25 days of cultivation was equal to 1.12 mg/dm^3 and 0.32 mg/dm^3 for nitrogen and phosphorus, respectively. From the beginning of the experiment until its completion, the total phosphorus content was reduced by ~92% (from 8.71 to 0.73 mg/dm^3) and nitrogen by ~89% (from 31.5 to 3.45 mg/dm^3). The final values obtained indicate that the removal of phosphorus and nitrogen from wastewater, using microalgae *Chlorella sp.,* was very efficient. The content of TP and TNb in the obtained solution after separation of algae biomass was lower than in the UF permeate (3.84 mg/dm^3 and 13.0 mg/dm^3, respectively) and in the UF/NF permeate (0.47 mg/dm^3 and 8.1 mg/dm^3, respectively).

Furthermore, it was also found that the final phosphorus and nitrogen content in the culture medium of algae was also lower compared to the retentate after bacterial treatment (TP – 2.7 mg/dm^3, TNb – 12.2 mg/dm^3). Therefore, an attempt to inoculate *Chlorella sp.* in this sample, which still contained nutrients, was made. The retentate treated with the bacteria did not exceed the standards for wastewater discharge into the environment. However, further declines in nitrogen and phosphorus content could result in the possibility of water reuse in an industrial plant, for example, as technical water for boiler or cooling systems. Fig. 5 shows the results of the experiment which took 16 days. Introducing the inoculum to the liquid after bacterial treatment resulted in initial increases in nitrogen (from 12.2 to 12.6 mg/dm^3) and phosphorus content (from 2.7 to 3.4 mg/dm^3) as well as pH (from 8.7 to 9.1). The nutrients remaining in the solution after bacterial treatment turned out to be the excellent sources for algae growth. As a result of the study, it was found that the microalgae absorbed almost all of the nitrogen and phosphorus from the medium, i.e. ~93% of TNb (final value 0.872 mg/dm^3) and ~99% m/m of TP (final value 0.037 mg/dm^3).
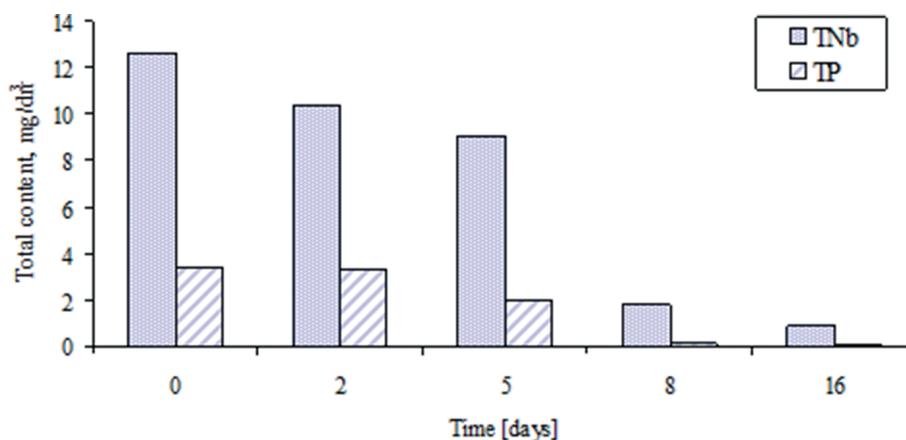
Fig. 5. **Changes in the total nitrogen (TNb) and phosphorus (TP) content in the UF retentate, after bacterial treatment used as a medium for the cultivation of microalgae**

Owing to the combination of two different biological processes (bioaugmentation with microalgal biomass production), the efficiency of the removal of nitrogen and phosphorus compounds from the retentate after ultrafiltration of dairy wastewater has considerably increased. Within several days of the experiment, after separation of algal biomass, the purified water met the environmental requirements for the discharge of wastewater into waters or soil within the content of these substances. Biomass, after dehydration and essential technological processing, can be a valuable raw material with high energy potential [49]. In the literature there are also examples of the use of microalgae capable of accumulating large quantities of lipids, among others, to remove specific impurities from wastewaters (e.g., antibiotics) during biomass production [50].

Conclusions

The obtained results have shown that an effective treatment of dairy wastewater can be successfully achieved using an integrated UF/NF system preceded by a pre-filter bag. However, the UF retentate is characterized by a high organic loading as well as high levels of nitrogen and phosphorus, which can cause environmental problems. The methods proposed for biological treatment, using bacterial and algal culture, effectively solved this problem. As a result of coupling these two methods, the concentration of TNb in purified water decreased <1.0 mg/dm^3 and TP <0.1 mg/dm^3. In addition, raw material (algae biomass) was obtained.

References

1. Steinhoff-Wrześniewska A., Rajmund A., Godzwon J.: Water consumption in selected branches of food industry. *Ecological Engineering*, 2013, 32, pp. 164–171 [in Polish].

2. Kasztelan A., Kierepka M.: Impact of the food industry on the environment in Poland. Polish Association of Agricultural and Agribusiness Economists. *Scientific Yearbooks* 2014, 16(2), pp. 109–116 [in Polish].

3. Vourch M., Balannec B., Chaufer B., Dorange G..: Treatment of dairy industry wastewater by reverse osmosis for water reuse. *Desalination*, 2008, 219 (1–3), pp. 190–202.

4. Cassano A., Rastogi N.K., Basile A.: Membrane technologies for water treatment and reuse in the food and beverage industries. *Advances in Membrane Technologies for Water Treatment*, 2015, 18, pp. 551–580.

5. Govindasamy-Lucey S., Jaeggi J.J., Martinelli C., Johnson M.E., Lucey J.A.: Standardization of milk using cold ultrafiltration retentates for the manufacture of swiss cheese: Effect of altering coagulation conditions on yield and cheese quality. *J. Dairy Sci*. 2011, 94 (6), pp. 2719–2730.

6. Kumar P., Sharma N., Ranjan R., Kumar S., Bhat Z.F., Jeong D.K.: Perspective of membrane technology in dairy industry: A Review. *Asian-Australasian Journal of Animal Sciences*, 2013, 26(9), pp. 1347–1358.

7. Suárez A., Fidalgo T., Riera F.A.: Recovery of dairy industry wastewaters by reverse osmosis. Production of boiler water. *Sep. Purif. Technol*., 2014, 133, pp. 204–211.

8. Huang L.P., Dong T., Chen J.W., Li N.: Biotechnological production of lactic acid integrated with fishmeal wastewater treatment by Rhizopus oryzae. *Bioprocess Biosyst. Eng*., 2007, 30(2), pp. 135–140.

9. Bajić B.Ž., Rončević Z., Puškaš V., Miljić U., Dodić S.N., Grahovac J.A., Dodić J.M.: White wine production effluents used for biotechnological production of xanthan. *J. Proc. and Energy in Agriculture*, 2015, 19, pp. 52–55.

10. Hena S., Fatimah S., Tabassum S.: Cultivation of algae consortium in a dairy farm wastewater for biodiesel production. *Water Resources and Industry*, 2015, 10, pp. 1–14.

11. Laurens L.M.I., Chen-Glasser M., McMillan J.D.: A perspective on renewable bioenergy from photosynthetic algae as feedstock for biofuels and bioproducts. *Algal Research*, 2017, 24(A), pp. 261–264.

12. Lateef A., Nawaz Chaudry M., Ilyas S.: Biological treatment of dairy wastewater using activated sludge. *Science Asia*, 2013, 39, pp. 179–185.

13. Carrasco E.F., Omil F., Garrido J.M., Arrojo B., Méndez R.: Advanced monitoring and supervision of biological treatment of complex dairy effluents in a full-scale plant. *Biotechnol. Prog.*, 2004, 20, pp. 992–997.

14. Demirel B., Yenigun O., Onay T.T.: Anaerobic treatment of dairy wastewaters: A review. *Process Biochem.*, 2005, 40(8), pp. 2583–2595.

15. Mutua D.N., Njagi E.N.M., Orinda G.O., Obondi G., Kansiime F., Kyambadde J., Omara J.B., Odong R., Butungi H.: Biological treatment of meat processing wastewater using lab-scale anaerobic-aerobic/anoxic sequencing batch reactors operated in series. *J. Bioremediat. Biodegrad.*, 2016, 7(4), pp. 1–6.

16. Porwal H.J., Mane A.V., Velhal S.G.: Biodegradation of dairy effluent by using microbial isolates obtained from activated sludge. *Water Resources and Industry*, 2015, 9, pp. 1–15.

17. Herrero M., Stuckey D.C.: Bioaugmentation and its application in wastewater treatment: A review. *Chemosphere*, 2015, 140, pp. 119–128.

18. Loperena L., Saravia V., Murro D., Ferrari M.D., Lareo C.: Kinetic properties of a commercial and a native inoculum for aerobic milk fat degradation. *Bioresour. Technol.*, 2006, 97(16), pp. 2160–2165.

19. Loperena L., Ferrari M.D., Díaz A., Ingold G., Pérez L.V., Carvallo F.R., Travers D., Menes R.J., Lareo C.: Isolation and selection of native microorganisms for the aerobic treatment of simulated dairy wastewaters. *Bioresour. Technol.*, 2009, 100(5), pp. 1762–1766.

20. Nzila A., Razzak S.A., Zhu J.: Bioaugmentation: An emerging strategy of industrial wastewater treatment for reuse and discharge. *Int. J. Environ. Res. Public Health*, 2016, 13(9), pp. 846.

21. Labbé J.I., Ramos-Suárez J.L., Hernández-Pérez A., Baeza A., Hansen F.: Microalgae growth in polluted effluents from the dairy industry for biomass production and phytoremediation. *JECE*, 2017, 5, pp. 635–643.

22. Chisti Y.: Biodiesel from microalgae. *Biotechnol. Adv.*, 2007, 25(3), pp. 294–306.

23. Bharathiraja B., Chakravarthy M., Ranjith Kumar R., Yogendran D., Yuvaraj D., Jayamuthunagai J., Praveen Kumar R., Palani S.: Aquatic biomass (algae) as a future feed stock for bio-refineries: A review on cultivation, processing and products. *Renew, Sust. Energ. Rev.*, 2015, 47, pp. 634–653.

24. Young G., Nippgen F., Titterbrandt S., Cooney M.J.: Lipid extraction from biomass using co-solvent mixtures of ionic liquids and polar covalent molecules. *Sep. Purif. Technol.*, 2010, 72(1), pp. 118–121.

25. Dębowski M., Zieliński M., Rokicka M., Kupczyk K.: The possibility of using macroalgae biomass from natural reservoirs as a substrate in the methane fermentation process. *Int. J. Green Energy*, 2015, 12(9), pp. 970–977.

26. Pandey A., Lee D.J., Chisti Y., Soccol C.R. (eds.): *Biofuels from algae*. Elsevier, 2014.

27. Zhang Y., White A.M., Colosi L.M.: Environmental and economic assessment of integrated systems for dairy manure treatment coupled with algae bioenergy production. *Bioresour. Technol.*, 2013, 130, pp. 486–494.

28. Wang C., Yu X., Lv H., Yang J.: Nitrogen and phosphorus removal from municipal wastewater by the green alga *Chlorella sp. J. Environ. Biol.*, 2013, 2(34), pp. 421–425.

29. Kumar A., Ergas S., Yuan X., Sahu A., Zhang Q., Dewulf J., Malcata F.X., van Langenhove H.: Enhanced CO2 fixation and biofuel production via microalgae: recent developments and future directions. *Trends Biotechnol.*, 2010, 28(7), pp. 371–380.

30. Lu Q., Zhou W., Min M., Ma X., Ma Y., Chen P., Zheng H., Doan Y.T.T., Liu H., Chen Ch., Urriola P.E., Shurson G.C., Ruan R.: Mitigating ammonia nitrogen deficiency in dairy wastewater for algae cultivation. *Bioresour. Technol.*, 2016, 201, pp. 33–40.

31. Rai U.N., Singh N.K., Upadhyay A.K., Verma S.: Chromate tolerance and accumulation in *Chlorella vulgaris* L: Role of antioxidant enzymes and biochemical changes in detoxification of metals. *Bioresour. Technol.*, 2013, 136, pp. 604–609.

32. Religa P., Kowalik-Klimczak A., Gierycz P.: Study on the behavior of nanofiltration membranes using for chromium(III) recovery from salt mixture solution. *Desalination*, 2013, 315, pp. 115–123.

33. Balannec B., Gésan-Guiziou G., Chaufer B., Rabiller-Baudry M., Daufin G.: Treatment of dairy process waters by membrane operations for water reuse and milk constituents concentration. *Desalination*, 2002, 147(1-3), pp. 89–94.

34. Cuartas-Uribe B., Alcaina-Miranda M.I., Soriano-Costa E., Bes-Piá A.: Comparison of the behaviour of two nanofiltration membranes for sweet whey demineralization. *J. Dairy Sci.*, 2007, 90(3), pp. 1094–1101.

35. Luo J., Ding L., Qi B., Jaffrin M.Y., Wan Y.: A two-stage ultrafiltration and nanofiltration process for recycling dairy wastewater. *Bioresour. Technol.*, 2011, 102(16), pp. 7437–7442.

36. Das B., Sarkar A., Sarkar A., Bhattacharjee S., Bhattacharjee Ch.: Recovery of whey proteins and

lactose from dairy waste: A step towards green waste management. *Process Saf. Environ. Prot.*, 2016, 101, pp. 27–33.

37. Hausmann A., Sanciolo P., Vasiljevic T., Weeks M., Schröen K., Gray S.R., Duke M.: Fouling of dairy components on hydrophobic polytetrafluoroethylene (PTFE) membranes for membrane distillation. *J. Membr. Sci.*, 2013, 442, pp. 149–159.

38. Loperena L., Ferrari M.D., Saravia V., Murro D., Lima C., Ferrando L., Fernández A., Lareo C.: Performance of a commercial inoculum for the aerobic biodegradation of a high fat content dairy wastewater. *Bioresour. Technol.*, 2007, 98(5), pp. 1045–1051.

39. Singhal N., Perez-Garcia O.: Degrading organic micropollutants: The next challenge in the evolution of biological wastewater treatment processes. *Front. Environ. Sci.*, 2016, 4, pp. 1–5.

40. Posavac S., Dragičević T.L., Hren M.Z.: The improvement of dairy wastewater treatment efficiency by the addition of bioactivator. *Mljekarstvo*, 2010, 60(3), pp. 198–206.

41. Dragičević T.L., Hren M.Z., Grgas D., Buzdum I., Čurlin M.: The potential of dairy wastewater for denitrification. *Mljekarstvo*, 2010, 60(3), pp. 191–197.

42. Mulkerrins D., Dobson A.B.W., Colleran E.: Parameters affecting biological phosphate removal from wastewaters. *Environ. Intern.*, 2004, 30, pp. 249–259.

43. Świerczyńska A., Bohdziewicz J., Amalio-Kosel M.: Activity of activated sludge microorganisms in the co-treatment of the leachates in the SBR bioreactor. *Ecol. Chem. Eng. A.*, 2014, 8, pp. 895–902.

44. Wagner M., Loy A.: Bacterial community composition and function in sewage treatment systems. *Curr. Opin. Biotechnol.*, 2002, 13(3), pp. 218–227.

45. Kurzbaum E., Shalom O.B.: The potential of phosphate removal from dairy wastewater and municipal wastewater effluents using a lanthanum-modified bentonite. *Applied Clay Sci.*, 2016, 123, pp. 182–186.

46. Dziosa K., Makowska M.: Monitoring of *Chlorella sp.* growth based on the optical density measurement. *Maintenance Problems*, 2016, 101(2), pp. 197–206.

47. Belotti G., de Caprariis B., De Filippis P., Scarsella M., Verdone N.: Effect of *Chlorella vulgaris* growing conditions on bio-oil production via fast pyrolysis. *Biomass and Bioenergy*, 2014, 61, pp. 187–195.

48. Kwietniewska E., Tys J., Krzemińska I., Kozieł W.: *Microalgae – cultivation and application of biomass as a source of energy: A review*. Acta Agrophysica Monographiae. Lublin: Inst. of Agrophysis, Polish Academy of Sciences, 2012.

49. Cheah W.Y., Ling T.Ch., Show P.L., Juan J.Ch., Chang J.-S., Lee D.-J.: Cultivation in wastewaters for energy: A microalgae platform. *App. Energy*, 2016, 179, pp. 609–625.

50. Guo W., Zheng H.S., Li S., Du J.S., Feng X.C., Yin R.L., Wu Q.L., Ren N.Q., Chang J.S.: Removal of cephalosporin antibiotics 7-ACA from wastewater during the cultivation of lipid-accumulating microalgae. *Bioresour. Technol.*, 2016, 221, 284–290.

Ewa WOSKOWICZ*, Monika ŁOŻYŃSKA, Maciej ŻYCKI, Anna KOWALIK-KLIMCZAK
ŁUKASIEWICZ Research Network – Institute for Sustainable Technologies, Radom, Poland
* Corresponding author: ewa.woskowicz@itee.radom.pl

HYBRID PROCESSES COMBINING MICROFILTRATION AND ADSORPTION/ION EXCHANGE FOR DAIRY WASTEWATER TREATMENT

Key words: activated carbon, ion exchange resins, dairy wastewater, microfiltration.

Abstract: This study investigated the efficiency of synthetic dairy wastewater treatment using three commercial activated carbons (AC) originating from various raw materials and prepared with different granulations, such as powdered activated carbon and granular activated carbon from wood and granular activated carbon from coconut shell. The additional step after the treatment with AC was ion exchange using mixed-bed ion resins for the enhancement of impurities removal from dairy wastewater. This allowed selecting powdered activated carbon coupled with ion exchangers as the most effective system for the treatment of real dairy wastewater. Integrating these processes with microfiltration has allowed increasing the removal efficiency of both organic and inorganic impurities by 90%.

Wykorzystanie układu hybrydowego: mikrofiltracja – adsorpcja i wymiana jonowa do oczyszczania ścieków mleczarskich

Słowa kluczowe: węgiel aktywny, żywice jonowymienne, ścieki mleczarskie, mikrofiltracja.

Streszczenie: W pracy zbadano efektywność oczyszczania modelowych ścieków mleczarskich z wykorzystaniem trzech komercyjnych węgli aktywowanych (AC) o różnym uziarnieniu, wykonanych z surowców roślinnych. Były to: drzewny węgiel aktywny w postaci proszkowej i granulowanej oraz granulowany węgiel aktywny z łupin orzecha kokosowego. W celu zwiększenia efektywności oczyszczania usuwania zanieczyszczeń w kolejnym etapie zastosowano proces wymiany jonowej z wykorzystaniem mieszanki żywic jonowymiennych. Pozwoliło to wytypować najskuteczniejszy adsorbent w połączeniu z procesem wymiany jonowej do oczyszczania rzeczywistych ścieków mleczarskich. Do wstępnego oczyszczania rzeczywistych ścieków mleczarskich wykorzystano mikrofiltrację oraz membranę ceramiczną, a następnie układ – węgiel aktywny/złoża jonowymienne. W ten sposób zintegrowane procesy pozwoliły zwiększyć skuteczność usuwania zarówno zanieczyszczeń organicznych, jak i nieorganicznych po procesie mikrofiltracji ścieków mleczarskich.

Introduction

The rapid development of industry consuming large amounts of water results in an increase in the level of water pollution. Wastewaters from industry and urban agglomerations, increasing consumption of surfactants, artificial fertilizers, and the decomposition of organic matter contribute to the disposal of significant amounts of various pollutants into surface waters. A number of physical, biological, and chemical methods have been used in wastewater treatment processes, such as filtration, coagulation, advanced oxidation, and membrane processes [1-4]. As they are often insufficient in complete removal of pollutants, this stimulated the search of some alternatives as adsorbents originating from non-conventional agricultural bio-products such as wood, coconut shell, and vegetables processed into activated forms of charcoals. The activated charcoals are usually used as one of the last steps of the treatment cycles, where the variety of pollutants in water at very low concentrations, because the other methods do not bring the expected results. Adsorption using activated carbon is a technology with a wide spectrum of applications,

i.e. in the processes of removing primarily organic, but also inorganic pollutants from both the air and water [5]. The efficiency of the treatment of the liquid phase using activated carbon in the reduction of pollutant parameters is greatly influenced by adsorbent porous structure, including pore volume and size distribution, specific surface area, the presence of functional groups, electrostatic interactions, hydrophobicity, ash content, molecular weight, structure, the chemical properties of the adsorbate, and the parameters of treated water (pH, ion concentration in solution, oxygen content) [6-13]. The determined properties of activated carbon are shaped during the processing stages, such as the carbonization of raw material in an inert atmosphere. During this process, most of the non-carbon elements (oxygen, hydrogen, nitrogen, and sulphur) are eliminated in the form of gaseous products, and the elemental carbon atoms form layers composed of irregularly connected aromatic rings, between which free spaces are formed, forming the porous structure of activated carbons [14].

Another alternative for conventional treatment methods are ion exchange resins in the form of beads. Ion exchange is a process of mobile exchange of ions from the medium over other ions of the same electric sign contained in the structure of resin beads. Among the ion exchangers, there are both cationic resins, which are able to exchange the ions containing positive charge, as well as anionic resins capable of exchanging the ions with negative charge [15]. A great solution to improve the quality of water is to use mixed beads that exchange both cations and anions creating a stronger driving force. Mixed-bed ion resin materials are commonly used in water purification for polishing process water which can be reused in the industry.

Nevertheless, the lack of effectiveness in overcoming the problem of variety of impurities in wastewaters makes the traditional treatment unprofitable. In order to enhance the performance of wastewater treatment plants,
in recent years, integrated systems for water purification has become increasingly common [3,4,16]. Activated carbon is generally used both as a primary treatment, to facilitate other purification processes, and as the final tertiary stage in the purification of the wastewater. Both powdered and granular activated carbons can be used in water treatment, but the granular type has the advantage of the capability of regeneration [17].

The aim of this work was to study the possibility of using different sorbents for the treatment of dairy wastewater. In the first step, the performances of three types of activated charcoals were studied, such as powdered and granular made from plants and granular prepared from coconut shell activated carbons integrated with mixed ion resin beads in the treatment of dairy wastewater. As a result, the most efficient charcoal was selected to treat real dairy wastewater in the integrated system: microfiltration/activated carbon/mixed ion resins. The efficiency of the treatment methods and the quality of treated water was assessed based on the analysis of selected pollution parameters. Moreover, the obtained results allowed us to develop the conception and construction of a module using activated carbon and ion resins for post-treatment of industrial waste streams.

1. Experimental

Materials

The efficiency of dairy wastewater treatment was verified for three different types of commercially available activated carbons, such as powdered (AC 1) and granular (AC 2) made of wood and granular made of coconut (AC 3) activated carbon. AC 1 and AC 2 were provided by VWR and AC 3 was provided by Tropical Company. The characteristics of the activated carbons used for the treatment of dairy wastewater are presented in Table 1.

Table 1. Characteristics of activated carbons used in the treatment of dairy wastewater

Symbol	Type of activated carbon	Granulation	Specific surface area
AC 1	Powdered (wood)	50-75 μm	2500 m²/g
AC 2	Granular (wood)	0.5-1.0 mm	1000 m²/g
AC 3	Granular (coconut shell)	0.5-1.0 mm	1100 m²/g

All of these carbons were used in a hybrid system with mixed-bed ion resins (cationic and anionic). The cationic ion resin was AMBERLITE IRN77 resin and
anionic resin was AMBERLITE™ IRA410. Both were provided by VWR. The main characteristics are presented in Table 2.

Table 2. Characteristics of ion exchangers used after treatment with activated carbons

Ion resin	Mobile ion	Bead size	Exchange capacity
Cationic	H+	0.6-0.70 mm	≥ 1.90 mval/L
Anionic	Cl-	0.6-0.75 mm	≥ 1.25 mval/L

The construction of the prototype uses 'Star-sep TM' ceramic membrane from Mantec designed for use in a cross-flow regime (Table 3). The filtration module was equipped with six 19-channel membranes with a nominal pore diameter of 0.2 μm (max. 0.65 μm), a length of 1200 mm, and the filtration area of 0.33 m². The total filtration area of the installed membranes was approximately 2 m².

Table 3. Characteristics of ceramic membrane used to pretreat dairy wastewater

Parameter	Ceramic membrane 'Star-Sep^{TM}'
External diameter	32 mm
Number of channels	19
Channel shape	Star
Length	1200 mm
Filtration area	0.33 m²
Pore size	0.2 μm

Methods

In order to check the performance of activated carbon-ion exchangers for wastewater treatment, in the first step, the synthetic dairy wastewater was based on powdered milk. The concentrations of the analysed pollution parameters are given in Table 4. The processes of the adsorption of pollutants in wastewater were conducted in the laboratory set-up, which allowed us to propose and design real industrial sorption module (Fig. 1). The volume of columns used in the experiments was 20 mL. The activated carbons were put in columns – 1 g. The cation and anion resins were mixed equally, and the total mass was 2 g, which was then put into a separate column. The model dairy wastewater with a volume of 50 mL was first filtered through the activated carbon and then filtered again through mixed-bed ion exchange resin. The effectiveness of the treatment of model wastewater was evaluated for Filtrate and Filtrate I (Fig. 1) based on the percentage efficiency removal of pollutions expressed as chemical oxygen demand (COD), total bound nitrogen (TNb), and sulphates. It was calculated with the formula $(1 - C_1/C_2) \cdot 100\%$, where C_1 – the concentration of the pollutant in the wastewater after the treatment, mg/L, and C_2 – the concentration of the pollutant in the wastewater before the treatment, mg/L. The analyses were conducted using cuvette tests with a spectrophotometer UV-VIS DR6000 from HACH Lange.
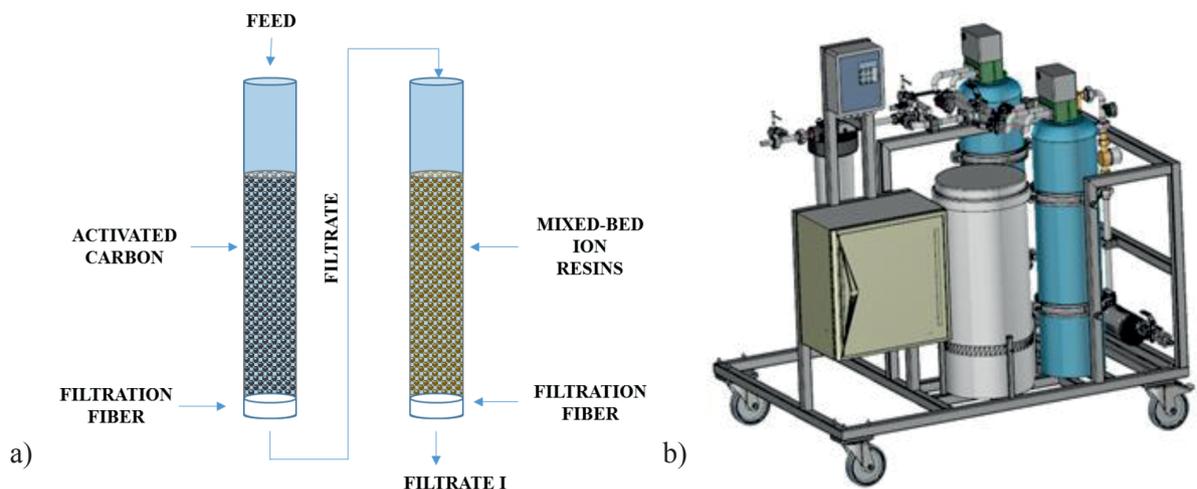

Fig 1. Scheme of two-stage wastewater treatment laboratory set-up using activated carbon and ion-exchange resins (a) and 3D visualization of designed industrial sorption module

Activated carbon-ion exchange integrated steps used for the treatment of synthetic dairy wastewater allowed selecting the most efficient adsorbent and ion exchange resin material for the post-treatment of real dairy wastewater after prior pressure driven process such as microfiltration. Dairy wastewater with a volume of 100 L was pumped from the feed tank through the membrane module at a pressure that was adequate for the membrane technique that was used (1.4–2.0 bar) and the 80 L of permeate was collected. After passing through the filtration module, the feed was separated into two different streams: a stream of purified filtrate (permeate), and a stream of concentrate (retentate).

The Filtrate stream was collected in a separate tank and a retentate stream was recycled to the feed tank. As a result, the concentrations of compounds that were retained by the membrane were gradually increasing. Microfiltration (MF) was performed with a membrane installation using a ceramic membrane with a pore size of 0.2 μm. The microfiltration system was previously described in the work [18]. The retentate flow was set to the maximum level (1200–1250 L/h). The samples of permeate from the process was subjected to filtration through the selected sorbent and mixed-bed ion exchange resins. The values of parameters selected for testing in real wastewaters are given in Table 4.

Table 4. Initial values of pollution parameters in dairy wastewaters

Parameter	Synthetic dairy wastewater	Real dairy wastewater	
	Untreated	Untreated	Treated with MF
COD [mg O_2/L]	879	2090	629
TNb [mg/L]	249	47	38
Sulphates [mg/L]	475	176	49

2. Results and discussion

Performance of activated carbon-ion exchange resins in the treatment of synthetic dairy wastewater

The first stage of the study involved the analysis of the performance of activated carbons named AC 1, AC 2, and AC 3 along with mixed-bed ion resins (C/A) as an additional step for model dairy wastewater treatment. This was determined by the investigations of the removal efficiencies of pollution parameters such as COD, TNb, and sulphates. Comparative experiments using all of the activated carbons allowed observing that the highest removal efficiency of chemical oxygen demand in synthetic wastewater was obtained using powdered activated carbon (AC 1) (Fig. 1). The effectiveness of AC 1 was almost 50% higher than AC 2 and over 50% higher than AC 3 activated carbon. This was associated with the highest surface of powdered activated carbon. In this case, the additional step using mixed bed ion exchange resin allowed the enhancement of the removal efficiency of COD of about 10% for each of the tested activated charcoal (Fig. 2). The additional treatment after powdered activated carbon with a mix of cation and anion resin allowed reducing COD by almost 80% (Fig. 2).
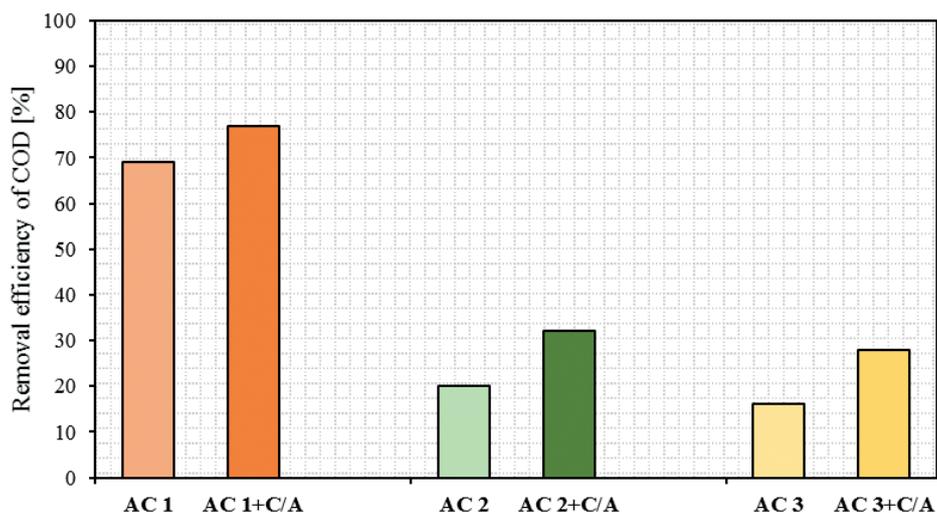

Fig. 2. Removal efficiency of chemical oxygen demand (COD) using activated carbons and coupled with mixed ion exchange resin

The performances of activated carbons were also investigated for the reduction of parameter of TNb (Fig. 3). It was found that the highest removal efficiency was again obtained by AC 1 and equal to 13%; however, the difference between particular activated carbon was not very significant. It was found that mixed-bed ion resins allow increasing the removal efficiency by about 45%. This might indicate that most of nitrogen was originated from the ion form. The smallest percentage reduction of TNb was observed for the AC 3 made from coconut shell (Fig. 3).
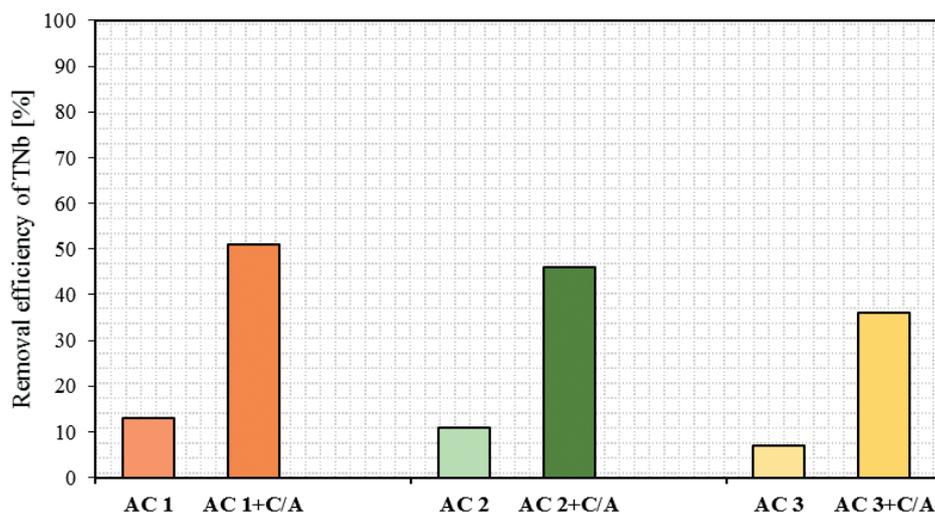

Fig. 3. Removal efficiency of total bound nitrogen (TNb) in model dairy wastewater using activated carbons and coupled with mixed ion exchange resin

In the case of the removal efficiency of sulphates from synthetic dairy wastewater, none of the activated carbons were highly efficient (Fig. 4). As sulphates were mainly present in the ionic form, their concentration was greatly reduced with the filtration through columns containing mixed cationic and anionic Amberlite-resins.
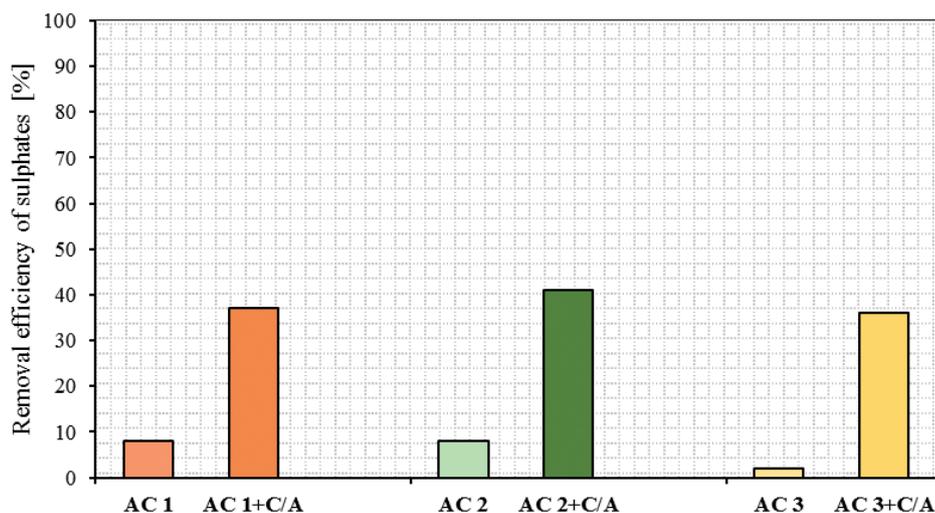

Fig. 4. Removal efficiency of sulphates in model dairy wastewater treatment with activated carbons and coupled mixed-bed ion exchange resin

Based on the obtained results, the powdered activated carbon was selected as the most efficient for the treatment of dairy wastewater. It was particularly noted for reducing the COD parameter quantifying the amount of mainly organic but also inorganic matter. However, the mixed bed ion exchangers were much more efficient for the reduction of ion concentrations. Differences in the amount of adsorbed pollutions using a particular sorbent have been attributed to surface area and the presence of surface functional groups and electrostatic interactions [19].

Real dairy wastewater treatment with integrated system

Treatment of real dairy wastewater was started with microfiltration (MF) conducted with a ceramic membrane in order to remove suspended solids. Then, based on the highest efficiency of synthetic wastewater treatment with activated carbon, the AC 1 was selected for further treatment of the wastewater along with mixed-bed ion resins. It was noted that microfiltration itself is not sufficient to highly reduce concentrations of pollutants in dairy wastewater (Fig. 5). Powdered activated carbon used with cation-ion exchangers reduced the organic impurities content expressed as COD by over 90%, which was 20% more than MF. The TNb level decreased only 19% when using MF. This means that impurities containing nitrogen compounds could freely pass through the pores of the ceramic membrane resulting in low removal efficiency. However, the integrated system of powdered activated carbon and ion exchange resins after MF yielded a 80% reduction of TNb. For the removal efficiency of sulphates from wastewater, only C/A as an additional post-treatment step allowed the reduction of the content of sulphates by nearly 90% (Fig. 5).
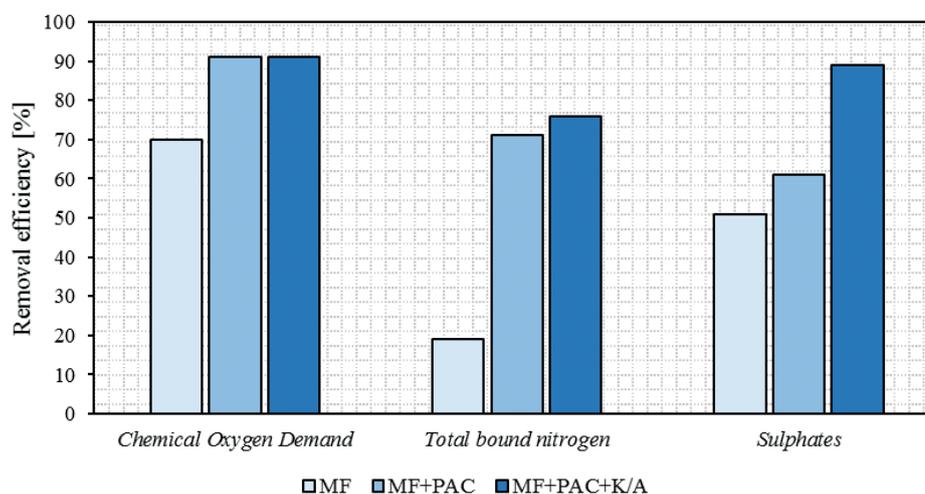

Fig. 5.   Removal efficiency of chemical oxygen demand (COD), total bound nitrogen (TNb) and sulphates with MF used as a single process, coupled with powdered activated carbon and both activated carbon and mixed-bed ion resins

The low efficiency of MF used as a single process for dairy wastewater treatment can found in Levine's work [20], which shows that particles of organic compounds such as polysaccharides or fatty acids in filtered water are smaller than the pore diameters of microfiltration membranes and can freely pass contaminating the water.

Using powdered activated carbon is an alternative to the water purification process in granular activated carbon filters [21]. The main advantage of the powdered activated carbon compared to granular one is the low investment cost and the flexibility of application. It can be dosed periodically when the quality of the collected water requires an additional treatment process. Activated carbon in the form of powder is useful to treat organic impurities, especially those contributing to odorous smell in dairy wastewater, which also results from inorganic compounds [22]. Using the integrated ion-exchange resins for the removal of charged particles and activated carbon for organic molecules might be an effective solution for the treatment or post-treatment of industrial wastewater. Employing membrane processes such as microfiltration as a pre-treatment integrated with adsorption and ion exchange can result in the enhancement of reducing impurities, which, in consequence, might contribute to the system development and optimization of high quality water production that can be reused in the particular industry. Thus, it is necessary to continue the work toward selecting appropriate process conditions for adsorption of pollutants on various types of sorbents. For this purpose, it was necessary to design and build a research post-treatment plant involving columns for sorbents such as activated carbon and ion exchange resins, which can work in a technological line with microfiltration module as a pre-treatment step (Fig. 6). This module consists of two columns working both individually or in parallel which can be used depending on the required quality of treated water. During the laboratory study, it was confirmed that, at the outlet of the columns, a non-woven filter with a pore size of 5 μm should be employed at the outlet of the columns, which allows the retention of solid particles released from activated carbon. The additional element of the module is the brine tank used for the regeneration of ion exchange resins. The whole system is planned to be used for post-treatment of wastewaters regenerated with membrane processes.
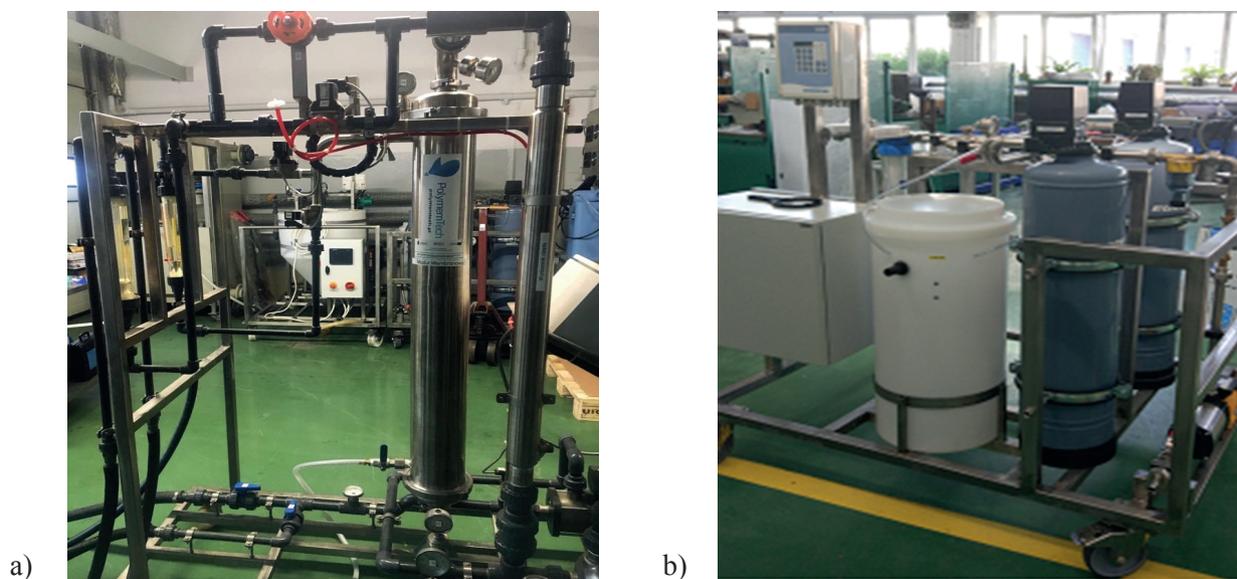
Fig. 6. Technological line involving microfiltration plant (a) and sorption module (b) consisting of columns for both activated carbon and ion exchange resins.

Conclusions

The results obtained in the study have shown that the most efficient tested activated carbon for the removal of most impurities in synthetic dairy wastewater was powdered activated carbon, which then was integrated with mixed-bed ion resins in order to enhance the removal efficiencies. This integrated system was used to treat real dairy wastewater after prior microfiltration through ceramic membrane. It turned out that powdered activated carbon coupled with Ambulate ion resins employed after microfiltration greatly affected the performance of dairy wastewater treatment. This resulted in the removal of unwanted pollution originating from both organic matter and ions expressed as chemical oxygen demand, total bound nitrogen, and sulphates. Thus, in further work, the designed module will be used to post-treat the technological liquids in order to obtain water that can be reused in industrial plants.

References

1. Amuda O.S, Amoo I.A., Ajayi O.O.: Performance optimization of coagulant/flocculant in the treatment of wastewater from a beverage industry. *Journal of Hazardous Materials*, 2006, 129, pp. 69–72.
2. Kowalik-Klimczak A., Stanisławek E.: Reclamation of water from dairy wastewater using polymeric nanofiltration membranes. *Desalination and water treatment*, 2018, 128, pp. 364–371.
3. Stanisławek E., Kowalik-Klimczak A.: Integration of advanced oxidation process with nanofiltration for dairy effluent treatment. *Challenges of Modern Technology*, 2017, 8, pp. 3–6.
4. Kowalik-Klimczak A., Stanisławek E., Grądkowski M.: Możliwości regeneracji wody ze zużytych kąpieli myjących z przemysłu mleczarskiego w procesie nanofiltracji. *Inżynieria i Aparatura Chemiczna*, 2017, 56(3), pp. 76–77 [in Polish].
5. Moore B.C., Cannon F.S., Westrick J.A., Metz D.H., Shrive C.A., DeMarco J., Hartman D.J.: Changes in GAC pore structure during full-scale water treatment at Cincinnati: a comparison between virgin and thermally reactivated GAC. *Carbon*, 2001, 39, pp. 789–807.
6. Boehm H.P.: Some aspects of the surface chemistry of carbon blacks and other carbons. *Carbon*, 1994, 32, pp. 759–769.
7. Newcombe G., Drikas M.: Adsorption of NOM onto activated carbon: electrostatic and non-electrostatic effects. *Carbon*, 1997, 35, pp. 1239–1250.
8. Pendleton P., Wong S. H., Schuman R., Levay G., Denoyel R., Rouquerol J.: Properties of activated carbon controlling 2 methylisoborneol adsorption. *Carbon,* 1997, 35, pp. 1141–1149.
9. Newcombe G.: Activated carbon and soluble humic substances: adsorption, desorption, and surface charge effects. *Journal of Colloid and Interface Science,* 1994, 164, pp. 452–462.
10. Faur-Brasquet C., Kadirvelu K., Le Cloirec P.: Removal of metal ions from aqueous solution by adsorption onto activated carbon sloths: adsorption competition with organic matter. *Carbon,* 2002, 40, pp. 2387–2392.
11. Vidicv R.D., Suidan M.T., Traegner U.K., Nakhla G.F.: Adsorption isotherms: illusive capacity and role of oxygen. *Water Research,* 1994, 24, pp. 1187–1195.

12. Corapcioglu M.O., Huang C.P.: The adsorption of heavy metals onto hydrous activated carbon. *Water Research,* 1987*,* 21, pp. 1031–1044.

13. Srivastava V.C., Mall I.D., Mishra I.M.: Adsorption of toxic metal ions onto activated carbon: Study of sorption behaviour characterization and kinetics. *Chemical Engineering and Processing: Process Intensification,* 2008, 48, pp. 1269–1280.

14. Bansal R.C., Goyal M.: Adsorpcja na węglu aktywnym. Warszawa: *Wydawnictwo Naukowo-Techniczne*, 2009 [in Polish].

15. Kabsch-Korbutowicz M.: Zastosowanie procesu wymiany jonowej do usuwania naturalnych substancji organicznych z wody. *Ochrona Środowiska*, 2013, 35(1), pp. 11–18 [in Polish].

16. Konieczny K., Rajca M., Bodzek M., Kwiecińska A.: Water treatment using hybrid method of coagulation and low pressure membrane filtration. *Environment Protection Engineering*, 2009, 35, pp. 5–23.

17. Bahadori A.: *Essentials of Oil and Gas Utilities: Process Design, Equipment, and Operations.* Gulf Professional Publishing, 2016.

18. Łobodzin P., Piątkiewicz W., Grądkowski M.: Regeneration method of aqueous, technological liquids using a dedicated microfiltration system. *Solid State Phenomena,* 2015, 237, pp. 271–277.

19. Mezohegyi G., van der Zee F.P., Font J., Fortuny A., Fabregat A.: Towards advanced aqueous dye removal processes: A short review on the versatile role of activated carbon. *Journal of Environmental Management*, 2012, 102, pp. 148–164.

20. Levine, A.D., Tchobanoglous G., Asano T.: Characterization of the size of contaminants in wastewaters: treatment and reuse implications. *Journal (Water Pollution Control Federation)*, 1985, 57(7), pp. 805–816.

21. Kårelid V., Larsson G., Björlenius B.: Pilot-scale removal of pharmaceuticals in municipal wastewater: comparison of granular and powdered activated carbon treatment at three wastewater treatment plants. *Journal of Environmental Management*, 2017, 193, pp. 491–502.

22. Kushwaha J.P., Srivastava V.C., Mall I.D.: Treatment of dairy wastewater by commercial activated carbon and bagasse fly ash: parametric, kinetic and equilibrium modelling, disposal studies. *Bioresource Technology*, 2010, 101, pp. 3474–3483.

Andrzej MAJCHER*, Mirosław NESKA, Mirosław MROZEK
ŁUKASIEWICZ Research Network – Institute for Sustainable Technologies, Radom, Poland
* Corresponding author: andrzej.majcher@itee.radom.pl

WASTE HEAT RECOVERY WITH THE USE OF THERMOELECTRIC GENERATORS – A RESEARCH STATION

Key words: thermoelectric generator, waste heat, heat energy recovery.

Abstract: Closing technological cycles by means of reducing the amount of waste and its management is one of the main issues addressed in manufacturing companies. Low temperature heat is an example of technological waste which may take the form of hot flue gases, cooling liquids from industrial processes, or hot water from heating vents or operating installations. One of the methods of managing low temperature heat from the above sources is converting it into electricity using thermoelectric generators (TEG). The article presents an experimental research station for heat energy recovery. The paper includes a description of a control system which enables adjustment and control of the parameters of generated electricity. Moreover, proprietary software to analyse, archive, and create databases of heat exchange parameters and electronic converters are discussed. The station has a modular structure, enabling its further expansion, both through the use of various heat sources and different cooling systems.

Stanowisko badawcze odzysku ciepła odpadowego z wykorzystaniem termogeneratorów

Słowa kluczowe: termogenerator, ciepło odpadowe, odzysk energii cieplnej.

Streszczenie: Zamykanie obiegów technologicznych poprzez redukcję ilości odpadów i ich zagospodarowanie są jednymi z głównych zagadnień podejmowanych w przedsiębiorstwach produkcyjnych. Przykładem odpadu technologicznego jest energia cieplna o parametrach niskotemperaturowych w postaci: gorących spalin, gorących lub ciepłych cieczy chłodniczych procesów przemysłowych, ciepłej wody z upustów ciepłowniczych czy instalacji eksploatacyjnych. Jedną z metod zagospodarowania energii tego typu źródeł niskotemperaturowych jest przetworzenie jej na energię elektryczną z zastosowaniem termogeneratorów (TEG). W artykule przedstawiono opracowane eksperymentalne stanowisko do badań eksperymentalnych takich układów. Opisano system sterowania, umożliwiający regulację i kontrolę parametrów generowanej energii elektrycznej. Omówiono autorskie oprogramowanie umożliwiające analizę, archiwizację i tworzenie baz danych parametrów wymienników ciepła oraz przekształtników elektronicznych. Stanowisko posiada konstrukcję modułową, umożliwiającą jego dalszą rozbudowę, zarówno poprzez wykorzystanie różnych źródeł ciepła, jak i różnych układów do wytwarzania chłodu.

Introduction

Reduction of CO2 emissions and improvement of the energy balance of production processes are the main two factors that influence the generation of new methods for energy recovery and waste management, specifically the waste heat energy [1]. Low temperature heat [2] is a product of a technological or production processes, and it is also a result of the exploitation of natural heat sources as well as forced heating processes. It is considered a waste heat, and it is currently used to a minimal extent, because waste heat management, in general, faces two major obstacles, i.e. low thermal parameters and diverse physicochemical properties of the waste in question. Most often it is returned to the environment, thus deteriorating the environmental conditions. Therefore, a number of waste heat utilization projects are being undertaken. The approach is to transform the hot waste heat into cold or useful heat [3, 4]. Experts also work on the use of waste heat from hot flue gases generated in the process of pellet combustion in low-power boilers, to produce electricity using a thermoelectric power generation

system [5]. Solutions that use heat recovery processes from hot exhaust gases are still being developed, e.g., by using innovative segmental thermogenerator modules, whose efficiency is estimated at about 9% [6]. Electricity generated from such cells can be used directly as direct current or converted into alternating current with DC/AC converters [7]. The research station presented in the article enables the testing of waste heat energy recovery systems in which the final product is electricity. The device generates electricity through the conversion of thermal energy into direct current. Moreover, it converts DC into AC.

1. Construction of the research station

The research station has a modular structure (Fig. 1) which enables its rapid modification and further development through the use of various low temperature heat sources, different cooling systems, and thermoelectric generators. The basic elements of the station are modules which allow the storage and exchange of high temperature thermal energy (B_{HT}), storage and exchange of low temperature thermal energy (B_{LT}), heat exchangers hot (W_{HT}) and cold (W_{LT}), and a set of thermoelectric generators (TEG).

**Fig. 1 Block diagram of the research station**

Further modules of the research station are a DC/AC converter module (DC/AC), a storage module with high thermal parameters (S_{HT}), a storage module with low thermal parameters (S_{LT}), a control system module (CPU), and PC computer (PC). High temperature heat exchange module (Q_{HT}) and low temperature heat exchange module (Q_{LT}) can be added to the system if necessary.

2. Construction of the research station

Figure 2 presents the construction of the research station. Storage and heat exchange modules with high and low temperature parameters (Figs. 2.2 and 2.3) were developed as cylindrical tanks of a capacity equal to $800\ dm^3$ and a spiral coil placed inside, which has a heat

a)   b)

Fig. 2   Model of the research station in 3D (a) and its realization (b): 1) frame, 2) B_{LT}, 3) modules B_{HT}, 4) control cabinet of CPU, DC/AC and PC modules, 5) modules W_{HT}, W_{LT}, and a TEG module se

transfer area of *3 m²*. The coils forbid direct contact of liquids in the exchangers; hence, the possibility of using liquids with different freezing and evaporation temperatures is possible. Consequently, it can be used to extract heat from sources with different temperatures.

The maximum temperature for heating the liquid in the tank is set at 95°C for water, which stores heat energy while the minimum temperature for cooling the liquid is 4°C. Similarly, the storage and heat exchange modules with low thermal parameters are adapted to cooperate with different heat collection systems, an example of which is a dry or wet cooling tower [8], a fanless cooling tower, or an adsorption aggregate [9–11]. The research station is also equipped with a block of modules, i.e. a set of thermoelectric generators (Fig. 3) with hot and cold side heat exchangers.

The design of the block of modules allows testing of one to four individual units placed inside a thermally insulated case (Fig. 4).

The case is made of bolted aluminium profiles that enable extension and modification.
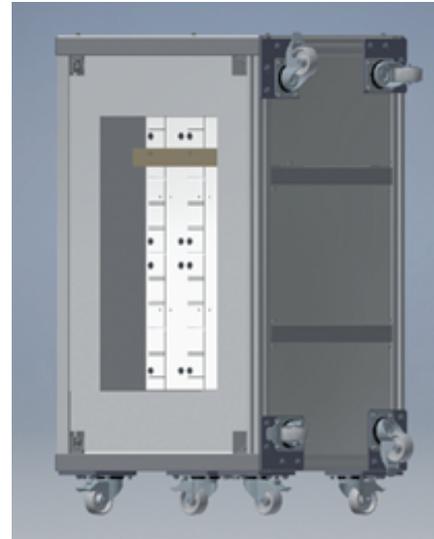

Fig. 3.　Construction diagram of a thermally insulated case with a single block of heat exchanger modules for testing thermoelectric generators.
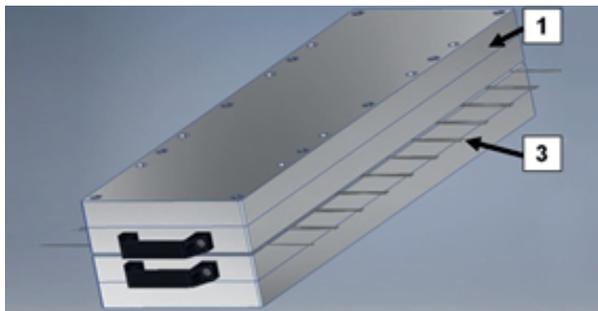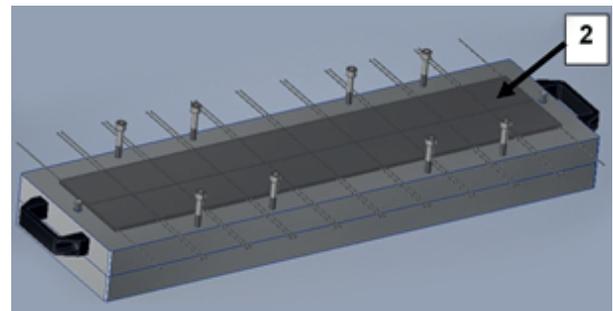

a)　　　　　　　　　　　　　　　　　　　b)

Fig. 4.　Construction diagram of a single set of heat exchanger modules with a water circuit for testing thermoelectric generators: a) unit drawing, b) location of thermoelectric generators inside the unit, 1) hot side exchanger, 2) thermoelectric generators, 3) cold side exchanger

The design of the block makes it possible to assemble the modules vertically or horizontally. The entire unit is also mobile. A unit placed in the block consists of aluminium heat exchangers and liquid thermoelectric generators (Fig. 4). The modules of exchangers have the same design for both hot and cold sides of the thermoelectric generators. A single heat exchanger module is a two-section heat exchanger (Fig. 5) in which the heating or cooling liquid flows inside, depending on the function of the module.
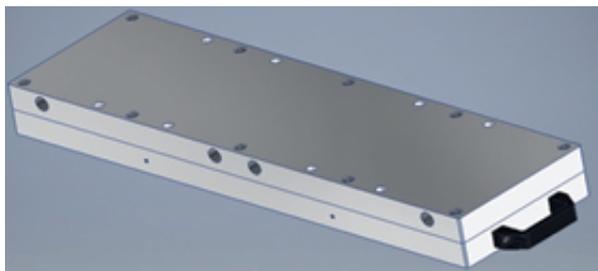
a)　　　　　　　　　　　　　　　　　　　b)

Fig. 5.　Construction diagram of a single hot/cold side exchanger module with a water circuit for testing thermoelectric generators: a) unit drawing, b) two-section water exchanger circulation

In a single set of heat exchanger modules, space has been provided to accommodate a set of twenty individual thermoelectric generators. The construction is designed to enable the reconfiguration of electrical connections of individual thermoelectric generators. The station is operated using a control system containing a measuring and control system, a DC/AC converter, and a PC computer, placed in the control cabinet (Fig. 2).

Thermogenerator of the TEC1-12730 type were used in the research station for waste heat recovery [12]. It is supplied with energy from the high temperature parameters storage and the heat exchange module, which is fed with waste heat energy. The heat exchange medium used in this circuit is water and its thermal parameters in the B_{HT} module are monitored by temperature, pressure, and level sensors. The water flow in the circuit between B_{HT} and W_{HT} modules is implemented using a *Yonos ECO* pump [13]. The measuring elements of the WHT module circuit are DUK ultrasonic flow meter [14], TP-375 temperature sensors [15], and a SEN pressure sensor [14].

Fig. 6. Elements dispersing thermal energy located outside: 1) external coolant tank, 2) external fanless cooler

The energy of the W_{LT} module of the cold side of the thermoelectric generator is discharged to the low temperature parameters storage and the heat exchange module, in which the heat is collected using elements of heat energy dissipation. The heat exchange medium used in this circuit is also water. The components and measuring elements in this circuit are the same as in the W_{HT} module circuit. The heat dissipating element in this system is a fanless external fin exchanger together with an external coolant container (Fig. 6). The heat transfer from the B_{LT} module to the S_{LT} module is carried out by the flow of the coolant in an additional circuit. Ethylene glycol (*Ergolid A with 35% concentration*) was used as the cooling liquid [16].

3. The control system

The research station is equipped with a control system monitoring its components using information provided by the measuring system. The cDAQ-9189 [17] controller with a set of analogue and digital I/O modules was used here. The controller allows the measurement of both slow-changing signals (temperature, flow) as well as high-amplitude waveforms associated with the generation of 230 V, 50 Hz electricity.

The controller works with a PC on which the proprietary control and measurement software, developed in the LabVIEW environment, has been implemented. The software enables the visualization of the work of the entire research station (Fig. 8). It allows the operator to change the controllers of individual components, on-line analysis of measurement data, as well as archiving and creating databases from the acquired measurement data, which relates to the conversion of generated electricity. The main supervisory functions of the software include the monitoring of the station's parameters, setting the parameters of its components, recording the measured parameters, and detecting and alarming in case of emergency. These functions are implemented in seven windows of the system software.

The *INSTALLATION* window (Fig. 8) contains a schematic illustration of all the station's elements with characteristic temperatures, flows, and pressures in the system. The window enables the activation of hot and cold water circulation pumps and the control of valves in their circuits. The voltage, current, and power of the waveform generated in individual sets with thermoelectric generators are also monitored here. The software enables forcing automatic operation of thermoelectric generators in conditions without electrical load, but also with electronic resistance load *Rigol DL3021A* [18]. The system also works with the load of the proprietary *DC/AC* converter and with the load of the commercial *DC/AC* converter.

The next software windows shown in the program tree are *DETAILS, Temperatures, TEG, DC, AC,* and *ALARMS* windows. The *DETAILS* window allows for reading and setting parameters related to the deeper layer of the station's control. The *Temperatures* window illustrates the temperature waveforms and allows the operator to select and preview any waveform, automatically or manually scale the chart axis, and save it as a text file. The *TEG* window enables 3D imaging of temperature distribution in units with thermoelectric generators and their scaling. The *DC* window visualizes the parameters of the DC output (current, voltage, power) from thermoelectric generators modules and enables the collection of discrete data for determining the current-voltage characteristic and power characteristic of the thermoelectric generators module. The *AC* window presents current, voltage, and power waveforms of *DC/AC* converters operating without load or connected to the power grid. The *ALARMS* window records emergency situations occurring during the functioning of the station, such as errors in communication between the computer and the controller, errors in reading the input signals of the controller, or exceeding the permissible values of the station parameters.
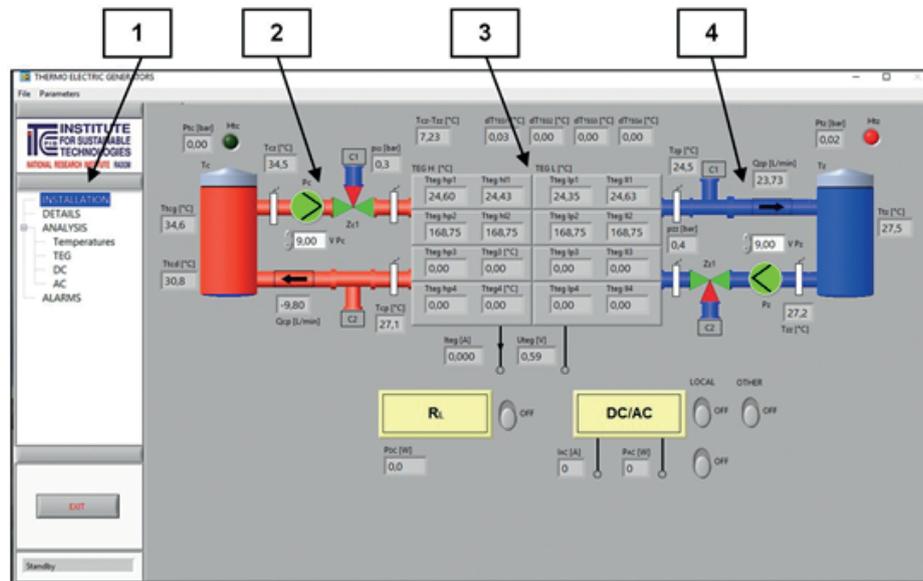
Fig. 7.   Main window of the workplace control system software for testing low temperature heat recovery systems: 1) program tree, 2) circulation of the hot sides, 3) block of modules for testing thermoelectric generators, 4) circulation of the cold sides

An important element of the control system is the proprietary DC/AC converter. It can give energy to the power grid (on-grid) or work in a local grid (off-grid). The converter generates electricity up to 1 kW and a constant input voltage range from 10 to 90V.

4. Verification of the station's functionality

The research station allows for carrying out tests of thermoelectric cells with different geometrical dimensions as well as different thermal and electrical parameters. The station also enables the use of waste heat and its conversion into heat with adjustable temperature and flow parameters (Fig. 8). This process takes place in a high temperature heat storage and heat exchange module. On the one hand, the use of water guarantees obtaining and maintaining the maximum temperature (95 ° C) in the B_{HT} module. On the other hand, the use of water as coolant allows for the minimum temperature of 4°C in the system. By using a heat storage and exchange module with low thermal parameters, continuous and stable heat collection is ensured.
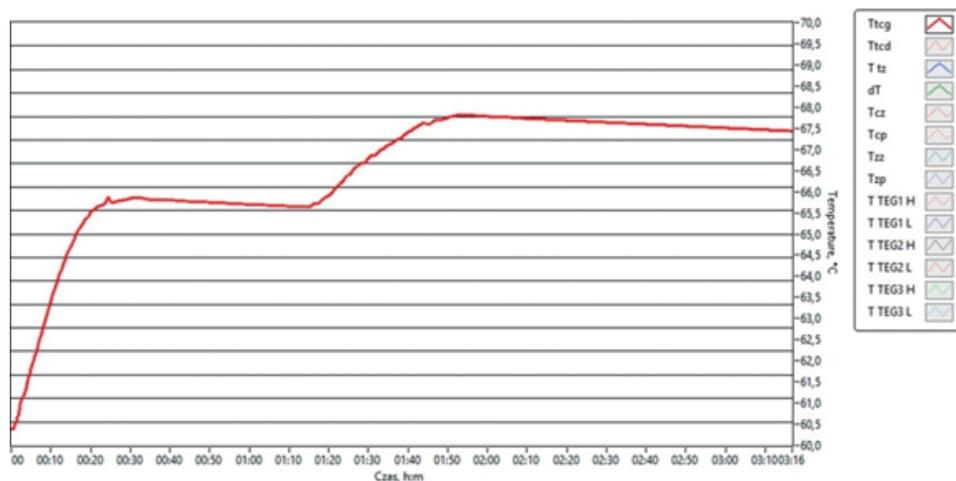

Fig. 8.   Graph of temperature changes in the hot water tank obtained under the conditions of the PI controller for two ranges of temperature settings.

The BLT module allows heat collection with adjustable temperature and flow parameters as well as further heat transfer to the heat dissipation system (Fig. 9).
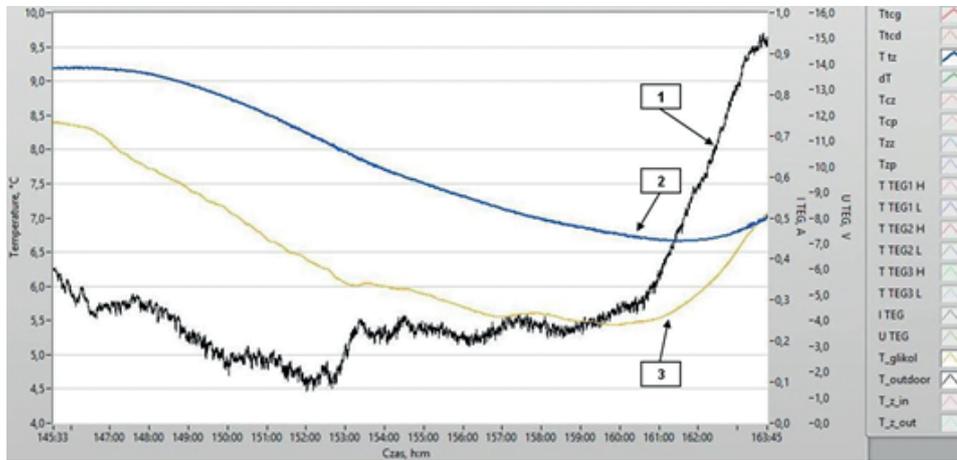
Fig. 9. Graph of temperature changes: 1) outside, 2) in the cold water tank, 3) in the external coolant tank

The prototype research station is used to test not only individual sets of modules, but also large sets of thermoelectric generators. It is designed to test thermoelectric cells of different volumes placed in layers, cascades, and electrically mounted in any configuration – in series and/or in parallel.
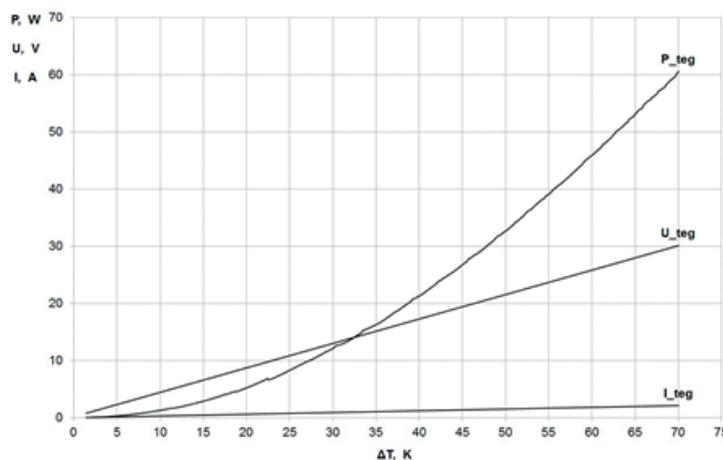

Fig. 10. Changes in electrical parameters at the output of a set of thermoelectric cells: I_teg – current characteristic, U_teg – voltage characteristic, P_teg – power characteristic

The station is equipped with two sets of modules which were separately verified. A single set contains twenty thermoelectric generators. The results from the verification of a single set are shown in Figure 10. During the test, a temperature difference of 70K was induced on the thermoelectric generators. As a result, the response of the system which generated electric power at the average level of 60W was obtained.

5. Summary

The research station for waste heat recovery using thermoelectric generators described in this article allows for the use of lost low-temperature energy and its conversion into electricity. The tests confirmed the correctness of operation of the system and the ability to generate electricity as a result of the temperature difference between the covers of the thermoelectric generators. The research station can be used to verify operation of low power systems that use a small number of thermoelectric cells in which the output product is only DC [5]. It can also be used in research on thermoelectric cells, not only those with single high-efficiency segment modules, but also larger TEG generators with a single generator electrical power of 1kW [6]. The presented solution also enables the conversion of thermal energy from waste heat sources with unstable parameters to thermal energy with utility parameters. The station presented can be used to dissipate thermal energy in the SLT module during a natural fall in temperature at night. As a result, a significant reduction in electricity consumption may be achieved. Furthermore, the adsorption cooling system [19, 20] supplied with heat energy can be used

in the developed station to generate supplementary "coolness." This may allow for more efficient use of waste heat energy, and it may also strengthen the heat removal process in the lower heat source and, as a result, increase the temperature difference between the covers of thermoelectric generators. The research station for waste heat recovery may be additionally equipped with systems powered by solar energy, which may affect its autonomy and provide alternative thermal energy in devices with a highly unstable source of waste heat [21].

References

1. Zarzycki R.: Wykorzystanie ciepła odpadowego z układu sprężania CO_2 do produkcji wody lodowej. *Zeszyty Naukowe Instytutu Gospodarki Surowcami Mineralnymi i Energią Polskiej Akademii Nauk*, 2016, 95, pp. 169–180 [in Polish].

2. Alam K.C.A., Akahira A., Hamamoto Y., Akisawa A., Kashiwagi T.: A four-bed mass recovery adsorption refrigeration cycle driven by low temperature waste/renewable heat source. *Renewable Energy*, 2004, 29, pp. 1461–1475.

3. Pyrka P.: Modelowanie trójzłożowej chłodziarki adsorpcyjnej. *Zeszyty Energetyczne*, 2014, I, pp. 205–216 [in Polish].

4. Wang R.Z., Oliveira R.G.: Adsorption refrigeration - An efficient way to make good use of waste heat and solar energy. *Progress in Energy and Combustion Science*, 2006, 32(4), pp. 424–458.

5. Brazdil M., Pospisil J.: Thermoelectric Power Generation Utilizing the Waste Heat from a Biomass Boiler. *Journal of Electronic Materials*, 2013, 42(7), pp. 2198–2202.

6. Wojciechowski K., Merkisz J., Fuć P., Tmankiewicz J., Zybała R., Leszczyński J., Lijewski P., Nieroda P.: Prototypical thermoelectric generator for waste heat conversion from combustion engines. *Combustion Engines*, 2013, 154(3), pp. 60–71.

7. Gospodarczyk A., Majcher A., Mrozek M.: Trójfazowy przekształtnik mocy AC/DC. *Zeszyty Problemowe - Maszyny Elektryczne*, 2013, 2(99), pp. 219–225 [in Polish].

8. Catalog data of the companies: M.A.S., Juwent.

9. Neska M.: *Analiza adsorpcyjnych układów chłodzenia*. In: Całus D., Flasza J., Szczepański K., Michalski A., Luft R. (eds.): *Możliwości i horyzonty ekoinnowacyjności. Samowystarczalność energetyczna i poprawa jakości powietrza*. Warszawa: Wyd. Instytut Ochrony Środowiska – PIB, 2017, pp. 96–108 [in Polish].

10. Neska M., Majcher A.: *Koncepcja sterowania adsorpcyjnego układu chłodniczego małej mocy*. In: Całus D., Oźga K., Popławski T., Michalski A., Szczepański K. (eds): *Możliwości i horyzonty ekoinnowacyjności. Zielona Energia*. Częstochowa: Wyd. Politechniki Częstochowskiej, 2018, pp. 141–153 [in Polish].

11. Neska M.: Refrigeration systems with one adsorption bed. *Journal of Machine Construction and Maintenance*, 2019, 113(2), pp. 121–129.

12. HB Corporation catalog data.

13. Wilo: *Main website*. [Online]. 2019. [Accessed 30 November 2019]. Available from: https://wilo.com/en/index.html

14. Kobold Messring: *Main website*. [Online]. 2019. [Accessed 30 November 2019]. Available from: https://www.kobold.com/en

15. Czaki Thermo-Product: *Main website*. [Online]. 2019. [Accessed 30 November 2019]. Available from: https://www.czaki.pl/en

16. Boryszew ERG: *Main website*. [Online]. 2019. [Accessed 30 November 2019]. Available from: http://www.boryszew.com.pl/?page=en-home

17. National Instruments: *Main website*. [Online]. 2019. [Accessed 30 November 2019]. Available from: https://www.ni.com

18. RIGOL TECHNOLOGIES catalog data.

19. Mohammed R.H., Mesalhy O., Elsayed M.L., Chow E.M.L.: Assessment of numerical models in the evaluation of adsorption cooling system performance. *International Journal of Refrigeration*, 2019, 99, pp. 166–175.

20. Semprini S., Asenbeck S., Kerskes H., Druck H.: Experimental and numerical investigations of an adsorption water zeolite heat storage for refrigeration applications. *Energy Procedia*, 2017, 135, pp. 513–521.

21. Gazda W., Stanek W.: Energy and environmental assessment of integrated biogas trigeneration and photovoltaic plant as more sustainable industrial system. *Applied Energy*, 2016, 169, pp. 138–149.

Mirosław MROZEK, Andrzej MAJCHER *, Mirosław NESKA
ŁUKASIEWICZ Research Network – Institute for Sustainable Technologies, Radom, Poland
* Corresponding author: andrzej.majcher@itee.radom.pl

THERMOELECTRIC HEAT EXCHANGER

Key words: waste heat, renewable energy, thermoelectric generator, heat exchanger, TEG thermoelectric modules, thermocouples.

Abstract: The article presents a heat exchanger with thermoelectric generators, which consists of two single sheet heat exchangers, between which thermoelectric generators are placed. The heat exchanger in question is used to convert waste heat energy into DC electricity. The construction of the heat exchanger is described in detail in the article, and the study of temperature distribution of both the high and the low temperature side is presented. The basic parameters of the heat exchanger are also given. They were determined with the current-voltage characteristics method, and then they were compared with the values established in the conventional way.

Termoelektryczny wymiennik ciepła

Słowa kluczowe: ciepło odpadowe, energia odnawialna, termogenerator, wymiennik ciepła, moduły termoelektryczne TEG.

Streszczenie: W artykule przedstawiono wymiennik ciepła z termogeneratorami, który składa się z dwóch pojedynczych płytowych wymienników wymiennika ciepła, pomiędzy którymi umieszczone są termogeneratory. Wymiennik służy do przetwarzania energii cieplnej w energię elektryczną prądu stałego. Przedstawiono konstrukcję wymiennika oraz badania rozkładu temperatury stron o wysokiej i niskiej temperaturze. Opisano podstawowe parametry wymiennika, wyznaczone metodą charakterystyki prądowo-napięciowej. Porównano je z wartościami wyznaczonymi w klasyczny sposób.

Introduction

Waste heat is currently processed to a minimal extent. In the most cases, it returns to the environment thus worsening the environmental conditions and energy balance of manufacturing processes. Thermoelectric generators can answer the problem, and they can be used to properly manage waste heat energy. TEG thermoelectric modules [1–3] are used to directly convert thermal energy into electricity. Their construction does not require any moving parts or working fluids, they start up immediately, they can work in any position, they do not need any spare parts and maintenance, they have a long service life (20–30 years), and they work in a wide temperature range. It has been proved that the supply of higher thermal energy to the thermocouple results in higher conversion efficiency and the amount of recovered electricity. The technological progress and lowering prices mean that it is economically and technically justified to use thermocouples for generating electricity even from low-temperature heat [8].

The efficiency of thermoelectric modules is the ratio of the electrical power released in the external circuit to the amount of heat supplied to the QH module. Presently, the efficiency of thermocouples is 5-8%. Improvements of those modules result in achieving better thermoelectric properties that allow efficiency above 10% [10–12]. One thermoelectric module can generate up to 20 W of electrical power. Such values are achieved by modules in which the temperature difference between the sides exceeds 300°C [13]. For ΔT<100°C values, the achieved powers are usually not more than 5W and the generated voltages do not exceed 5V [8]. When a thermocouple is used to power, e.g., a measuring system, these values are sufficient. The use of thermocouples for the production of electricity with higher values reaching many kilowatt hours requires the use of several interconnected modules. TEG modules are placed in a heat exchanger. The parameters of a single thermoelectric generator depend

on the type of thermoelectric material used. These are primarily efficiency and maximum power for a given temperature difference.

The article presents the design of a thermoelectric heat exchanger and the results of measuring the temperature distribution of both the high and the low temperature side worked out in the task realised in the frame of the EU project "Establishment of the Intelligent Specialization Centre in the field of Innovative Industrial Technologies and Technical and Environmental Safety." The basic parameters of the exchanger were determined with the current-voltage characteristics method [14]

and compared with the parameters obtained in the conventional way. The conditions necessary to increase the efficiency of obtaining electricity are also given.

1. Heat exchanger design

The heat exchanger consists of four aluminium sheets (Figs. 1, 2). There are 20 thermoelectric modules (type TEC1-12730) between the top two and bottom two sheets. The dimensions of a single sheet are a length of 680 mm, a width of 200 mm, and a thickness of 34 mm.
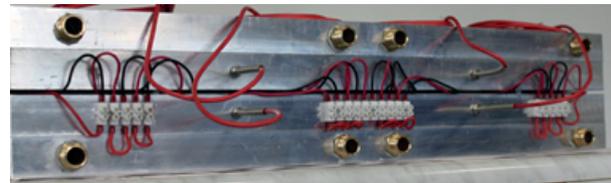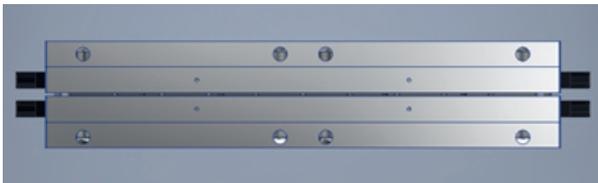

Fig. 1. Heat exchanger for liquid-liquid thermoelectric modules: a) 3D model of thermoelectric heat exchanger and its implementation (b)

In each outer aluminium sheet, two coil-shaped ducts were milled to supply heat (top sheet) and to dissipate heat (bottom sheet) (Fig. 2). Inlet and outlet openings were drilled on the side of each sheet. The heat transmission medium is water. It was assumed that

the exchanger will be used for low temperature heat management at a temperature of about 90°C, i.e. just below the boiling point of water. The design allows for even temperature distribution in planes parallel to the planes of thermoelectric modules.
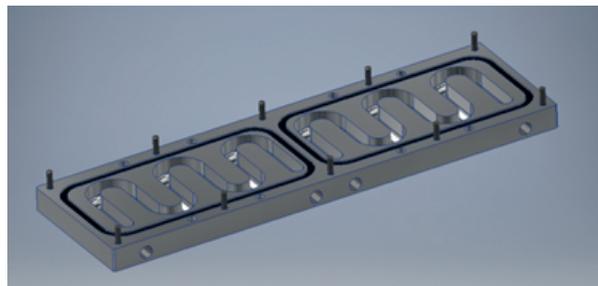

Fig. 2. The heat exchanger for thermoelectric modules. View from the inside

2. Temperature distribution in the heat exchanger

The temperature distribution in the heat exchanger was measured for water at a temperature of 59°C supplied to the hot side of the exchanger (upper sheet)

and for water at a temperature of about 25°C supplied to the cold side (lower sheet). The results are shown in Fig. 3 and Fig. 4.
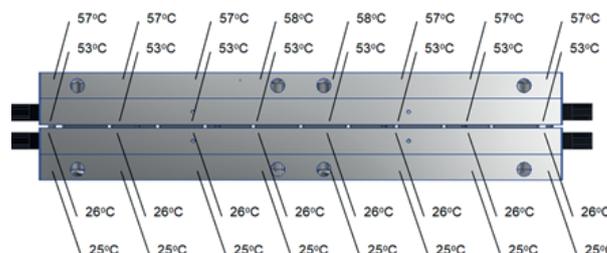

Fig. 3. Temperature values at individual points of the heat exchanger side part
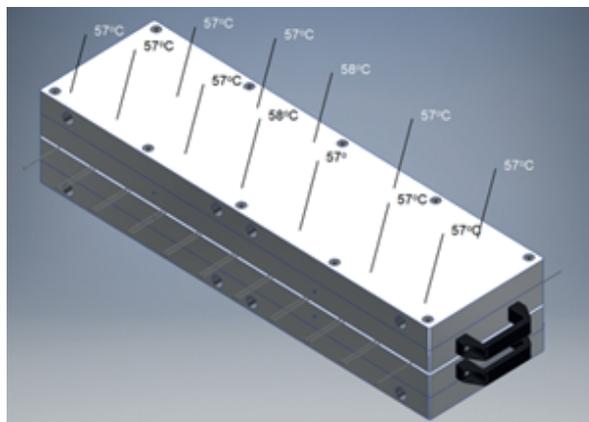
Fig. 4. Temperature values at individual points of the upper part (hot side) of the heat exchanger

The values of voltages generated by individual thermocouples without load and with load were also measured. The results are shown in Fig. 5 and Fig. 6.
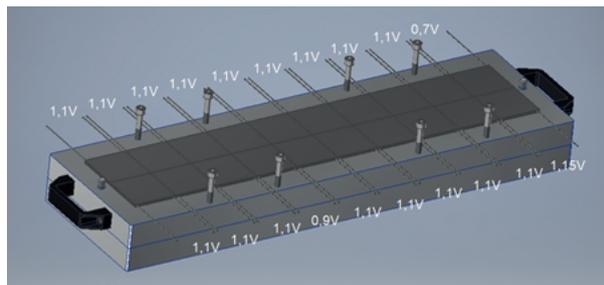

Fig. 5. Voltage values generated in the heat exchanger by individual thermocouples in idle state

Fig. 6. Voltage values generated in the heat exchanger by individual thermocouples under load

The temperature distribution in the heat exchanger is even, both on the hot and cold side, especially in places where the heat exchanger contacts thermocouples. This is very important for the effective recovery of electricity. In case one thermocouple receives less heat than other modules, it will limit the electricity produced.

Despite the even distribution of temperatures, not all thermocouples generated the same voltage. One thermocouple was clearly less efficient; the voltage on it was U_0=0.7V in idle state and U_L=0.1V under load. It was caused by an assembly error, i.e. an uneven distribution of thermal compound between the thermocouple and the heat exchanger plane. Other thermocouples generated voltages in the same range of values, i.e. U_0=1.1V in idle state and U_L=0.5V under load. The resultant voltage of all thermocouples connected in series was U_0=21.4V in idle state and U_L=10.2V under load at I_L=0.97A. In the case of a disconnection of the least efficient thermocouple, the resultant voltage of the remaining 19 thermocouples was U_0=20.7V in idle state and U_L=10.1V under load at I_L=0.98A. After disconnecting the least efficient module, the current increased slightly, and the total generated power remained at almost the same level (P=9.9W). In conclusion, the larger the heat flux flows through the thermocouples and the greater the differences between the electric energy generated by the individual thermocouples, the greater will be the counteraction of the weakest thermocouple [15].

3. Basic parameters of the exchanger with thermoelectric generators

A single thermoelectric module has specific parameters that result from the thermoelectric material used. Manufacturers provide its parameters and characteristics for a given temperature difference ΔT for a given module. The use of multiple thermoelectric modules connected together and placed in a heat exchanger does not mean that the resulting power will be directly proportional to the number of modules and the efficiency of one module. It depends on the design of the heat exchanger and the resulting thermal resistance between the exchanger and the individual modules. Nevertheless, it is possible to determine the resultant electrical parameters of a heat exchanger built of many individual thermocouples using the current-voltage characteristics method for one thermocouple [14].

The method consists in determining the current-voltage characteristics of the thermoelectric generator on the basis of current and voltage time histories at the transition from short-circuit to open and from open to short-circuit at a given temperature ΔT (Fig. 7).
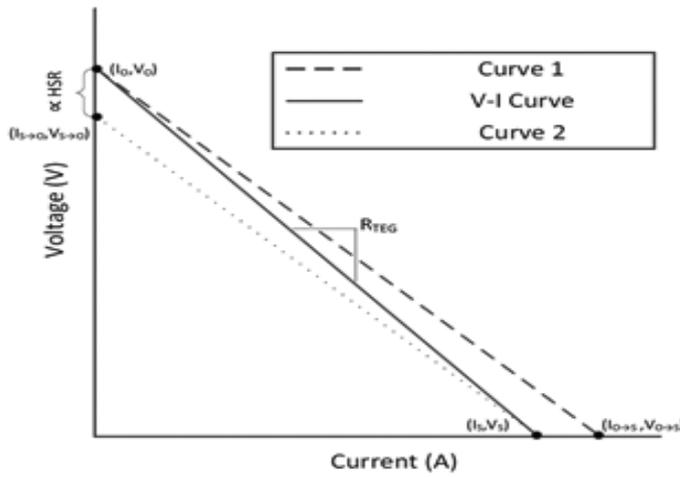

Fig. 7.   Method for determining the V-I characteristics on the basis of measured characteristic points [14]

Determination of characteristic points on the waveforms (Fig. 8, Fig. 9) allows one to calculate the $I_{MP}=I_S/2$ current and the voltage $U_{MP}=V_S/2$ for the maximum power $P_{MP}=I_{MP}*V_{MP}$ and the internal resistance of $R_{TEG}=V_O/I_S$ of the thermocouples.

When the value of thermal energy QH supplied to the thermocouple is known, the efficiency and thermal resistance of HSR can also be calculated according to the following formula:

$$HSR = \frac{\Delta T(V_{S\to O} - V_O)}{2(Q_{HO}V_{S\to O} - Q_{HS}V_O)} \qquad (1)$$

QHO and QHS are the heat supplied to the thermocouple (1) in the open state and short circuit state, respectively.
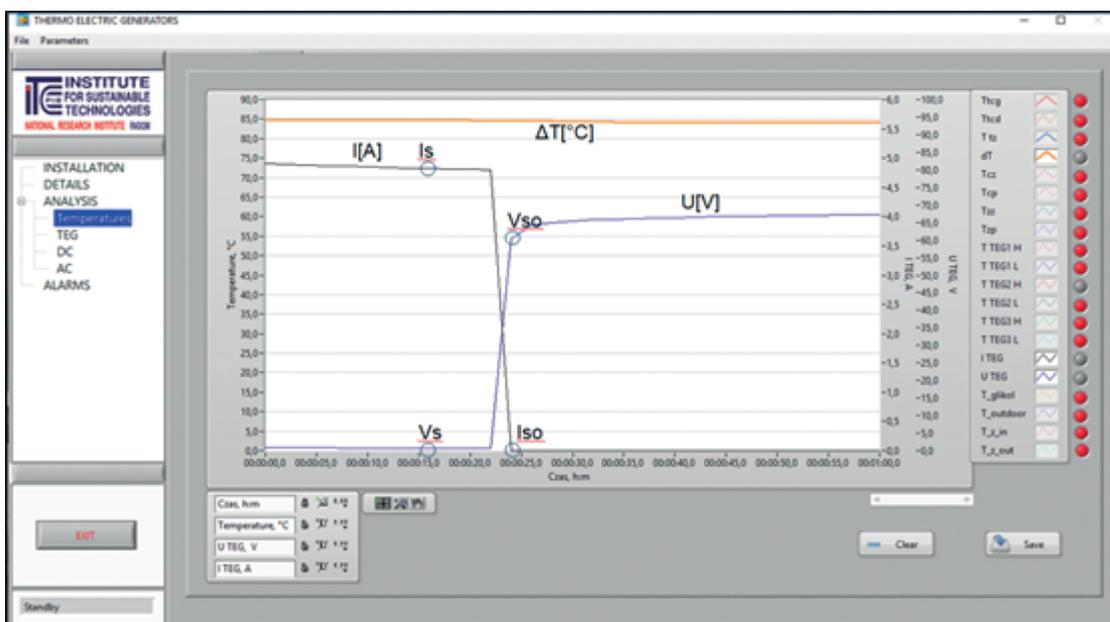
**Fig. 8. Transition from short circuit to open state at ΔT = 85 °C**
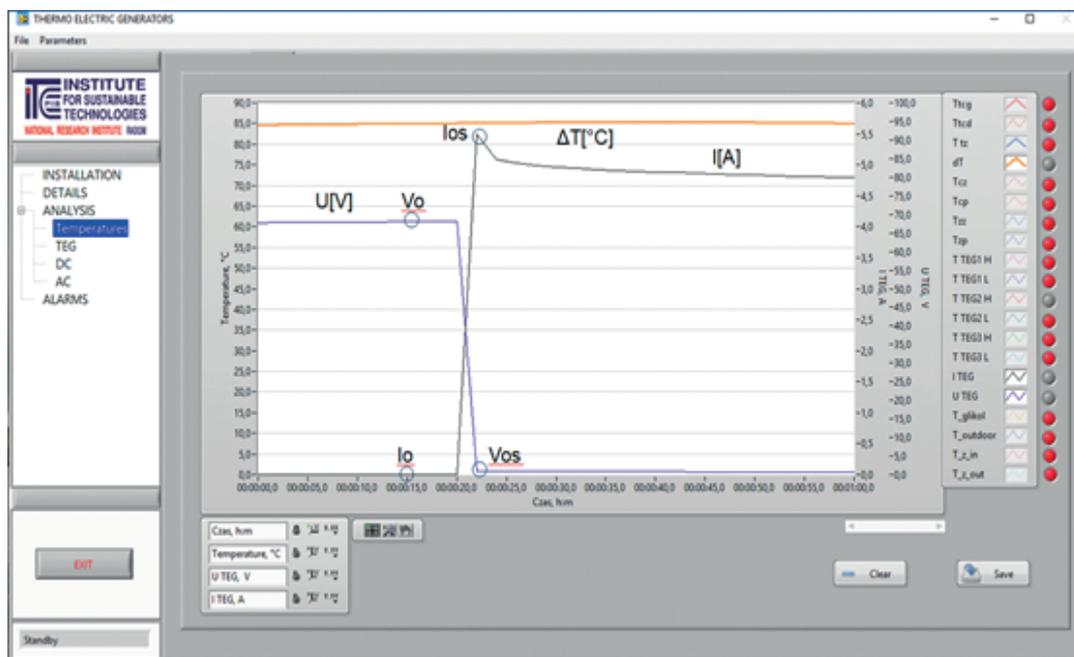
Fig. 9. Transition from open to short-circuit at ΔT = 85 °C.

The recorded time series for ΔT=85°C at the transition from the short to the open state (Fig. 8) allowed determining the characteristic points: Vs = 0V, Is = 4.9A, Vso = 60V, and Iso = 0A. When moving from an open state to a short-circuit state (Fig. 9), the characteristic points are Vs = 0V, Is = 4.9A, Vso = 60V, Iso = 0A. It is possible now to prepare the current-voltage characteristics of the tested exchanger with thermoelectric generators according to the described method (Fig. 10).
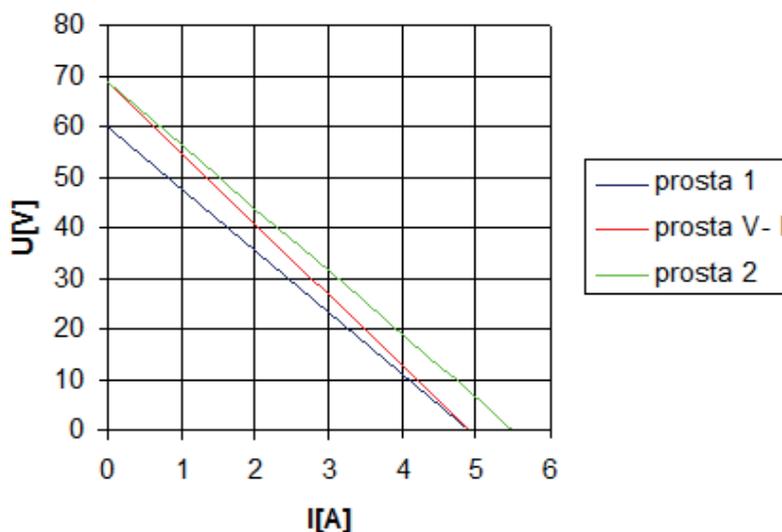

Fig. 10. Current-voltage characteristics of the tested thermoelectric generator for ΔT=85°C

Consequently, the determined parameters have the following values: current I_{MP}=2.45A and voltage U_{MP}=34.5V for maximum power P_{MP}=84.5W and R_{TEG}=14.1Ω. The graph in Fig. 11 shows the relationship between voltage and power as a function of the exchanger current obtained with the conventional method for temperature difference ΔT=85°C. This method consists in collecting measurement data of currents and corresponding voltages for a specific temperature difference. Based on the collected measurements, a graph of U=f(I) and P=f(I) was created, where P=U*I. The P=f(I) graph is an inverted parabola that has its extreme [16]. The extreme of this parabola is the maximum power point of MPP. The maximum power value read is approximately 85W and coincides with the calculated PMP value (P_{MP}=84.5W).
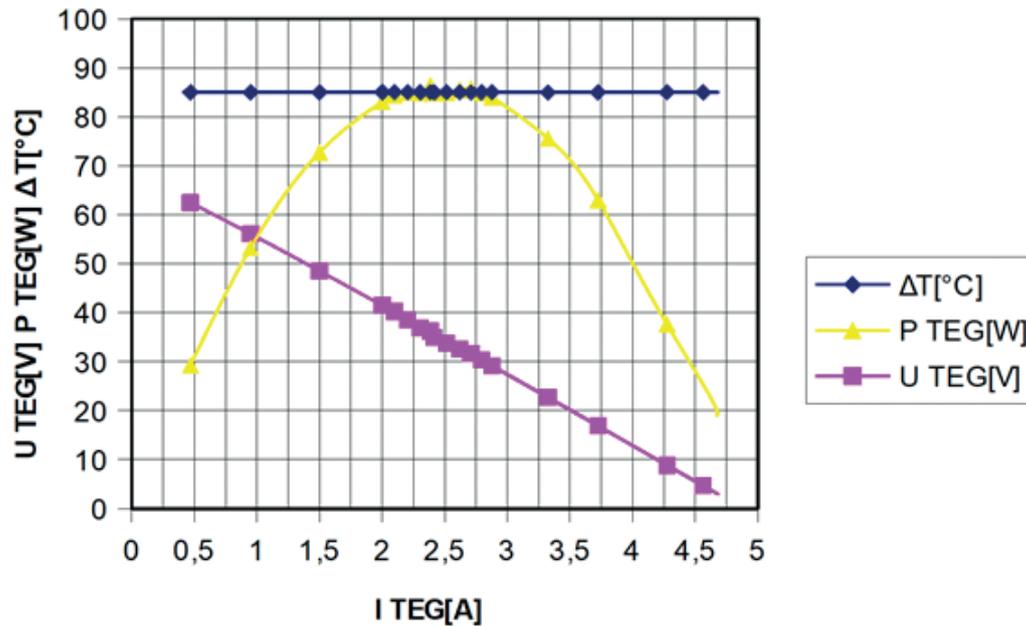
Fig. 11. Graph ΔT [° C], PTEG [W], and UTEG [V] as a function of ITEG current [A] of a thermoelectric generator (20 thermocouples connected in series).

Summary

The thermoelectric heat exchanger is used to properly manage waste heat energy. Its design and the use of water as a refrigerant ensures easy heat transfer to thermoelectric generators. A single thermocouple has specific parameters that result from the thermoelectric material used. In the case of many thermoelectric generators connected in series and placed in a heat exchanger, the resulting power depends on the design of the heat exchanger and the resultant thermal resistance between the heat exchanger and individual thermoelectric generators. Using the method described in the article, one can quickly determine the resultant maximum power of such a heat exchanger for a given temperature difference. In addition, this method allows one to determine the internal resistance and thermal resistance after making measurements at only four characteristic points, provided that thermoelectric generators are under a constant output load. Compared to the conventional method in which several points are determined at different load values, it accelerates the characterization of this type of thermoelectric systems.

The method was used in the test stand, described in a separate article, which was created in the previously mentioned project and is used for testing waste heat recovery systems.

It is important to evenly distribute the temperature on the covers of individual modules, both on the hot and the cold side, in order to efficiently converse the heat energy into electricity in a heat exchanger with many thermoelectric generators. The design of the heat exchangers should strive for the most uniform delivery of heat energy to all thermoelectric modules.

References

1. Brazdil M., Pospisil J.: Thermoelectric Power Generation Utilizing the Waste Heat from a Biomass Boiler. *Journal of Electronic Materials*, 2013, 42(7), pp. 2198–2202.
2. Wojciechowski K., Merkisz J., Fuć P., Tmankiewicz J., Zybała R., Leszczyński J., Lijewski P., Nieroda P.: Prototypical thermoelectric generator for waste heat conversion from combustion engines. *Combustion Engines*, 2013, 52(3), pp. 60–71.
3. Kalpana K., Muthumeena V., Sheerin S. and Sriranjani M.: Thermoelectric Generator and PV Panel Integrated Hybrid Energy Harvesting System. *International Journal for Modern Trends in Science and Technology*, 2017, 3(5), pp. 173–177.
4. Ohara B., Wagner M.: Residential Solar Combined Heat and Power Generation using Solar Thermoelectric Generation. *Journal of Electronic Materials*, 2015, 44, pp. 2132–2141.
5. Aggarwal R.K., Markandas S.: Thermoelectric generation using combination of solar and geo-thermal energy. *International Journal of Advanced Research*, 2013, 1(5), pp. 53–58.
6. Sztekler K., Wojciechowski K., Komorowski M.: The thermoelectric generators use for waste heat utilization from conventional power plant. *E3S Web of Conferences*, 2017, 14, 01031.

7. Trojanowski Ł.: Stabilizator temperatury płaszcza wodnego oparty na modułach Peltiera [BSc Thesis]. Warsaw University of Technology, 2008 [in Polish].

8. Jadwiszczok P., Sidorczyk M.: Produkcja energii elektrycznej z ciepła za pomocą ogniw TEG: charakterystyki termoelektryczne termogeneratorów. *Rynek instalacyjny*, 2016, 4, pp. 38–42 [in Polish].

9. Poudel B, Hao Q., Ma Y., Lan Y., Minnich A., Yu B., Yan X., Wang D., Muto A., Vashaee D., Chen X., Liu J., Dresselhaus M.S., Chen G., Ren, Z.: High-thermoelectric performance of nanostructured bismuth antimony telluride bulk alloys. *Science*, 2008, 320(5876), pp. 634–638.

10. Hochbaum A.I., Chen R.K., Delgado R.D., Liang W.J., Garnett E.C., Najarian M., Majumdar A., Yang P.D.: Enhanced thermoelectric performance of rough silicon nano wires. *Nature*, 2008, 451(10), pp. 163–167.

11. Królicka A., Hruban A., Mirowska A.: Nowoczesne materiały termoelektryczne – przegląd literaturowy. *Electronic Materials*, 2012, 40(9), pp. 19–34 [in Polish].

12. Rezania A., Rosendahl L.A.: *Thermal effect of a thermoelectric generator on parallel microchannel heat sink. Energy*, 2012, 37(1), pp. 220–227.

13. Tellurex: *G2-56-0570 Thermoelectric Power Generation Module Specifications* [Online]. 2019. [Accessed 10 December 2019]. Available from: https://www.tellurex.com/media/uploads/product_pdfs/g2-56-0570-specifications.pdf

14. McCarty R., Piper R.: Voltage–current curves to characterize thermoelectric generators. *Journal of Electronic Materials*, 2015, 44(6), pp. 1896–1901.

15. Mrozek M., Majcher A.: Application of thermoelectric generators for electrical energy production with a low-temperature heating source. *Journal of Machine Construction and Maintenance*, 2017, 4, pp. 123–130.

16. Zaremba A., Rodziewicz T., Wacławek M.: Algorytmy śledzenia punktu mocy maksymalnej (MPPT) w systemach fotowoltaicznych. *Proceedings of ECOpole*, 2012, 6(2), pp. 805–810 [in Polish].

Andrzej KOMOREK *, Konrad OLESIEJUK, Paweł PRZYBYŁEK, Robert SZCZEPANIAK
Department of Aviation, Polish Air Force University, Dęblin, Poland
* Corresponding author: a.komorek@law.mil.pl

DEVICES FOR THE SAMPLES PREPARATION FOR DETERMINATION OF IMPACT STRENGTH OF ADHESIVE JOINTS TESTED TO CLEAVAGE

Key words: impact strength, adhesive joint, preparation device.

Abstract: The impact strength tests of adhesive joints loaded for cleavage using a wedge-shaped impactor are generally described in the Polish Standard PN-EN ISO 11343. In order to conduct the tests, it is necessary to prepare bonded samples consisting of two specially formed elements. To form sample elements, it is necessary to take advantage of a special device, which is not adequately described in the standard. In view of the fact that the test method is quite common, some information, however general, with regard to the moulding device is available in the literature. Therefore, the authors have developed a device which was later validated in research with sample elements made from steel and an aluminium alloy. After the formation of adherends, it is necessary to connect them by means of a glued joint; however, it also requires a special handle due to an unusual shape of the samples. The handle is to stabilize samples and generate an appropriate clam required in the process of bonding at the time of making the connection. Both newly designed devices were made as prototypes so as to be able to check the correct operation of the designed constructions. Various tests were made in which the sample elements were moulded until obtaining a proper shape. During the test, particular elements of the device were adjusted so that the shape of the obtained samples would be in compliance with the parameters specified in the standard. On completion of the adjustments, it was possible to obtain specific repeatable elements. The obtained samples were inspected visually, and, on this basis, modifications were made. Then successive series of samples were prepared. Finally, the samples were subjected to a quality assessment. The results of the work are presented in the paper.

Przyrządy do przygotowania próbek do badania udarności połączeń klejowych na rozczepienie

Słowa kluczowe: udarność, połączenie klejowe, przyrząd do przygotowania próbek.

Streszczenie: W artykule zaprezentowano metodykę badań wytrzymałości udarowej połączeń klejowych na rozczepienie z wykorzystaniem impaktora w kształcie klina. Jest to metodyka opisana ogólnie w Polskiej Normie PN-EN ISO 11343, według której prowadzi się badania udarności połączeń klejowych. W celu przeprowadzenia badań wymagane jest przygotowanie próbek klejonych, składających się z dwóch odpowiednio uformowanych elementów. Do formowania elementów próbek niezbędny jest specjalny przyrząd, o którym nie można uzyskać żadnych informacji na podstawie Normy. Ze względu na to, iż metoda badania jest rozpowszechniona w świecie, pewne informacje dotyczące przyrządu formującego dostępne są w literaturze, jednak są to informacje ogólne. Dlatego samodzielnie opracowano tego typu przyrząd i przeprowadzono badania walidacyjne z elementami próbek wykonanymi ze stali i stopu aluminium. Po uformowaniu elementów próbek należy je połączyć za pomocą spoiny klejowej, do czego również jest wymagany specjalizowany uchwyt ze względu na nietypowy kształt próbek. Zadaniem uchwytu jest stabilizacja złożonych próbek oraz wytworzenie odpowiedniego docisku wymaganego w procesie klejenia w czasie wiązania kleju. Obydwa zaprojektowane urządzenia wykonano w formie prototypowej w celu sprawdzenia poprawności działania zaprojektowanych konstrukcji. Przeprowadzono próby kształtowania elementów próbek do wymaganej formy, podczas których poddawano regulacji poszczególne elementy przyrządu, tak aby kształt otrzymanych próbek był zgodny z parametrami określonymi w Normie. Po przeprowadzonych regulacjach możliwe jest uzyskiwania właściwych, powtarzalnych elementów. Powierzchnie klejone uformowanych elementów próbek przygotowano przez obróbkę strumieniowo-ścierną z odtłuszczaniem, a następnie naniesiono klej, złożono i zamocowano w uchwycie do klejenia w celu weryfikacji jego przydatności. Otrzymane próbki poddano oględzinom wzrokowym i na tej podstawie wprowadzono modyfikacje, a następnie wykonywano kolejne serie próbek oraz przeprowadzono ocenę ich jakości. W efekcie powstały dwa specjalizowane, pomocnicze przyrządy do przygotowania próbek do badań udarności. Wyniki badań zaprezentowano w artykule.

Introduction

The impact strength of adhesive joints has been studied since 1980s, when it was observed that more frequently used adhesive connections may be exposed to impact loads. The problem is related to various types of means of transport in which adhesive joints replaced other types of connections. Currently, the transport industry uses a large number of adhesive connections [1] in which a significant percentage are construction joints. A continuously increasing use of adhesive joints led to various research projects aimed at determining the strength and durability in various operating conditions. Impact strength is one of such properties. Additionally, it is a feature that may be vitally important for the safety of structures. If it refers to means of transport, it can also contribute to human safety. Therefore, it is worthwhile and necessary to conduct impact strength research of adhesive joints [2].

Currently, there are numerous methods for the assessment of adhesive joints impact strength [1, 3, 4] and two of which are standard methods. The first one is a method in which a special block sample is subjected to impact load as a result of which an adhesive joint is destroyed by shear [5]. This method was discussed in several relevant studies indicating its defects as well as discussing research issues [6]. The other method uses a specially bonded adhesive sample consisting of two components. In the course of a trial, it is split by means of the impact wedge. In order to carry out impact testing, it is necessary to prepare samples. However, this can be achieved by possessing appropriate auxiliary tools, which are not described in the standard or any other scientific articles. The article refers to papers associated with the construction as well as research into auxiliary equipment for sample preparation, which are necessary to study the impact strength of adhesive joints in the aspect of cleavage.

1. Project assumptions

The main objective of the project was to create easy-to-use, long lasting, and effectively operating devices that facilitate the proper moulding of steel and duralumin samples and also the stabilization of the samples during adhesive curing which should ensure the repeatability of the characteristics of the manufactured samples. It was assumed that the final outcome of the on-going work was to devise two support tools for sample preparation: a tool for moulding metal sample elements and a tool for samples bonding.

It was assumed that the device for the preparation of sample elements should ensure the formation of one sample element in a single cycle; whereas, the device for bonding should allow gluing at least five samples simultaneously.

The moulding device is to transfer the moment resulting from tightening the screws onto the elements which are directly in contact with sample elements to ensure their proper bending. It was necessary to take into consideration the place of bending, its angle, and resilient properties, which vary in the case of steel and duralumin samples. For this reason, it is impossible to build one universal device for all types of materials used for the creation of samples. When bending, there are plastic and elastic strains, which disappear on completion of the bending process. The effect is secondary deformation, i.e. changes in the dimensions of the bonded element in relation to the dimensions imposed by the template at the time of bending. The value of the deformation depends upon the material type and its thickness, the angle of bending, and thermal treatment. Its value is usually determined experimentally. In order to facilitate conducting such an experiment, the project had to take into account the possibility of any changes in the angle value under which the material is bended, depending on the needs and the required corrections. Other parameters, such as particular dimensions (Fig. 1), which determine the usefulness of samples for testing, are specified in the Polish Standard PN-EN ISO 11343 [7].
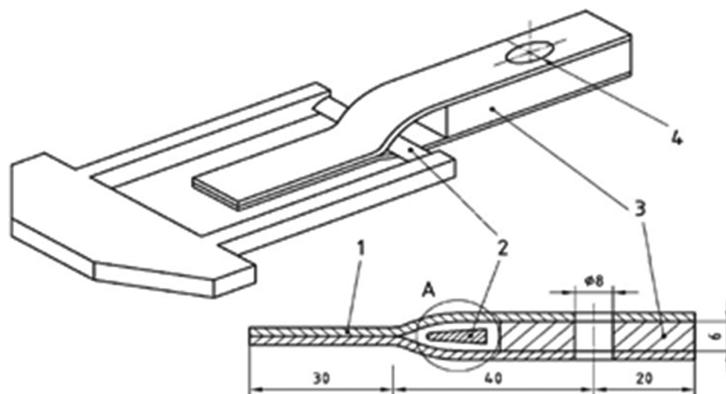

Fig. 1.   Dimensions of a glued sample used in the examination of impact strength. 1. Sample, 2. Wedge, 3. Spacer, 4 Screw hole
The projects of the devices were prepared in SOLIDWORKS software.
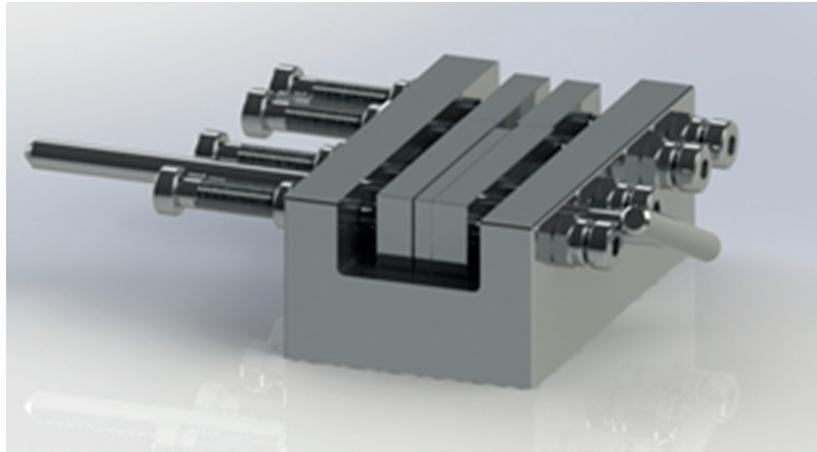
Fig. 2. Device for forming sample elements

The moulding device (Fig. 2), in accordance with the project, consists of the following components:

A steel frame of the device (Fig. 3) with eight holes, drilled through, with a grooved thread M8 x 1.25 mm, distributed axially against opposite holes, four on each side, separated into two holes per clamping element (cover plate). In each hole, a cylindrical-head screw with a hexagon socket M8 x 35 mm and a nut was screwed on. In the frame, two through holes, 8 mm in diameter, were made, on both sides, axially in relation to each other, intended to introduce the locking pin.
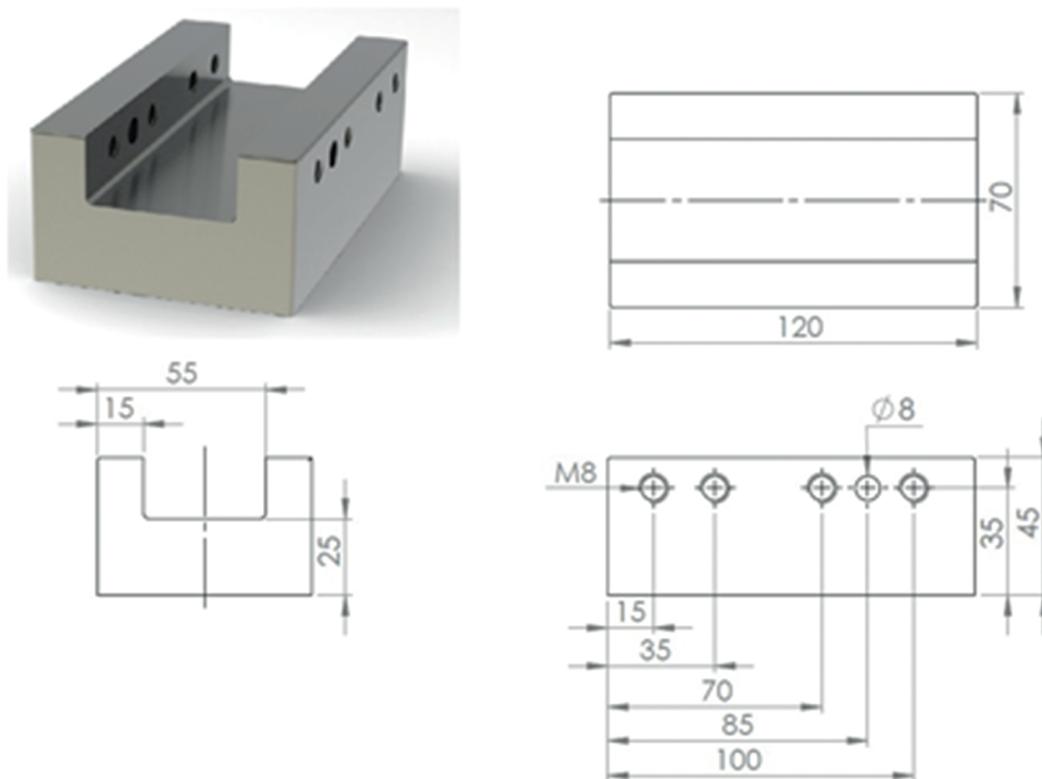

Fig. 3. The frame of device

- Locking pin made of a steel rod, 8 mm in diameter and 180 mm long, with a welded crossbar, 60 mm in length, is used to facilitate its introduction and removal.
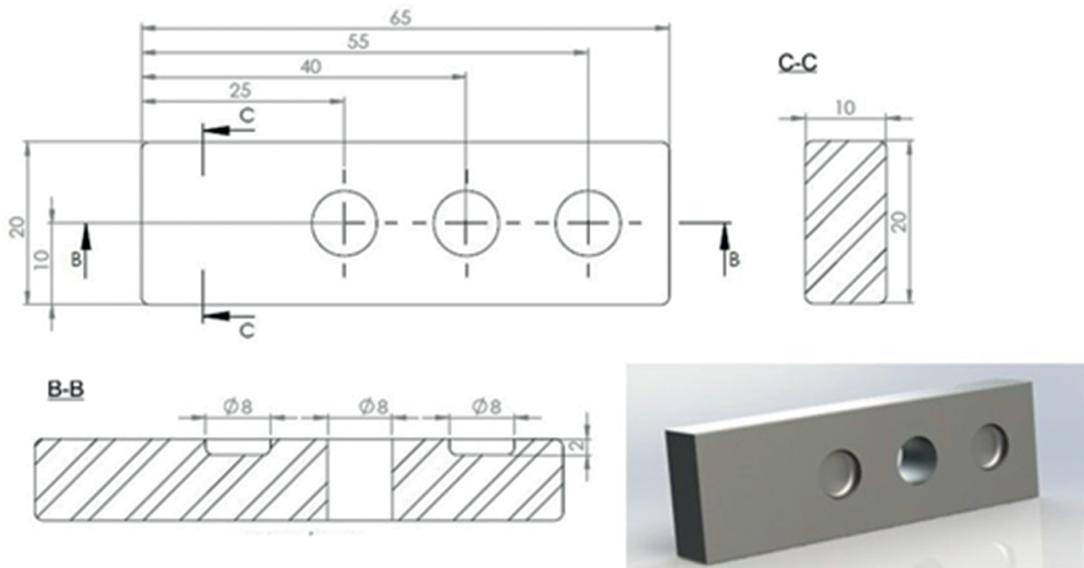
Fig. 4. Long cover plate

- Pressing the working elements (cover plates) distributed in pairs, in a parallel manner: two longer ones (Fig. 4) sized 65 x 20 x 10 mm, with two holes, 8 mm in diameter and 2 mm deep, intended to introduce the endings of the clamping screws in order to stabilize the cover plates at the time of its tightening, along with an extra through hole, 8 mm in diameter, intended for the introduction of the locking pin. Two shorter ones (Fig. 5), sized 37 x 20 x 10 mm, each with two holes, 8 mm in diameter and 2 mm deep, serving a similar purpose as in the case of long cover plates.
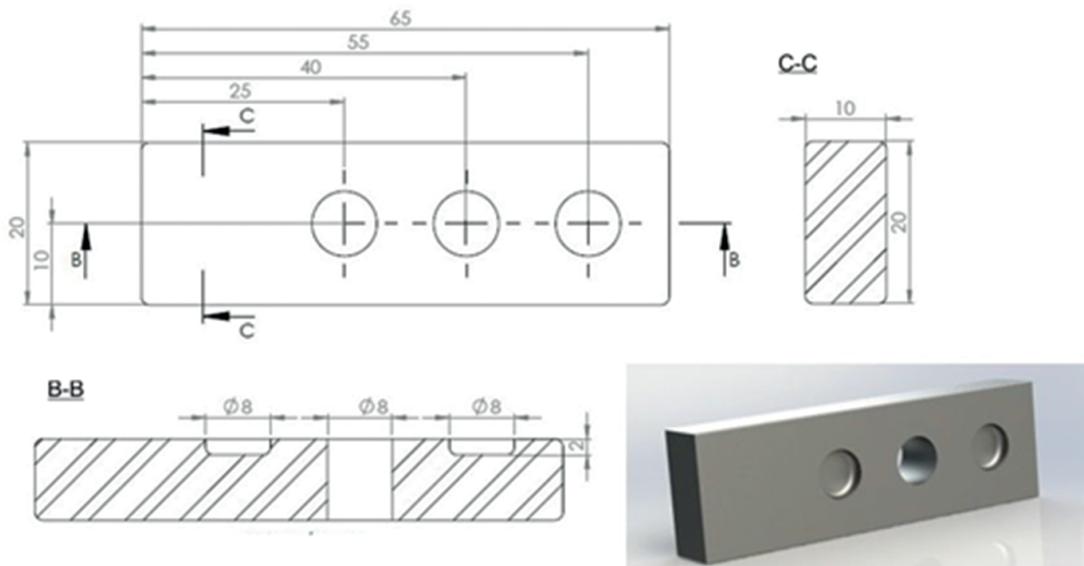
Fig. 5. Short steel cover plate

- A steel spacer sized 60 x 20 x 3 mm with a drilled through hole, 8 mm in diameter, is used to enter the locking pin and to determine the distance between the cover plates in order to obtain a desired angle of bending of the sample elements.

The bonding process will be conducted properly provided the bonded surfaces are in contact and remain stationary against one another during gluing. This is important to provide an appropriate joint and a sample shape. The second device (Fig. 6) is intended to stabilize and clamp the bonded samples during gluing at an appropriate force.
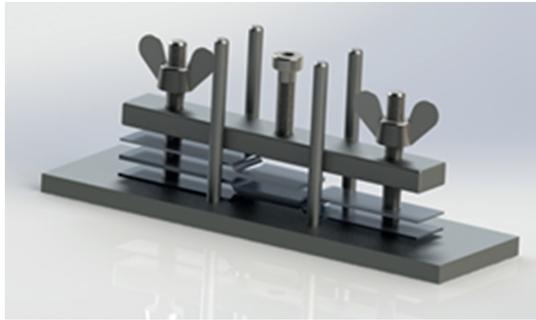
Fig. 6. Device for stabilizing glued samples

The device is composed of the following:
- A base (Fig. 7) made up of a steel flat, sized 200 x 60 x 8 mm: Inside the base, there are two M8 screws welded, 70 mm long, placed symmetrically along the long axis of the base, at a distance of 45 mm away from the edge. The screws have M8 wing-nuts put on. The screws are intended for the longitudinal stabilization of sample elements and also for blocking the crossbar, when clamping the samples. In the base, four steel rods, 6 mm in diameter, were also fixed symmetrically in pairs at a distance of 75 mm from the shorter edge of the base and 17 mm from the longer edge, intended for cross stabilization of sample elements.
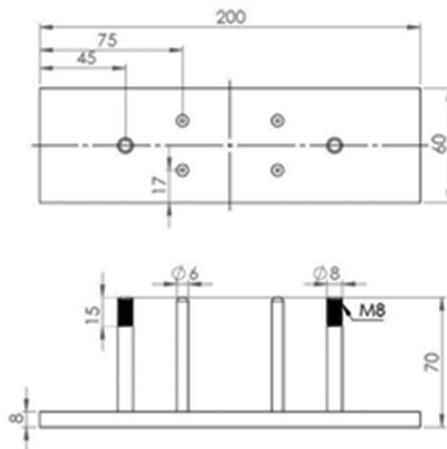
Fig. 7. Device base with screws and guides

- Steel spacers sized 27 x 20 x 4 mm placed between individual samples on the bonded section are used in order to provide an appropriate distance.
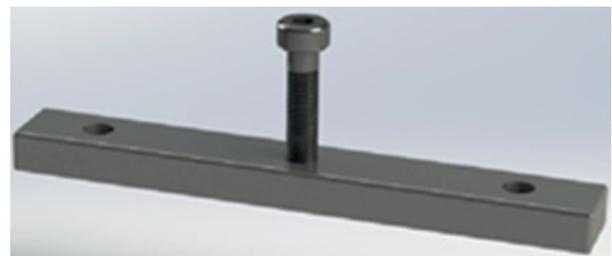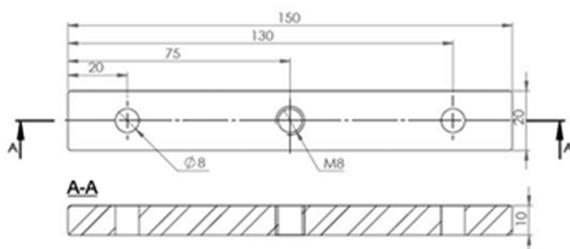
Fig. 8. Crossbar of the device with a clamping screw

- A steel crossbar (Fig. 8), sized 150 x 29 x 19 mm with two holes which are 8 mm in diameter, distributed symmetrically along the longitudinal axis, at a distance of 20 mm from the shorter edge, is intended to fix the cross bar on screws, and also with one grooved whole with M8 thread, which is to be found in the intersection point in the symmetry axis. In the hole, a cylindrical-head screw and a hexagon socket M8 x 35 mm was turned in, intended to exert pressure on the glued sample section.

2. Making devices

Based on the assumptions, taking into account the adopted principle of operation of the devices, prototype devices were made. Its main task was to confirm the correct design of the project.
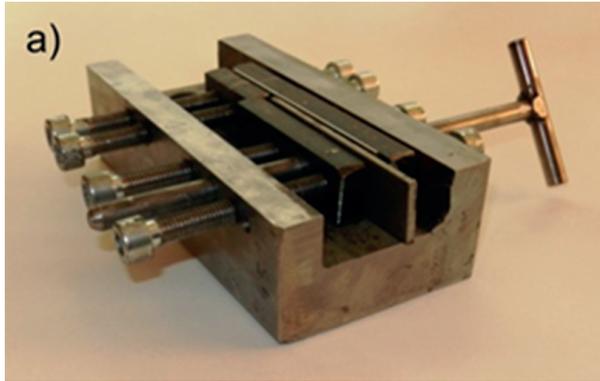
Fig. 9.   Prototype devices: a) to form sample elements, b) for stabilizing glued samples

The frame of the prototype device (Fig. 9a) was made from two steel elements which were connected by welding. Next, the frame had all the designed holes drilled and grooved. Finally, the frame was subjected to grinding. The cover plates were made from S355 flat steel.

The second device (Fig. 9b) was made by fixing two rods, grooved with the M8 thread, and four steel bars, 6 mm in diameter, in previously drilled holes in the base of the flat steel.

## 3. Validation and usage of equipment

After making the prototype devices, the sample elements were moulded. Before fixing them in the device, first it was necessary to drill holes in them, 8 mm in diameter, in the element axis, 20 mm away from the shorter edge. The holes were used to introduce the locking pin, stabilizing the position of the sample elements in the frame. The sample elements, prepared in such a way, were individually fixed in the device. In order to facilitate the position of the cover plates, the distance between their external edge and the side frame edge were assumed as a reference point. In addition, one constant was assumed for the reference point, which was one edge of the longer cover plate in the zero position. Thus, it was constantly in contact with the side edge of the frame. The other cover plate edge and the other cover plate were subject to adjustment. The parallel cover plates were treated as the clamping element.
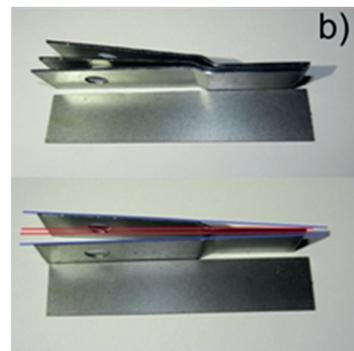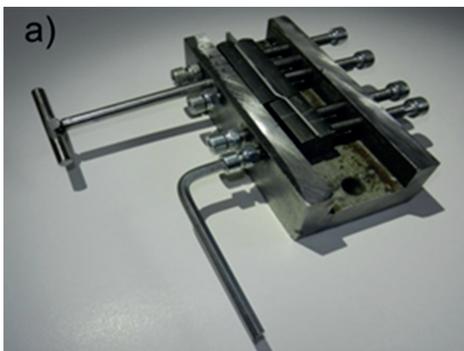
Fig. 10. Moulding sample elements (a), and improperly formed steel elements (b)

At first, steel components made from S235 steel, (Fig. 10a), were formed. The first attempts to set all the cover plates in a parallel configuration resulted in sample elements with a bending whose angle was too obtuse and whose bending angles had too gentle radii (Fig. 10b). The red lines indicate the parallel surfaces of shorter bends of the formed elements, whereas the blue lines represent an improper angle of longer bends.

It was necessary to regulate the cover plates as well as adjusting the pressing force so as to obtain correct bending angles. Therefore, at specified points (I, II, III, IV), the distance between the stones and the edge of the device frame were changed (Fig. 11).

Successive adjustment attempts are presented in Tab. 1.
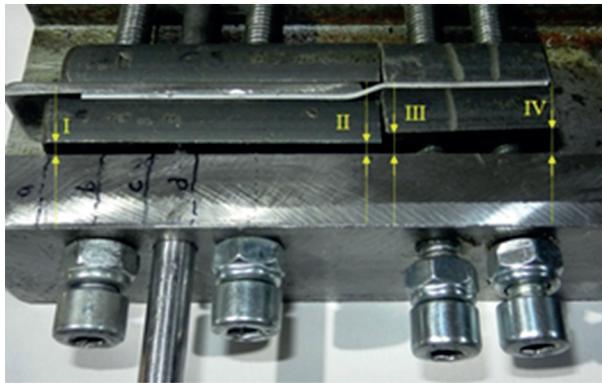
Fig. 11. Measurement points when adjusting the device
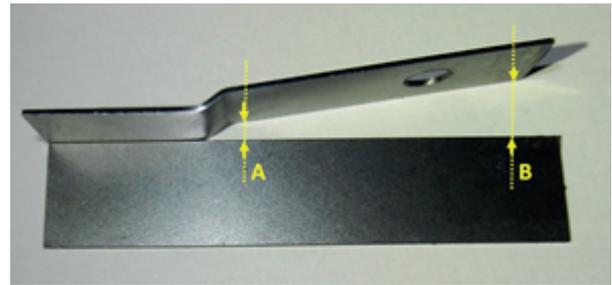
Fig. 12. Measurement points of effects of forming elements

Table 1. Values of adjusting cover plates and the results of forming sample steel elements

|	Distance between the cover plate edge and the device frame [mm]				Deviation between sample elements [mm]	
No.	I	II	III	IV	A	B
1	1.2	0	3	3	3.1	2.8
2	0.7	0	3	3.6	3.2	4
3	0.7	0	3.1	2.9	3	4.3
4	0.7	0	2.8	3.7	2.3	0.5
5	1.5	0	3	3.2	2.8	2.6
6	1.5	0	3.2	3,5	3.1	2.9
7	1.2	0	3.1	3.6	3.2	2.9
8	1.2	0	3.2	3.6	3	3
9	1.2	0	3.2	3.6	3	3
10	1.2	0	3.2	3.6	3	3

Measuring the distance between the long cover plate (I and II) and the short cover plate (III and IV) from the device frame was made with a calliper. Smaller distances were measured with a feeler gauge. The measurement of the moulding results was made by measuring the distance between the long arms of the bent sample element, after applying its shorter arm to the flat surface (Fig. 12).

A satisfactory result was achieved already after eight attempts. The accuracy of the dimensions of the sample components was also on a high level, similarly to the repeatability of the results.

Next, the device was calibrated in order to be able to form duralumin samples. The measurements were taken on the same principle as steel samples (Table 2).

Table 2. The values of adjusting cover plates and the results of moulding steel elements

	Distance between the cover plate edge and the device frame [mm]				Deviation between sample elements [mm]	
No.	I	II	III	IV	A	B
1	1.2	0	4	1.9	4.5	10
2	1.2	0	4	2.7	4	7.8
3	1.2	0	3	3	2.7	4.2
4	1.4	0	3	3	2.8	4
5	1	0	3.3	3	3.1	3.6
6	1.4	0	2.7	3	2.3	3.6
7	1.8	0	3	3	3	4
8	1.8	0	3.2	3.2	2.8	4.5
9	1.2	0	3.9	2.4	3.6	9
10	1.4	0	3	3.6	3	4.3
11	1.2	0	3	3,5	3	4.2

12	1.2	0	3	4	3	3.7
13	1.2	0	2.8	4.6	2	1
14	1.2	0	3.1	4.5	2,5	0
15	1.2	0	3.3	3.7	3	3
16	1.2	0	3.3	3.7	3	3
17	1.2	0	3.3	3.7	3	3

In this case, the difficulty in making the adjustments was due to the fact that the examined aluminium alloy (2017A) is characterized by larger elastic deformations than previously moulded steel. As a result, it was necessary to increase the angles of bending of sample elements to such a degree that resilience does not exert a negative impact on their shape after moulding. However, this led to a situation (Fig. 13) in which the cover plates began to significantly affect the surface of the bent sample elements and, in extreme cases, causing their destruction by cutting.
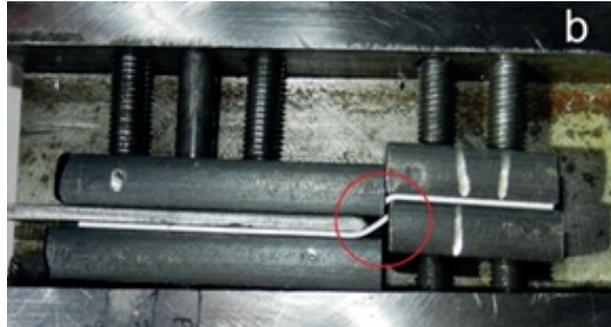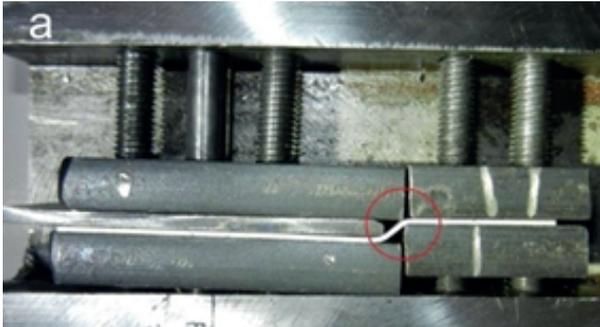
Fig. 13. Damage and destruction of an element by the edges of cover plates

To overcome this shortcoming, it was decided to change the 3 mm spacer for a 5 mm spacer, thus increasing the distance between the spacers by 2 mm.

The action had an intended consequence. Changing the thickness of the spacer sufficiently improved the capabilities of the device in the formation of sharper angles. It also facilitated manufacturing samples of required parameters (Fig. 14).

An intensive use combined with attempts of testing the strength of the device, by tightening successive screws with considerable force, close to destroying the thread, led to the emergence of cracks (Fig. 15) in places in which the frame elements were connected. In order to avoid such cases, the body of the device should be built by the method of a mechanical treatment from one piece of metal.

Fig. 14. Elements of the samples bent by means of the device during adjustment (a) and after setting the optimal parameters (b)
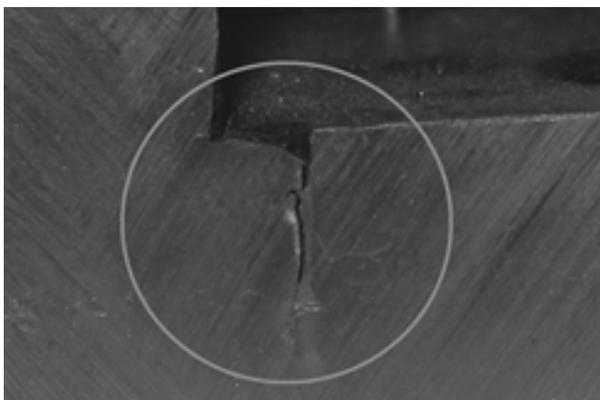
Fig. 15. Cracks in the device frame
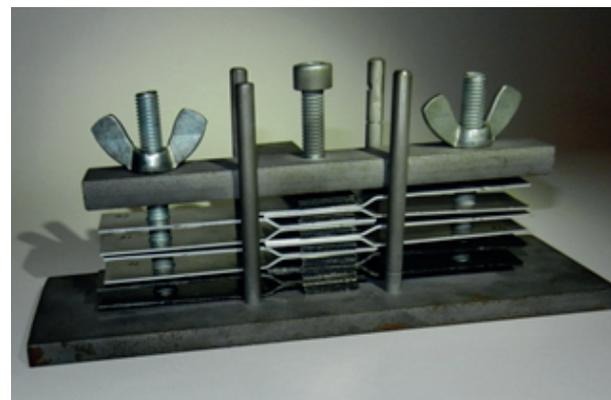
Fig. 16. Samples fixed in the device during bonding

The designed tools were made from non-alloy tool steel. In order to protect the manufactured instruments from corrosion and to obtain appropriate aesthetic properties, the tools were oxidized.

When using the moulding device, the prepared sample steel elements were prepared for bonding, and next, using the second device, they underwent the process of gluing (Fig. 16).

Both during inserting and extracting the samples from the device, it was possible to observe minor difficulties in moving the complex sample components through the threaded lead screw. While for the already hardened samples, it does not constitute a major problem, in the case of placing samples in the device and moving them prior to gluing, this can be an impediment. In the final version of the device, the screws were replaced by steel rods of the same diameter; however, they were threaded only over a distance of 25 mm so as to be able to lock the crossbar with a clamping screw.

Conclusions

On the basis of the conducted experimental research, it was proved that the assumptions made in the design of the devices were suitable. The prepared devices are functional and the samples made by them have got the parameters required by the norm.

The device for forming the samples is adjustable, which makes its application versatile, as it allows moulding sample elements of different materials. In the examinations, the sample elements were made up of average quality steel and aluminium alloy; however, after an adjustment of the device, it is possible to form elements made up of any materials.

The bonding device allows simultaneous bonding of up to seven irregular shape samples. Clamping the bonding can be adjusted by tightening the clamping screw using a dynamometer.

References

1. Machado J.J.M., Marques E.A.S., da Silva L.F.M.: Adhesives and adhesive joints under impact loadings: An overview. *The Journal of Adhesion*, 2018, 94(6), pp. 421–452.

The obtained samples (Fig. 17) were checked for the parameters specified in the standard. After measuring them with a calliper, it was found that the samples met the dimensional requirements.

They were made using the specially manufactured tools. They were tested by means of a proper dropping hammer Instron Ceast 9340. The tests confirmed the correctness of the prepared samples.

Fig. 17. Glued samples

2. Machado J.J.M., Marques E.A.S., Silva M.R.G., da Silva L.F.M.: Numerical study of impact behaviour of mixed adhesive single lap joints for the automotive industry. *International Journal of Adhesion and Adhesives*, 2018, 84, pp. 92–100.

3. Sato C.: *Impact behaviour of adhesively bonded joints*. In: Adams R.D. (ed.): *Adhesive Bonding: Science, Technology and Applications*. Cambridge: Woodhead Publishing, 2005, pp. 164–188.

4. da Silva L.F.M., Dillard D.A., Blackman B., Adams R.D.: *Testing Adhesive Joints: Best Practices*. Wiley & Sons, 2012.

5. Komorek A., Godzimirski J.: The influence of selected adhesive properties and the manner of surface preparation upon the impact strength of adhesive joints. *Journal of KONES Powertrain and Transport*, 2018, 25(4), pp. 463–470.

6. Adams R.D., Harris J.A.: A critical assessment of the block impact test for measuring the impact strength of adhesive bonds. *International Journal of Adhesion and Adhesives*, 1996, 16, pp. 61–72.

7. PN-EN ISO 11343: *Kleje. Oznaczanie wytrzymałości dynamicznej wysokowytrzymałych połączeń klejowych na rozczepienie pod wpływem warunków udarowych – Metoda uderzenia klinem*. Polski Komitet Normalizacyjny, 2007 [in Polish].

Joanna ŁABĘDZKA*

ŁUKASIEWICZ Research Network – Institute for Sustainable Technologies, Radom, Poland
* Corresponding author: joanna.labedzka@itee.radom.pl

AMALGAMATION OF BUSINESS INTELLIGENCE WITH ENTERPRISE RESOURCE PLANNING SYSTEMS FOR INDUSTRY 4.0

Key words: Business Intelligence, BI, Enterprise Resource Planning, ERP, Industry 4.0., information technology, decision-making, strategic management, information management.

Abstract: Businesses today are incredibly data rich, and dealing with large amount of data, so making some inferences and conclusions, depending on the organisation size and complexity of its processes, it has been a challenge, especially that the next disruptive phase in manufacturing, i.e. Industry 4.0 (I4.0) is already underway.
Business Intelligence (BI) and Enterprise Resource Planning (ERP) have become key issues for business activities as well a necessity for further phases of the industrialisation. Their importance has been recognised especially in supporting decision making by building an analytic capability and providing a holistic framework for technical systems in production, quality management, predictive modelling and maintenance, simulation techniques, etc. The introduction of Industry 4.0 requires the digitalisation of data stored in distributed systems and organisational and technological processes. The integration allows one to facilitate the collection, integration, and analysis of data in order to affect the process of development of technical innovations and support the planning and managing in efficient and productive manner.
Therefore, the main purpose of this paper was to discuss the importance of BI and ERP amalgamation for the process of the digitalisation and maximisation of company resources stored in distributed transactional systems in the context of Industry 4.0.

Konsolidacja koncepcji Business Intelligence z systemami klasy ERP dla potrzeb przemysłu 4.0

Słowa kluczowe: Business Intelligence, BI, planowanie zasobów przedsiębiorstwa, ERP, Przemysł 4.0., podejmowanie decyzji, zarządzanie strategiczne, zarządzanie informacją.

Streszczenie: Współczesny biznes i przemysł charakteryzuje wielowymiarowość danych, duża dynamika zmian oraz konieczność podejmowania elastycznych decyzji, co stanowi także wyzwanie dla narzędzi informatycznych oraz metod zarządzania. Systemy *Business Intelligence* (BI) i *Enterprise Resource Planning* (ERP) stały się kluczowymi platformami analizy i przetwarzania danych, a także podstawą dalszych etapów zaawansowanej industrializacji. Ich znaczenie doceniono szczególnie na płaszczyźnie wspomagania decyzji poprzez budowanie zdolności analitycznych, dostarczanie *real-time* danych oraz integrację wielowymiarowych przekrojów informacyjnych.
Business Intelligence (BI) to nie tylko koncepcja, ale także zestaw technologii, które ułatwiają gromadzenie, integrację i analizę danych w celu wspomagania procesów decyzyjnych. Z drugiej strony w większości organizacji wszystkie dane potrzebne do analiz są najczęściej przechowywane w systemach planowania zasobów przedsiębiorstwa klasy ERP. Zatem głównym celem tego artykułu jest omówienie znaczenia konsolidacji systemów klasy BI i ERP dla potrzeb procesu digitalizacji i maksymalizacji zasobów informacyjnych składowych w rozproszonych systemach transakcyjnych w kontekście koncepcji Przemysłu 4.0.

Introduction

The concept of using information systems to support decision-making has been a goal of companies since the introduction of business computer technology [1]. There are numerous IT solutions facilitating various levels of management. The following are just some examples: ERP (*Enterprise Resource Planning*), BI (*Business Intelligence*), MRP (*Manufacturing Resource Planning*), DMS (*Document Management*

System), WMS (*Warehouse Management System*), CRM (*Customer Relationship Management*), and KMS (*Knowledge Management System*). These solutions offer a range of features. However, a framework of BI and ERP is the key approach to improve business operations and eventually reaching an understanding of the environment of an organisation. Industry 4.0 calls for a future of agile and affordable manufacturing fuelled by the Internet of things [1], additive manufacturing [2], cloud computing [3], big data [4], etc., and ERP or BI will become the backbone of a network of connected environment. Therefore, those were selected for further analyses paying attention a little more to ERP systems, as the BI concept was presented in [5].

1. Mutual relationship between BI and ERP

After presentation of the BI and ERP approach to data, the relationship between those two concepts is defined in this section, because they serve different functions depending on business requirements.

Business Intelligence is understood as an overarching term that definitely concerns much more than a particular piece of information or IT software. The current holistic view of BI encompasses business objectives, performance management, people, processes, analytics, reporting, online analytical processing (OLAP), and query technologies, all sitting on an information processing and management infrastructure [6]. BI is characterised as a process of analysing, transforming, and presenting structured data from multiple sources and identifying actionable business opportunities. Business Intelligence is also defined as the ability to provide meaningful information at the right time so that the decision making can be informed and fact-based [7, 8]; therefore, its main purpose is to enrich the multidimensional business environment with so far uncovered opportunities.

However, BI requires large amount of various data to inference and guide the business, such as technical innovation process. One of the most sophisticated information systems currently known to be able to satisfy the need for data efficiency is the Enterprise Resource Planning system (ERP) [9]. ERP is treated as one of the more common categories of business software, especially among large businesses. ERP is defined as an enterprise-wide set of management tools that balances various business activities and assures cross-functional integration between sales, supply chain, operations, marketing, manufacturing, new product development, and human resources, etc. [10]. ERP, like MRP software, manages manufacturing processes, in particular, production planning, scheduling, and inventory management. Although the full range of ERP capabilities is much more extensive and involves keeping all of workflow data in one place,

all of business processes draw data from that location to inform insights. This helps ensure data quality, since it never gets duplicated between systems and increases data accessibility [11]. A main role of the ERP system is to collect, store, and interpret data from business activities, in order to improve the performance and reduce costs through the integration and automation of the processes.

The latest ERP is often called *postmodern ERP*, because it deconstructs ERP software from one big central program into logical components and it is defined as highly modular business process management software, which is a core of an effective way of centralising information and workflow processes through data management [12].

Considering also other definitions, for example, [6, 13, 14, 15, 16, 17, 18, 19], this paper takes into account narrow understanding of ERP, and defines it as a modular computer architecture that stores and integrates data from various cross-organisational levels with no data redundancy and creates a complex picture of the entire organisation.

The literature review has shown that BI and ERP facilitate the different facets of organisation and both are needed to enhance and improve the ability of companies to decision-making at all levels of management (Fig 1), especially that stress on quick data access, sharing and exchange is fundamental for I4.0.

BI and ERP systems are incorporated within a main business process, such as development and the introduction of a technical innovation to the market, mass manufacturing, etc., Enterprise Resource Planning functions at the transactional level emphasises organisation, performance evaluation and rewards, and are task- and outcome-oriented. ERP system as a software application with a centralised database with separate modules [22] can be used to manage an entire process of the product development from the concept stage, through prototyping, introducing to the market and evaluation. A central ERP database integrates data representing different functions within the organisation. It includes the operational processes that define the primary activities that a company needs to perform in order to successfully execute its business [23]. The Industry 4.0 compatible ERP system fully integrates with manufacturing execution systems. ERP helps to put the pieces of the puzzle together and provides a single operational view of the business in order to manage and improve industrial processes.

However, to move from the data level to long term oriented strategic level, Business Intelligence is required. The most current information technology is to feed BI-based systems with data from external systems, such as ERP, that from the other hand can be an ideal tool for developing BI applications.
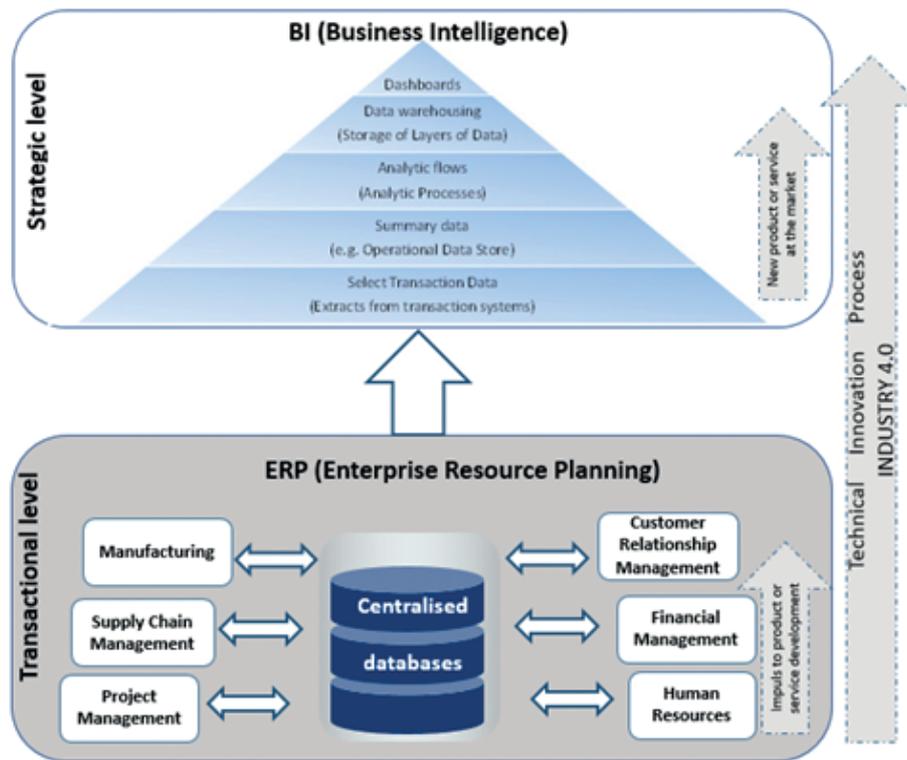
Fig. 1. The mutual relation between BI and ERP systems in a business environment
Source: The author on the basis of [20, 21]

BI uses the information and analysis from a transactional level to spur business growth and transformation innovations into market products. BI filled with ERP data allows organisations to access, analyse, and share information and knowledge about the whole process of manufacturing in order to track, understand, target, and manage business to improve its economic performance. It allows one to optimize future activities and to properly modify the organisational, financial, and technological aspects of the company's operations, so that it more effectively implements the set strategic goals. On that basis, more strategic, flexible decisions could be made with regards to future trends and patterns that influence business growth and innovation market [24].

Although ERP systems and Business Intelligence systems are complimentary, they are distinctly different. BI is proactive, comprised of forward-thinking principles and ideas, while ERP approach occurs on either a regular, on-going basis or as needed to support HR strategy. However, ERP and BI should be integrated and function together, since they are both important to create intelligent production environment toward I4.0.

2. Synergy of BI and ERP integration

ERP and BI create an integrated platform of enterprise data systems with the Internet of things (IoT) and cloud computing required in Industry 4.0 to make better-informed business decisions and operate as efficiently as possible. BI software can step in and take a weight off when it comes to the analysis of data stashed in the ERP system. Combining these two concepts provides a more comprehensive approach to business management and offers dynamic reporting, where companies can pinpoint lucrative business opportunities [25].

The synergy of ERP and BI appears on the software level, as the most current information technology is to load data from ERP into a data warehouse and then link to BI-based systems with BI tools (such as OLAP, data mining, query and reporting). BI software draws heavily upon the information stored in the ERP system, yet has the primary objective of analysing this information. Feeding on the information stored in the ERP software system, a BI system will take this data, analyse it, and present it back in an actionable and easy to interpret format [26]. On the organisational level, the synergy allows one to take advantage of the analytic data and proceed to strategic long-term oriented management to guide the business towards digitalisation and real-time data to increase customer value by streamlining processes, increasing quality, creating new revenue streams, and reducing production costs.

The convergence of ERP and BI systems is considered crucial, so BI is frequently tightly coupled with the ERP systems. Where ERP offers enterprise-wide data consistency and systemic integration, BI describes a set of concepts and methods to support and improve managerial decision making by using fact based support systems use-able by all levels of management [27].

Integration of ERP and BI enhances and improves the ability of companies to make decisions by leveraging the ability to manage data from the ERP system and the analytical capabilities of the BI system [28. This integration leads to optimal use of both ERP and BI systems and more specifically, the following benefits are provided [29, 30]:

- Allows one to control the recognition of corporate cash flow in real time;
- Facilitates the implementation of cooperation between departments;
- Reduces the time required to generate regular reports;
- Improves profitability by transaction data analysis and forecasting business trends;
- Enables finance staff to create financial revenue reports and expenses quickly;
- Improves accounts payable and vendor relationship management;
- Provides online access to the data, saving access time;
- Improves relations with customers through sales of in-depth data mining; and,
- Shares information with the sales department, and this allows one to make better decisions based on a macro view of the business.

Because the integration of ERP and BI systems provides a significant value for an organisation, i.e. cost and time savings, improved information and business processes, more efficient and quick decisions and market response, the next section proposes the scheme to feed the process of digitalisation of the company heading for the I4.0.

3. The ERP and BI-based framework for Industry 4.0

Traditional management methods and structures are failing to adequately respond to an overwhelming flurry of information, discontinuous change, and hyper competition in Industry 4.0 that was also the rationale for developing the ERP and BI-based framework.

The presented framework merges all levels of decision making and takes into account the following elements of strategic management [31]:

- Business environment analysis (external environment scanning and analyse, strategic resources and capabilities identification, critical points isolation and clusters identification);
- Strategy formulation (review of strategic objectives knowledge database searching, strategic options identification and selection, key issues, scenario preparation);
- Strategy implementation (organisational design: structure, culture and control, development of implementation structure, budgeting and allocation resources, discharge of functions and activities); and,
- Evaluation and control (analysis and assessment).

The conceptual framework identifies the Enterprise Resource Planning and Business Intelligence characteristics and their competencies in the strategic management for requirements of Industry 4.0 (Fig. 2).
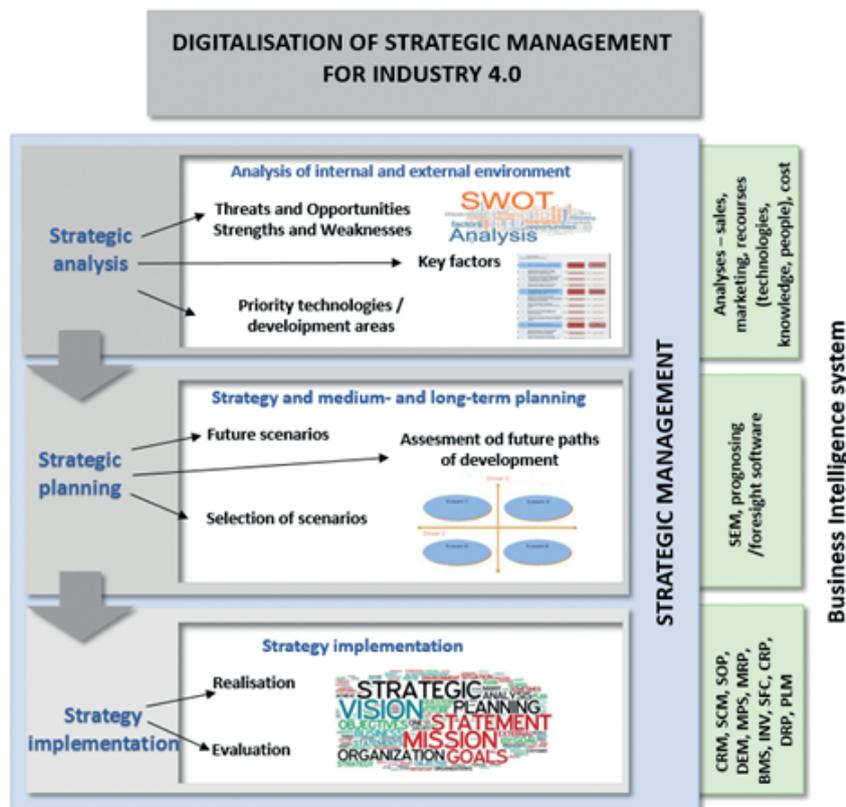

Fig. 2. The framework of ERP and BI-based digitalisation for Industry 4.0 requirements

The developed framework based on the strategic management process within Industry 4.0 proposes the use of BI and ERP class computer systems to support and automate individual business processes, and it aligns strategic tasks with ERP and BI competencies. Operational processes generate transactional data stored in the ERP system, and BI sources data from the ERP via extraction and provides the transformation and consolidation diverse data into meaningful performance indicators.

At the stage of strategic analysis, the proposed framework includes procedures, databases and computer systems to analyse the following: financial results, costs, indicators, financial flows, sales plans vs. results, profitability, marketing, production costs, efficiency and quality at all stages of the process. The strategic planning phase considers advanced software packages performing complex, sophisticated analyses and comparisons of human resources, human capital, order completion, inventory status, quality and performance assessment, as well as software for forecasting, foresight, and strategic planning (SEM). At the implementation stage, the proposed methodology includes IT tools for *Customer Relationship Management* (CRM), *Supply Chain Management Systems* (SCM), *Sales and Operations Planning* (SOP), *Demand Management* (DEM), *Master Production Schedule* (MPS), *Materials Resource Planning* (MRP), *Product structure subsystem* (BMS), *Material Transaction Subsystem* (INV), *Production control* (SFC), *Capacity Requirements Planning* (CRP), *Distribution Planning* (DRP), *Product Lifecycle Management* (PLM), etc.

The integration allows companies to take advantage of ERP data using BI reporting capabilities as Business Intelligence developed on the top of the ERP system and takes advantage of simplified data acquisition drawn from a homogenous source. The strategic management on each level (strategic analyses, planning and strategy implementation) sifts through large amounts of data in order to focus their resources more effectively and efficiently with the use of computer systems. BI provides refined information that could be used for advances Industry 4.0 requirements on the context of the data digitalisation. Created in that way, the data platform gives access to timely accurate data that processes large amounts of data and provides support for tactical, operational, and strategic decision making within the I4.0.

The framework that aggregates Business Intelligence and the ERP information system within Industry 4.0 and should become more and more integrated with organisational processes, bringing more productivity and better control to those processes.

Conclusions

The introduction of Industry 4.0 requires not only a shift to the digitalisation in manufacturing systems that connects physical assets and digital networks, but also predictive analysis tools for production and maintenance. The growth in an Industry 4.0 environment will be intrinsically linked with a business's ERP and BI systems that should be in a better position to meet the fast-paced and connected requirements of Industry 4.0. To be ready for digital transformation, ERP and BI software should provide business with a common platform, allow for central master data management, and offer real-time data processing, enabling all stakeholders in the business to have access to the latest, and most accurate data in real-time.

The paper presented the scheme for the amalgamation of ERP and BI systems within company introducing I4.0. On the basis of literature review, the mutual relationship between ERP and BI was more attentively explored. This indicated needs for BI and ERP integration, and simultaneously drew a synergic process. Only the synergy derived of the combination of strategic management techniques, information technology systems (for instance ERP and BI) and human resources management enhances organisational performance and improves the ability of companies to evidence-based decision-making, and brings a real I4.0.

References

1. Ganzha M., Paprzycki M., Pawlowski W., Szmeja P., Wasielewska K.: Semantic interoperability in the Internet of Things: An overview from the INTER-IoT perspective. *Journal of Network And Computer Applications*, 2017, 81, pp. 111–124.

2. Ford S., Despeisse M.: Additive manufacturing and sustainability: an exploratory study of the advantages and challenges. *Journal of Cleaner Production*, 2016, 137, pp. 1573–1587.

3. Wang T., Mei Y.X., Jia W.J., Zheng X., Wang G.J., Xie M.D.: Edge-based differential privacy computing for sensor-cloud systems. *Journal of Parallel and Distributed Computing*, 2020, 136, pp.75–85.

4. Cui Y.S., Kara S., Chan K.C.: Manufacturing big data ecosystem: A systematic literature review. *Robotics And Computer-Integrated Manufacturing*, 2020, 62, Article Number: 101861.

5. Łabędzka J.: Integrated understanding of Business Intelligence in technological innovation processes. *Journal of Machine Construction Maintenance*, 2018, 111(4), pp. 123–130.

6. Panian Z.: How to make business intelligence actionable through service-oriented architectures. *WSEAS Transactions on Business and Economics*, 2008, 5(5), pp. 210–221.

7. Rahimi E., Rostami N.A: Enterprise Resource Planning and Business Intelligence: The Importance of Integration. *International Journal of Management Academy*, 2015, 3(4), pp. 7–14.

8. Fink L., Yogev N., Even A.: Business intelligence and organizational learning: An empirical investigation of value creation processes. *Information & Management*, 2017, 54(1), pp. 38–56.

9. Jenkins L.: *MRP vs ERP: A Comprehensive Comparison of the Difference Between ERP and MRP Systems*. [Online]. 2019. [Accessed 3 October 2019]. Available from: https://selecthub. com/enterprise-resource-planning/mrp-vs-erp-differences-between-systems/

10. Kharuddin, S., Yau F.S., Senik R.: ERP Adoption Factors: The Effect of Institutional- and Economic-Based Theory. *Pertanika J. Soc. Sci.& Hum*, 2013, 21(S), pp. 149–170.

11. Wallace T.F., Kremzar M.H.: *ERP: making it happen: the implementers' guide to success with enterprise resource planning*. Ed. Wiley, 2001.

12. Jenkins L.: *Postmodern ERP: Just Another Buzzword?* [Online]. 2019. [Accessed 6 October 2019]. Available from: https://selecthub.com/enterprise-resource-planning/postmodern-erp-another-buzzword/

13. Baray S., Hameed S., Badii A.: Analyzing the factors responsible for effectiveness of implementation and integration of enterprise resource planning systems in the printing industry. *Journal of Enterprise Information Management*, 2008, 21, pp. 139–161.

14. Chou D., Bindu Tripuramallu H., Chou A.Y.: BI and ERP integration. *Information Management & Computer Security*, 2005, 13(5), pp. 340–349.

15. Klaus H., Rosemann M., Grable S., Segars A.: What is ERP? *Information Systems Frontiers*, 2000, 2(2), pp. 141–162.

16. Laudon J., Laudon K.: *Management Information Systems – Managing the Digital Firm*. 7th Edition. Prentice Hall, Inc., 2002.

17. Russman R., Seymour L.F., van Belle J.-P.: Integrating BI Information into ERP Processes Describing Enablers. In: *19th International Conference on Enterprise Information Systems (ICEIS 2017), Porto (Portugal), 26-29 April 2017*. Proceedings, 2017, 1, pp. 241–248.

18. Sheikh K.: *Manufacturing Resource Planning (MRP II) – With an introduction to ERP, SCM and CRM*. McGraw-Hill Publishing Limited, 2003.

19. Yen D., Chou D., Chang J.: A synergic Analysis for Web-based Enterprise Resource Planning Systems. *Computer Standards and Interfaces*, 2002, 24(4), pp. 337–346.

20. Vakalfotis N., Ballantine J., Wall A.: A Literature Review on the Impact of Enterprise Systems on Management Accounting. In: *8th International Conference on Enterprise Systems, Accounting and Logistics (ICESAL), Thassos Island (Greece), 11–12 July 2011*. Proceedings, 2013.

21. Innoverto: *Certified Effective Use of Business Intelligence*. [Online]. 2019. [Accessed 26 September 2019]. Available from: https://www.innoverto.com/register/cebi/

22. Bourgeois D.T.*: Information Systems for Business and Beyond*. The Saylor Academy, 2014.

23. MSG: *Learn Management Concepts & Skills Rapidly*. [Online]. 2019. [Accessed 15 October 2019]. Available from: https://www.managementstudyguide.com/

24. Muthukumar M., Karthikeyan K.: Business Intelligence Market Trends and Growth in Enterprise Business. *Int. J. Recent Innov. Trends Comput. Commun.*, 2016, 4(3), pp. 188–192.

25. ERP Desk: *ERP and BI Software: What's the Difference?* [Online]. 2017. [Accessed 15 October 2019]. Available from: https://it.toolbox.com/blogs/erpdesk/erp-and-bi-software-whats-the-difference-030217

26. Sales-i Marketing Team: *ERP vs BI software: What is the difference?* [Online]. 2019. [Accessed 15 October 2019]. Available from: https://www.sales-i.com/erp-vs-bi-the-difference

27. El Amrani R., Rowe F., Geffroy B.: The effects of enterprise resource planning implementation strategy on cross-functionality. *Information Systems Journal*, 2006, 16(1), pp. 79–104.

28. Davenport T.H., Harris J.G., De Long D.W., Jacobson Alvin L.: Data to Knowledge to Results: Building an Analytic Capability Accenture. *California Management Review*, 2001, 43(2), pp. 117–138.

29. Nofal M.I., Yusof Z.M.: Integration of Business Intelligence and Enterprise Resource Planning within Organizations. *Procedia Technology*, 2013, 11, pp. 658–665.

30. Agostino R.: *Business Intelligence: solving the ERP overload*. [Online]. 2004. [Accessed 15 October]. Available from: www.crystaldecisions

31. Melecky A., Machacek M.: The role of national and supranational fiscal rules – International evidence and situation in the Czech Republic. *Journal of Applied Economic Sciences*, 2010, 5. pp. 375–382.